ADAPTIVE MODEL PREDICTIVE CONTROL APPLIED TO SUBMERSIBLE PUMP LIFTED WELLS

Pedro de Azevedo Delou

Dissertação de Mestrado apresentada ao Programa de Pós-graduação em Engenharia Química, COPPE, da Universidade Federal do Rio de Janeiro, como parte dos requisitos necessários à obtenção do título de Mestre em Engenharia Química.

Orientadores: Argimiro Resende Secchi
Maurício Bezerra de Souza Júnior

Rio de Janeiro
Agosto de 2019

ADAPTIVE MODEL PREDICTIVE CONTROL APPLIED TO SUBMERSIBLE PUMP LIFTED WELLS

Pedro de Azevedo Delou

DISSERTAÇÃO SUBMETIDA AO CORPO DOCENTE DO INSTITUTO ALBERTO LUIZ COIMBRA DE PÓS-GRADUAÇÃO E PESQUISA DE ENGENHARIA (COPPE) DA UNIVERSIDADE FEDERAL DO RIO DE JANEIRO COMO PARTE DOS REQUISITOS NECESSÁRIOS PARA A OBTENÇÃO DO GRAU DE MESTRE EM CIÊNCIAS EM ENGENHARIA QUÍMICA.

Examinada por:

Prof. Argimiro Resende Secchi, D.Sc.

Prof. Maurício Bezerra de Souza Júnior, D.Sc.

Prof. Alessandro Jacoud Peixoto, D.Sc.

Eng. Mario Cesar Mello Massa de Campos, D.Sc.

RIO DE JANEIRO, RJ – BRASIL
AGOSTO DE 2019

Delou, Pedro de Azevedo

Adaptive Model Predictive Control Applied to Submersible Pump Lifted Wells/Pedro de Azevedo Delou. – Rio de Janeiro: UFRJ/COPPE, 2019.

XXI, 126 p.: il.; 29,7cm.

Orientadores: Argimiro Resende Secchi

Maurício Bezerra de Souza Júnior

Dissertação (mestrado) – UFRJ/COPPE/Programa de Engenharia Química, 2019.

Referências Bibliográficas: p. 104 – 116.

1. Adaptive Control. 2. Model Predictive Control. 3. Model Scheduling. 4. Kalman Filter. 5. Robust Control. 6. Electrical Submersible Pump. 7. Artificial Lift. I. Secchi, Argimiro Resende *et al.* II. Universidade Federal do Rio de Janeiro, COPPE, Programa de Engenharia Química. III. Título.

Para Tito e Nicolas, meus sobrinhos queridos que trouxeram nova vida e imensa alegria à família.

Agradecimentos

Primeiramente e acima de tudo, agradeço a Deus pela oportunidade da vida e pelo acompanhamento em minhas escolhas, me fortalecendo e me guiando pelos desafios.

Ao Professor Argimiro, gostaria de agradecer por todo apoio e suporte, não só durante a execução deste trabalho, mas em toda a minha trajetória como Pesquisador e Engenheiro Químico. Pelo exemplo de dedicação, simplicidade e excelência profissional. Pelas oportunidades de crescimento e pela confiaça depositada em minha formação.

Ao professor Maurício, pela confiança e suporte durante toda execução deste trabalho. Pelo incentivo para realizar um trabalho de qualidade, apontando as direções mais interessantes. Pela dedicação minuciosa nas correções de textos e apresetações.

À minha família, pelo apoio e suporte ao longo da minha trajetória de vida.

À minha companheira, Marina, pelo amor e carinho durante este período. Por me apoiar e aguentar os momentos difíceis de estresse e ansiedade. Sobretudo, por escolher dividir a vida comigo.

Aos amigos que a vida me deu, que fazem parte de quem eu sou e nem mesmo a distância diminui o amor e o carinho que tenho por eles: Vynicius, Arthur, Gabriel, Paulo, Viana, Isadora, Vanessa, Janaina, Raquel e Duda.

Aos amigos do Brasas, que diviram comigo as manhãs de sábado estudando inglês, entre uma discussão ou outra sobre pagar mais impostos ou sobre feminismo: Alexandre, Jessy, Pedro, Carol, Yuri (nosso "nem-nem") e *teacher* Naty.

Aos amigos que dividiram comigo a etapa sofrida de disciplinas do PEQ: Danillo, Sâmia, Bruna, Tetsuo, Luiz, Renato, Thiago, Zé e especialmente Lucas e Julia. O primeiro por estar sempre disposto a discutir os assuntos referêntes às disciplinas e a este trabalho, e a segunda por ter colaborado com o ínicio da metodologia, proposto o trabalho com a ESP e ter sido co-autora do paper que apresentamos no DYCOPS 2019. Além de terem se tornado grandes amigos.

Aos professores do PEQ que contribuíram em mais esta etapa da minha formação acadêmica. Especialmente ao Professor Príamo, pelos aconselhamentos de grande valia a cerca das minhas preocupações com a carreira profissional.

Aos colegas que, mesmo já tendo passado da etapa de disciplinas, voluntariamente voltaram para nos auxiliar através das monitorias: Daniel, Sergio, Otávio, Christian, Allyni e Ataíde.

Aos companheiros do LADES que tornam o dia a dia mais leve: Silvio, Thiago, Thamires, Maria, Daniel e Isabela.

Aos companheiros de trabalho no projeto RTO de pequeno porte: *monsieur* Paiva, Letícia e Dorigo.

Por fim, mas não menos importante, às instituições de fomento à pesquisa do Brasil, Cappes e CNPq, que financiaram parte desse trabalha e da minha trajetória acadêmica, e à Petrobras que finciou minha ida ao Dycops e os projetos de cooperação com a UFRJ.

"O cérebro eletrônico faz tudo
Quase tudo
Quase tudo
Mas ele é mudo

O cérebro eletrônico comanda
Manda e desmanda
Ele é quem manda
Mas ele não anda

Só eu posso pensar
Se deus existe, só eu
Só eu posso chorar quando estou triste
Só eu
Eu cá com meus botões de carne e osso
Eu falo e ouço

Eu penso e posso
Eu posso decidir se vivo ou morro por que
Porque sou vivo"
(Gilberto Gil)

Resumo da Dissertação apresentada à COPPE/UFRJ como parte dos requisitos necessários para a obtenção do grau de Mestre em Ciências (M.Sc.)

CONTROLE PREDITIVO ADAPTATIVO APLICADO A BOMBA SUBMERSÍVEL PARA ELEVAÇÃO DE POÇOS

Pedro de Azevedo Delou

Agosto/2019

Orientadores: Argimiro Resende Secchi
Maurício Bezerra de Souza Júnior

Programa: Engenharia Química

Bombas Elétricas Submersíveis (ESPs) são uma das tecnologias de elevação artificial de óleo mais difundidas para exploração em águas profundas. Na operação de uma ESP existe um grande número de parâmetros que devem ser monitorados e mantidos dentro de restrições operacionais com o objetivo de manter uma operação estável e ótima. Controle preditivo baseado em modelo (MPC) é uma das estratégias utilizadas para tal fim. Literaturas prévias propuseram o uso de MPC linear baseado em identificação, contudo nenhuma estratégia foi empregada para contornar as não linearidades do sistema, em vez disso o uso de apenas um modelo linear interno vem sendo empregado, além de considerar todas as variáveis relevantes do sistema com medidas disponíveis. Neste trabalho, o problema de perda das medidas das variáveis de estado é abordado. É mostrado que uma estratégia não-adaptativa, com um único modelo interno, carece de qualidade na estimação dos estados, e um MPC robusto não é possível com tal configuração. Portanto, um MPC adaptativo acoplado com filtro de Kalman é proposto e três estratégias de adaptação são comparadas. Duas estratégia de chaveamento baseada em interpolação de modelos locais são propostas e comparadas com a linearização sucessiva. Todas as estratégias garantem a acurácia e estabilidade do modelo interno em todo o intervalo de operação. As estratégias apresentaram uma performance similar à linearização sucessiva, evitando a necessidade de obtenção de um modelo linear local em cada tempo de amostragem através da interpolação entre um número de modelos lineares obtidos por identificação. Por fim, uma estratégia de estimação de parâmetros é proposta e acoplada ao MPC com o objetivo de contornar as incertezas de medida e as incertezas estruturais de modelo.

Abstract of Dissertation presented to COPPE/UFRJ as a partial fulfillment of the requirements for the degree of Master of Science (M.Sc.)

ADAPTIVE MODEL PREDICTIVE CONTROL APPLIED TO SUBMERSIBLE PUMP LIFTED WELLS

Pedro de Azevedo Delou

August/2019

Advisors: Argimiro Resende Secchi
Maurício Bezerra de Souza Júnior

Department: Chemical Engineering

Electric Submersible Pumps (ESPs) are one of the most widespread oil artificial lifting technologies for deepwater exploration. In the operation of an ESP there is a large number of parameters that must be monitored and held within operational constraints in order to guarantee stable and optimal operation. Model predictive control (MPC) is one of the strategies able to guarantee stable and optimal operation with constraints handling. Previous literature has proposed the use of linear MPC based on system identification, however no adaptive strategy has been employed to overcome system nonlinearities, instead a single internal model has been used. Moreover, all previous works have considered relevant system variables measurements to be available. In this dissertation, the problem of losing measurements of the state variables due to the aggressive subsea environment is addressed. We show that a non-adaptive single linear model strategy lacks in quality for state estimation and a robust MPC is not possible under this configuration. Therefore, an adaptive MPC coupled with Kalman Filter is proposed and three adapting strategies are compared. Two scheduling strategies based on linear interpolation of a set of local models are proposed and compared to successive linearization. All strategies guarantee internal model accuracy and stability over the whole operational range. The proposed scheduling strategies presented a similar performance compared to the successive linearization strategy, avoiding the need of obtaining a local linear model at each sampling time by interpolating among a number of linear models previously obtained by identification instead. In addition, a parameter estimation strategy is proposed and coupled to the MPC scheme so that measurement and model structural uncertainties are overcome.

Contents

List of Figures

List of Tables

List of Abbreviations

ACADO	Automatic Control and Dynamic Optimization, p. 33
ARMAX	Autoregressive Moving Average Model, p. 10
ARX	Autoregressive Exogenous Model, p. 10
CEKF	Constrained Kalman Filter, p. 25
CV	Controlled Variable, p. 38
DMC	Dynamic Matrix Control, p. 9
EHAC	Extended Horizon Adaptive Control, p. 10
EKF	Extended Kalman Filter, p. 25
EPSAC	Extended Prediction Self-Adaptive Control, p. 10
ESP	Electric Submersible Pump, p. 1
FIR	Finite Impulse Response, p. 16
FSR	Finite Step Response, p. 16
GPC	Generalized Predictive Control, p. 10
HIECON	Hierarchical Constraint Control, p. 12
IDCOM-M	Multivariable Identification and Command, p. 12
IDCOM	Identification and Command, p. 9
IFAC	International Federation of Automatic Control, p. 4, 35
ISS	Input-to-State Stability, p. 20
KF	Kalman Filter, p. 25
MAC	Model Algorithmic Control, p. 9

MHE	Moving Horizon Estimators, p. 25
MIMO	Multi-input, multi-output, p. 8
MPC	Model Predictive Control, p. 3
MRAC	Model Reference Adaptive Control, p. 22
MURHAC	Multipredictor Receding Horizon Adaptive Control, p. 10
MUSMAR	Multistep Multivariable Adaptive Regulator, p. 10
MV	Manipullated Variable, p. 36
NMPC	Nonlinear Model Predictive Control, p. 10
PCT	Perceptual Control Theory, p. 12
PDE	Partial Differential Equation, p. 29
PFC	Predictive Functional Control, p. 10
PID	Proportional, Integral and Derivative, p. 6
PLC	Programmable Logic Controller, p. 33
QDMC	Quadratic Dynamic Matrix Control, p. 9
QP	Quadratic Program, p. 12
RHC	Receding Horizon Control, p. 8
RTO	Real-time Optimization, p. 6
SAC	Scheduled Adaptive Control, p. 22
SEPTIC	Statoil Estimation and Prediction Tool for Identification and Control, p. 33
SKF	Scheduled Kalman Filter, p. 47
SMOC	Shell Multivariable Optimizing Control, p. 12
SSE	Sum of the Squared Errors, p. 51
STAC	Self-tuning Adaptive Controller, p. 24
UKF	Unscented Kalman Filter, p. 25
UPC	Unified Predictive Control, p. 10
VSD	Variable Speed Driver, p. 28

Chapter 1

Introduction

Artificial lift is a terminology employed for a group of technologies applied to an oil production well whenever the reservoir does not present enough pressure to naturally drive the oil up to the surface with an economical feasible flow rate, usually between 10 to 15 mbopd in deepwater wells (BRUHN *et al.*, 2003). It can be used in the early project phase of the oil field, but also in the end of the field life to boost production. The types of artificial lift to be applied in a well depend on several factors, such as oil viscosity, well and reservoir depth, gas-oil ratio, safety and so on. In a subsea context, with ultra deepwater reservoir, the most common artificial lift techniques are (THOMAS, 2001):

- Continuous gas-lift;
- Intermittent gas-lift;
- Electrical Submersible Pump (ESP).

Gas-lift technology makes use of the energy content of a compressed gas to lift the oil from the reservoir up to the surface. There are two operational modes, the continuous one has the aim to gasify the oil while the intermittent one has the aim to push it from a certain depth to the surface. It is common to have several valves along the gas-lift column to play the role of discharge and operation, in order to ease the damping fluid removal and the gas injection in different depths, respectively. Usually, gas-lift is an interesting technology to be applied for oils with high sand content and high gas-oil ratio, it can be used for very deep wells (up to 2,600 m) obtaining high flow rate (up to 1,700 m^3/d) with a relatively low implementation cost (THOMAS, 2001).

Electric Submersible Pumps consist of multi-stage centrifugal pumps installed in a subsea environment, far from the surface between hundreds to thousands of meters below the surface. The pressure boost provided by the ESP enables the fluid flow to the surface with the desired flow rate. Each stage of the pump

is composed of an impeller-diffuser group. The impeller is responsible for the transfer of the energy to the fluid as pressure and kinetic energy, while the diffuser converts part of the kinetic energy in more pressure (VARÓN *et al.*, 2013).

For a long time, production from subsea wells has been carried out by natural lift or by using artificial lifting methods such as gas-lift or water injection in the reservoir, which is not efficient due to unfavorable mobility difference between oil and water phases (PINTO *et al.*, 2003). However, these methods present low efficiency and they are not always feasible (MENDONÇA *et al.*, 2008). Petrobras discovered very important deepwater oil reservoirs in the 80's. However, the long distances, increase of BSW and loss of efficiency of the gas-lift in horizontal flowlines have motivated the company to invest in alternatives artificial lift technologies. That led Petrobras to install the world's first ESP in a subsea well in 1994. The well was located in a shallow waters region of the Campos Basin and it operated over almost 3 years until its first failure. Four years later, in 1998, the success of this prototype has stimulated the company to proceed with the world's first ESP installation in a deep waters of the Campos Basin (MENDONÇA *et al.*, 2008).

The use of ESP proved to be very efficient considering the high flow rates and the capability to deal with longer distances between well and platform. It is also able to increase the well lifetime in 1 to 2 years (MENDONÇA *et al.*, 2008). These are some of reasons that made the ESP to be the most applied artificial lift technology worldwide in deep waters (PAVLOV *et al.*, 2014). It is impossible to recognize the developments that the ESP technology has archived to the world's oil production without mentioning the pioneering role of Petrobras. The company has also been responsible for the largest subsea ESP project in the world, counting with 15 installed ESPs in the Jubarte field (HARRIS *et al.*, 2012).

The manual operation of the ESP consists in adjusting the pump rotational speed by means of a variable frequency drive in combination with the adjustment of the choke valve opening located on top of the well that feeds the manifold. The pump speed and well head choke valve must be adjusted in a coordinated manner such that the pump and well constraints are not violated. Failure to do so may lead to reduced operational efficiency and reduced lifetime of the pump, resulting in significant financial losses. Hence, the operation of an ESP is constrained by variables physical and safety limits (PAVLOV *et al.*, 2014).

For the aforementioned reasons, an automatic control of the ESP operation is desired in order to ensure safe and optimal operation of the ESP lifted well (PAVLOV *et al.*, 2014). Therefore, we consider the use of model predictive control (MPC) strategy, which is known to explicitly handle multivariable systems with constraints and optimize the operation (CAMACHO and BORDONS, 2007). Several predictive control approaches can be found depending on the control ob-

jectives of the specific application. For example, BINDER *et al.* (2014) prioritized keeping a constraint on the electric current, and the ESP inlet pressure within certain constraints. PAVLOV *et al.* (2014) focused on implementing a setpoint tracking for ESP intake pressure with minimization of ESP power. KRISHNAMOORTHY *et al.* (2016) controlled the ESP intake pressure to a desired setpoint while keeping the production choke as open as possible, in order to minimize the energy losses across it. In addiction, BINDER *et al.* (2015) developed a soft-sensor to estimate the viscosity and the well productivity index based on data measurements using a Moving Horizon Estimation technique. However, to this date, there are no records of adaptive strategies to handle the ESP system's nonlinearities, or estimate strategies coupled with MPC in order to overcome possible loss of measurement and parameter estimation. Therefore, the present work proposes the development of an adaptive MPC coupled with a Kalman filter strategy to simultaneously estimate the state variables and the fluid viscosity based on the output measurements for a scenario of loss of measurement of the state variables and the presence of the uncertain parameter.

1.1 Motivation

As previously said, ESP is one of the most common technologies for artificial oil lift. In spite of that, installation, maintenance, operation and cost of failure result in a multimillion-dollar investment. Therefore, it is very interesting to minimize the risk of economic loss, due to any intervention resulting in a major amount of money.

In the operation of a well production with an ESP, there are several parameters that have to be monitored. The manual operation, within safe limits and keeping stability, is hard, but can be done in spite of the difficulty. However, optimal operation is usually very close to these limits and manual strategies can result in constant violation of process constraints. The violation of these limits must be avoided because it can result in premature failure and reduce ESP life-time what, as has been said, result in a multimillion-dollar loss, specially if the loss of not being producing is taken into account.

In addition, PAVLOV *et al.* (2014) highlight the fact that 80% of the failures in the beginning of the ESP production is resulted from human factors. Therefore, an automatic system capable of dealing with process constrains and guaranteeing optimal and stable operation must be considered.

1.2 Objectives

The general objective of this work is to develop a robust control system capable of dealing with process nonlinearities, absence of state measurements and the presence of uncertain parameters to an Electric Submersible Pump system.

To accomplish this broad general objective, it was subdivided into specific three ones, they are:

(i) Develop a linear adaptive MPC capable of scheduling its internal model in order to present a better performance over the operational range.

(ii) Develop a linear adaptive MPC coupled with a Kalman filter strategy, using the same internal model scheduling strategy, capable of accurately estimating the state and presenting a satisfactory performance over the operational range.

(iii) Expand the adaptive strategy to enable accurate parameter estimation during the MPC operation.

1.3 Structure

Chapter 2 presents a brief Literature and Theory review over the main subjects related to the objectives of this dissertation. It starts with a contextualization of the control hierarchical structure, followed by a deep review over the fundamentals of MPC in Section 2.2, presenting the two main algorithms formulations and a discussion about robustness and stability. In addiction, Section 2.3 presents the main strategies of adaptive control and Section 2.4 presents the basis of Kalman filter, the precursor of the state estimation techniques. Finally, Section 2.5 formulates the nonlinear dynamic model that describes the ESP system studied and presents the main literature works that have been published.

Chapter 3 is a case study accomplishing the first specific objective of the present work, it is composed by an Introduction, Methodology, Results and Discussion and Conclusions sections. This chapter was published and presented in the Oil&Gas invited session in 12th IFAC Symposium on Dynamics and Control of Process Systems, including Biosystems (DYCOPS 2019).

Chapter 4 is a case study accomplishing the second specific objective of the present work, it is composed by an Introduction, Methodology, Results and Discussion and Conclusions sections. This chapter was presented in a poster session of the 1st Brazilian Process System Engineering (PSE-BR 2019).

Chapter 5 presents the full methodology developed in this work, accomplishing the third specific objective and, therefore, the general objective proposed.

Chapter 6 makes a brief summary of the developments carried out in the work, some proposes of futures works are outlined and it concludes the dissertation.

Finally, Appendix A presents the linearization strategy used and Appendix B presents the State-Space formulation of the linear MPC considering the feedthrough matrix, a formulation not easily found in literature and that was deducted for this work due to case study requirement.

Chapter 2

Literature and Theory Review

2.1 Control Hierarchical Structure

The control structure is usually organized in a hierarchical multilayer structure. Each layer is interconnected, receiving information from the layer immediately above, processing this information based on the strategy for what it serves in a predetermined time scale and send a set of actions for the immediately bellow layer. Figure 2.1 illustrates the control structure.

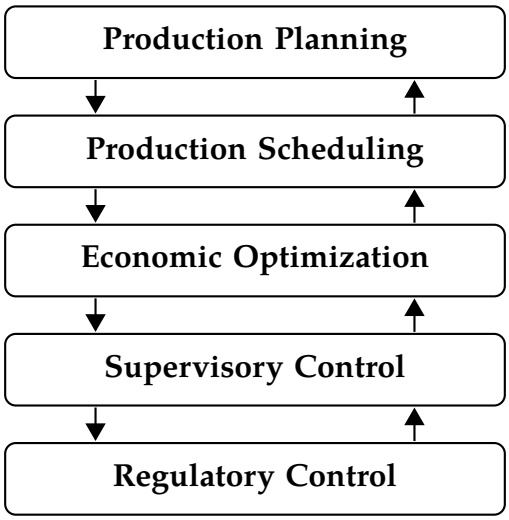

Figure 2.1: Hierarchical representation of the control structure.

In the operational level, there are three main layers: optimization, supervisory control and regulatory control. The common strategies used in each layer are RTO (real-time optimization), MPC and PID (proportional, integral and derivative) controllers, respectively.

The regulatory layer is responsible for maintaining the stability of the system actuating on the variables exposed to high frequency disturbances in the minor time scale of the control structure. It usually makes use of PID controller, but this

is not a rule, this responsibility can be fulfilled by a robust MPC as well, uniting the regulatory and supervisory layers in only one scheme (SHA'ABAN, 2015).

The supervisory layer makes use of advanced control algorithms, usually model based, in order to determine, under pre-established criteria, the best trajectory aiming to maintain or drive the system to the optimum steady state obtained by the optimization layer. MPC and its variations are the most widespread strategies to comply with the supervisory layer, they make use of a dynamic model of the system in order to determine the optimum trajectory by minimizing a quadratic cost function that penalizes the deviation between the controlled variables and its reference steady state taking constrains into account.

The optimization layer uses RTO strategy in order to obtain the optimum steady state of the system, considering economic and operational aspects. It makes use of a robust, usually nonlinear, static model of the plant to minimize an economical cost function.

The aforementioned hierarchical structure is a vertical one, some author discuss whether it is the best strategy or not. MARCHETTI *et al.* (2009a) highlight its main drawback as being the long sampling time of the optimization layer, which could delay the system optimum steady state determination under disturbances, leading to long periods of sub-optimum operation.

ELLIS *et al.* (2014) also point out that steady-state operations may not be the best economic strategy, suggesting that for some applications a dynamic operation could result in a faster and more efficient control.

Other authors focus on different approaches for control structures. For instance, adaptive control can be interpreted as a horizontal approach for update parameters of the vertical control structure. DARBY *et al.* (2011) make a profound review on RTO current practices where the control structure strategy is deeply discussed. MARCHETTI *et al.* (2009b) presents the recent advances in modifier-adaptation schemes for RTO of processes under uncertainties.

PRIOR and LOPEZ (1999) report a simplified RTO structure based on modules, in which each module is triggered on different time instants and send setpoints for multiple MPCs. They report a gain on RTO agility. GRACIANO *et al.* (2015) make use of a self-optimizing control approach, the main idea was to add a sensibility step to the RTO steps in order to identify the self-optimizing variables and only these variables are sent to the MPC layer. The idea is that the control of the self-optimizing variables would maintain the system close to its optimum operation until a new RTO cycle is done.

2.2 Model Predictive Control (MPC)

2.2.1 Introduction

Model predictive control or receding horizon control (RHC) is an on-line optimization based strategy used for large-scale multi-input, multi-output (MIMO) systems with a great capacity to deal with cross-linked coupled systems and process constraints that has been in development since the 70's. For that and other benefits, that MPC is widely accepted in the process industry (FORBES *et al.*, 2015).

There are many variations of MPCs algorithms, but in general terms all of them are based on the minimization of a performance index along a prediction horizon subjected to a process model and taking process constraints into account in order to calculate the control action (ELLIS *et al.*, 2014). The optimization is carried out every process sampling time and uses the actual measurement, or estimation when they are not available, of the system as the initial condition for the optimization procedure. The outputs are the optimal trajectory for the controlled variables over the prediction horizon, L, and the series of control actions for the manipulated variables that would drive the system to its optimal trajectory over the control horizon, N. From the series of control actions obtained, only the first one is applied to the system and the algorithm is repeated in the next sampling time (MACIEJOWSKI, 2002).

In the following, the three main aspects of the MPC will be discussed, they are: the cost function, the prediction model and the process constraints.

There are several variations for the cost index, which ultimately determines the main goal of the control strategy. The general aim is a setpoint tracking strategy, in which a multi-objective formulation that penalizes the quadratic deviation between the controlled variables, y, and the reference trajectory, y_{rt}, (CAMACHO and BORDONS, 2007):

$$J_{MPC} = \sum_{i=1}^{L} \left\| y_{k+i} - y_{k+i}^{rt} \right\|_{W_y}^2 + \sum_{i=1}^{N-1} \left[\left\| u_{k+i} - u_{k+i}^{t} \right\|_{W_u}^2 + \left\| \Delta u_{k+i} \right\|_{W_{\Delta u}}^2 \right] \tag{2.1}$$

in which W_y, W_u and $W_{\Delta u}$ are positive semi-definite weighting matrices which are tuning parameters that determine the degree of priority or suppression of respective variables. Also, the weighted 2-norm $\|x\|_Q^2$ is defined as $x^T Q x$.

One can also notice that the aforementioned formulation counts with the penalization of the deviation between the manipulated variables, u, and the targets, u^t, and the variation of the manipulated variables, Δu. Both of these effects can be prioritized or suppressed by the weight matrices settled elements values. It

is noteworthy that the first effect is responsible by the degree of freedom of the control while the second is responsible for the control effort and, therefore, the aggressiveness of the tuning (CAMACHO and BORDONS, 2007).

The prediction model is dynamic and usually linear. It has to be the most accurate possible, but also simple enough to minimize computational effort (FORBES *et al.*, 2015). Its form defines the solving algorithm of the strategy to be applied and there are algorithms for basically every forms of model (CAMACHO and BORDONS, 2007; QIN and BADWELL, 1997):

- **Impulse response models:** can be found in algorithms such as IDCOM and MAC. Some applications can be found in literature references (GROSDIDIER *et al.*, 1993; GROSDIDIER and KENNEDY, 1990; HEIRUNG *et al.*, 2015; KWONG, 2000). The model representation can be visualized as follows:

$$y(k) = \sum_{j=1}^{N} h_j u(k-j) \tag{2.2}$$

  in which, h_j is the sampled output when the process is disturbed by an unitary impulse, y is the output and u is the input;

- **Step response models:** can be found in algorithms such as DMC and QDMC. Recent applications can be found in literature references (CZERWIŃSKI and ŁAWRYŃCZUK, 2018; IANCU *et al.*, 2013; JORDANOU *et al.*, 2018; KLOPOT *et al.*, 2018; LI *et al.*, 2012; MOON *et al.*, 2018; NIVA and YLIKORPELA, 2012; WOJTULEWICZ and ŁAWRYŃCZUK, 2018). The model representation can be visualized as follows:

$$y(k) = y_0 + \sum_{i=1}^{N} g_i \Delta u(k-i) \tag{2.3}$$

  in which, g_i are the i^{th} sampled output values when the process is disturbed by a unitary step and Δu is the incremental input.

- **State Space models:** can be found in algorithms such as PFC and SMOC. Recent applications can be found in literature references (ABDULLAH *et al.*, 2017; ANZEHAEE *et al.*, 2018; CAMPETELLI *et al.*, 2010; NAMARA *et al.*, 2016; RAMDANI *et al.*, 2016; ZABET and HABER, 2017). The model repre-

sentation can be visualized as follows:

$$\begin{aligned} x(k) &= Ax(k-1) + Bu(k-1) \\ y(k) &= Cx(k) + Du(k) \end{aligned} \tag{2.4}$$

- **Transfer function models:** can be found in algorithms such as GPC, UPC, EPSAC, EHAC, MUSMAR and MURHAC. Recent applications can be found in literature references (CASTANO *et al.*, 2014, 2015; HODREA *et al.*, 2012; LIU *et al.*, 2017; SALAHSHOOR and KORDESTANI, 2014; SHI *et al.*, 2014; TRAN *et al.*, 2014). The model representation can be visualized as follows:

$$y(k) = G(z^{-1})u(k) \tag{2.5}$$

in which,

$$G(z^{-1}) = \frac{B(z^{-1})}{A(z^{-1})} = \frac{b_1 z^{-1} + b_2 z^{-2} + \cdots + b_{nb} z^{-nb}}{1 + a_1 z^{-1} + a_2 z^{-2} + \cdots + a_{na} z^{-na}} \tag{2.6}$$

- **Other input-output models:** other types of input-output models can be found in MPC combined with a system identification, such as ARX (DAHLIN *et al.*, 2018; DELOU; DEMUNER; SECCHI, 2018; ZHANG *et al.*, 2018a), ARMAX (DI CAPACI *et al.*, 2018; PASCHKE and ZAICZEK, 2018; YAN and ZHU, 2018).

- **Nonlinear models:** can be found in applications of NMPC by the use of nonlinear programing optimization strategies. Recent applications can be found in literature references (DIEHL *et al.*, 2018; KHUSAINOV *et al.*, 2018; PUSCHKE and MITSOS, 2018). A noteworthy application is neural network (MAO *et al.*, 2018; SADEGHASSADI *et al.*, 2018; STOGIANNOS *et al.*, 2018), which is an example of a nonlinear input-output model.

The last aspect of the MPC problem is the great efficiency on handling process constraints, which is one of the aspect of this technique that cannot be done by classic controllers such as PID (FORBES *et al.*, 2015). They are typically operational limit values such as valve openings, instrumentation calibrated range, safety bounds, and so on. However, physical constraints such as irreversibility of flows, species fraction bounds, etc. can also be imposed (CAMACHO and BORDONS, 2007).

To summarize, the MPC optimization problem can be reduced in a generalized manner to the following set of equations:

$$\begin{aligned} \min_{\Delta u} \quad & J_{MPC}(x(k), u(k)) \\ \text{s.t.} \quad & x(k) = f(x(k), u(k)) \\ & x(0) = x_0 \\ & g(x(k), u(k)) \leq 0, \quad \forall i \in [0, L) \end{aligned} \tag{2.7}$$

in which represents the minimization of a cost index subjected to a process model, with respect to the initial condition and the process constraints over a prediction horizon L.

2.2.2 Brief History of MPC

Three remarkable papers have been done about the evolution of MPC theory and applications in industry. The first one dates back to the 90's and the last almost 15 years later (LEE, 2011; QIN and BADWELL, 1997, 2003).

It is reported that the concepts of control modern theory were developed in the 60's by early work of Professor R. E. Kalman (1930 - 2016), in which he aimed to determine the conditions that a linear control system could be told to be optimal (KALMAN, 1960a,b). Although the early work, the first MPC applications were only reported in 1976 with the name of model predictive heuristic control (MPHC). Its algorithm used an impulse response model, a quadratic cost function over a finite prediction horizon, input and output constraints and optimal inputs are computed by heuristic iterations. It was named IDCOM (an acronym for Identification and Command) (RICHALET *et al.*, 1978). Later on, in 1979, a team of engineers at Shell Oil reported the first application of an unconstrained multivariable control known as dynamic matrix control (DMC), a development that had been on going since early 1970's (CUTLER and RAMAKER, 1980). The DMC algorithm considers a linear step response model for the system, a quadratic cost function over a finite prediction horizon and optimal inputs are computed by the solution of a least-squares problem. Both IDCOM and DMC are consider the first generation of MPC technology, in spite of their limitations they had caused a tremendous advance in process control field.

The constraints handling feature was only mastered by the development of QDMC. In which the DMC algorithm is adapted to fit in a quadratic program (QP) where constraints are explicit (GARCIA and MORSHEDI, 1986). The algorithm also considers a step response model for the system, a quadratic cost function over a finite prediction horizon and optimal inputs are computed as the solution to a

constrained QP. The second generation of MPC technology, which QDMC is part of, has the mark of rigorous constraints handling by placing the MPC problem in standard QP solvers.

Generalized predictive control rised by the adaptive control community as an attempt of dealing with the robustness problem that DMC was not able to deal. It was first reported in 1987 and the main feature was the use of transfer function as the system model (CLARKE *et al.*, 1987a,b). Despite its advantages on self-tuning regulator and robustness, the lack of efficiency on constraints handling was the main reason for the weak development of GPC.

The third generation of MPC algorithms are equipped with some peripheral resources, such as the concept of hard, soft and ranked constraints, mechanisms to deal with infeasible solution and strategies for dealing with real-time changes in the process. One of the first algorithms reported in this context was the Shell multivariable optimizing control (SMOC). It can use state-space internal models, general disturbances models and state estimators such as Kalman filter (MARQUIS and BROUSTAIL, 1988). Across the years, many other algorithms have been proposed, such as IDCOM-M (GROSDIDIER *et al.*, 1988), HIECON (RICHALET, 1993) and PCT (RICHALET *et al.*, 1987).

2.2.3 QDMC fundamentals

The quadratic dynamic matrix control proposed by GARCIA and MORSHEDI (1986) is an extension of the dynamic matrix control proposed by CUTLER and RAMAKER (1980) where the DMC formulation is fitted to a constrained QP problem. The QP structure can be visualized as follows:

$$\begin{aligned} \min \quad & \tfrac{1}{2}x^T Hx + c^T x \\ \text{s.t.} \quad & Ax \leq b \end{aligned} \tag{2.8}$$

in which H is a symmetric matrix of dimension $n \times n$, c is a vector of dimension n, A is a matrix of dimension $m \times n$ and b is a vector of dimension m. The fundamental of QDMC is to manipulate DMC matrices to fit into H, c, A and b from the QP and use known solvers to find the control law. Therefore, this section is dedicated to outline main aspects of the DMC matrices and how they are manipulated to generate the QDMC formulation based on CAMACHO and BORDONS (2007) and CUTLER and RAMAKER (1980).

DMC is based on a step response model, for a MIMO system it can be written

in the form of summations as:

$$y_j(t) = \sum_{k=1}^{m} \sum_{i=1}^{N} g_i^{kj} u^k(t-i) \tag{2.9}$$

in which g_i^{kj} is the step response coefficient of output j and input k. This notation considers that the processes is asymptotically stable and, therefore, it reaches a constant value after N sampling periods. In the matrix form:

$$y = \tilde{y} + G\Delta u + f \tag{2.10}$$

In which G is the dynamic matrix of dimension $(Lp) \times (Nm)$, y is the vector of predicted outputs of dimension (Lp), $\tilde{y}$ is the vector of predicted outputs regardless the control actions of dimension (Lp), u is the vector of future control actions of dimension (Nm) and f is the vector of the free response of dimension (Lp), which is the future control actions. Any feed-forward effect that might have any interest to detect can be written as measured disturbances adding another term in the Equation as $S\Delta d$. In which S is the matrix of step coefficients of the disturbances and Δd is the vector of variation of the disturbances. However, this discussion is not included in the present formulation. The predicted outputs and future control action vectors can be written based on the superposition principle due to model linearity as follows:

$$y = \left[y_1(t+1|t), ..., y_p(t+1|t), ..., y_1(t+L|t), ..., y_p(t+L|t)\right]^T \tag{2.11}$$

$$y = \left[\Delta u_1(t), ..., \Delta u_m(t), ..., \Delta u_1(t+N-1), ..., \Delta u_m(t+N-1)\right]^T \tag{2.12}$$

The free response is written as follows:

$$f = \left[f(t+1|t), ..., f_p(t+1|t), ..., f(t+L|t), ..., f_p(t+L|t)\right]^T \tag{2.13}$$

Finally, the MIMO dynamic matrix is as follows:

$$G = \begin{bmatrix} G_1 & 0_{m\times p} & ... & 0_{m\times p} \\ G_2 & G_1 & ... & 0_{m\times p} \\ \vdots & \vdots & \ddots & \vdots \\ G_L & G_{L-1} & ... & G_{L-N+1} \end{bmatrix} \tag{2.14}$$

In the DMC formulation, the free response is chosen to be the error between the initial prediction in the instant t and the actual measured controlled variable. This error is assumed to be constant along the prediction horizon.

$$f = \left[y_1^1(t) - \tilde{y}_1^0(t), ..., y_p^1(t) - \tilde{y}_p^0(t), ..., y_1^L(t) - \tilde{y}_1^0(t), ..., y_p^L(t) - \tilde{y}_p^0(t) \right]^T \tag{2.15}$$

So, the prediction outputs Equation can be written as:

$$\begin{bmatrix} y_1(t+1|t) \\ \vdots \\ y_p(t+1|t) \\ \vdots \\ y_1(t+L|t) \\ \vdots \\ y_p(t+L|t) \end{bmatrix} = \begin{bmatrix} \tilde{y}_1^1(t) \\ \vdots \\ \tilde{y}_p^1(t) \\ \vdots \\ \tilde{y}_1^L(t) \\ \vdots \\ \tilde{y}_p^L(t) \end{bmatrix} + \begin{bmatrix} G_1 & 0_{m\times p} & ... & 0_{m\times p} \\ G_2 & G_1 & ... & 0_{m\times p} \\ \vdots & \vdots & \ddots & \vdots \\ G_L & G_{L-1} & ... & G_{L-N+1} \end{bmatrix} \begin{bmatrix} \Delta u_1(t) \\ \vdots \\ \Delta u_m(t) \\ \vdots \\ \Delta u_1(t+N-1) \\ \vdots \\ \Delta u_m(t+N-1) \end{bmatrix} + \begin{bmatrix} y_1^1(t) - \tilde{y}_1^0(t) \\ \vdots \\ y_p^1(t) - \tilde{y}_p^0(t) \\ \vdots \\ y_1^L(t) - \tilde{y}_1^0(t) \\ \vdots \\ y_p^L(t) - \tilde{y}_p^0(t) \end{bmatrix} \tag{2.16}$$

Defining the vector of output references:

$$y^{rt} = \left[y_1^{rt}(t+1|t), ..., y_p^{rt}(t+1|t), ..., y_1^{rt}(t+L|t), ..., y_p^{rt}(t+L|t) \right]^T \tag{2.17}$$

Subtracting Equation 2.16 from 2.17 we have:

$$y^{rt} - y = y^{rt} - \tilde{y} - G\Delta u - f \tag{2.18}$$

Defining the errors vectors:

$$e = y^{rt} - y \tag{2.19}$$

$$\tilde{e} = y^{rt} - \tilde{y} - f \tag{2.20}$$

Therefore, Equation 2.18 can be written as:

$$e = \tilde{e} - G\Delta u \tag{2.21}$$

Regarding the above development and definitions, it is possible to write the cost function of the MPC optimization problem for DMC, based on Equation 2.1, as follows:

$$J_{QDMC} = \Delta u^T \left(G^T W_y G + W_u \right) \Delta u - 2\tilde{e}^T W_y G \Delta u + \tilde{e}^T W_y \tilde{e} \tag{2.22}$$

The last term of Equation 2.22 can be suppressed since it has no dependence on the decision variables, it just plays a displacement role that can be neglected. That said, it is possible to fit matrices H and c from Equation 2.8 in terms of Equation 2.22:

$$\begin{aligned} H &= G^T W_y G + W_y \\ c^T &= -2\tilde{e}^T W_y G \end{aligned} \tag{2.23}$$

The constrained MPC considers upper and lower bounds for the variation of

control actions, the control actions themselves and the controlled variables.

$$\begin{aligned} \Delta u^{lb} &\leq \Delta u(t) \leq \Delta u^{ub} \\ u^{lb} &\leq u(t) \leq u^{ub} \\ y^{lb} &\leq y(t) \leq y^{ub} \end{aligned} \tag{2.24}$$

With the proper mathematical handling, it is possible to fit the constraints into matrices A and b from Equation 2.8 as follows:

$$A = \begin{bmatrix} \tilde{I} \\ -\tilde{I} \\ \tilde{N} \\ -\tilde{N} \\ G \\ -G \end{bmatrix}, \; b = \begin{bmatrix} \Delta u^{lb} \\ \Delta u^{ub} \\ u^{ub} - u(t-1) \\ u(t-1) - u^{lb} \\ y^{ub} - \tilde{y} - f \\ \tilde{y} + f - y^{lb} \end{bmatrix} \tag{2.25}$$

The previous considerations summarize the fundamentals of QDMC approach; with them, it is possible to understand the basics of the algorithms. However, a robust MPC algorithm has to deal with several other issues regarding an operation of a complex nonlinear system, such as coping with infeasible solutions, nonlinear changes of operational point, stability of the controller, uncertainty of measurements, model and plant mismatch and so on. Therefore, the next sections are dedicated to discuss some of the issues regarding the use of a linear MPC-based controller to operate a nonlinear complex system.

2.2.4 State-space MPC

Even though finite impulse response (FIR) and finite step response (FSR) formulations were most used in the 90's (MACIEJOWSKI, 2002), there is a modern trend for state-space formulations (DARBY *et al.*, 2011). It presents an inherent flexibility to represent stable, unstable and integrating systems, also to account model unmeasured disturbances and a natural coupling with Kalman filter based estimators (DARBY *et al.*, 2011).

There are several references about state-space formulations in literature, most relevant and enlightening ones can be found in PEREZ (2012), RAWLINGS AND MAYNE (2009) and WANG (2009). These references and most formulations available do not consider the feedthrough matrix, D, in the augmented model supported in the fact that due to the receding horizon principle, a current entrance does not affect an output measurement instantly (WANG, 2009). Although this as-

sumption finds applications for most studied systems, the present work presents a case in which the feed-thorough matrix is needed, therefore we present a detailed algorithm in Appendix B.

2.2.5 Stability and Robustness of MPC

The MPC stability has always been a relevant topic for both industrial and academic communities. The fact that an infinite horizon controller is not feasible to be implemented on computer application and, therefore, a finite horizon strategy has to be done, results in the lack of guarantee of stability. In spite of that, industrial community has not given proper attention to this issue, as long as most applications were stabilized by a sufficiently large horizon and proper tuning (MAYNE, 2014). It was in 2000 that MAYNE *et al.* (2000) published a remarkable review summarizing the latest conclusions on MPC stability based on Lyapunov theory. This work has stated that "*Research on stability of model predictive controlled systems has now reached a relatively mature stage.*" (MAYNE *et al.*, 2000).

Although the main aspects of MPC stability for deterministic systems were well established by 2000, the uncertain systems remain a major field to be exploited even in the present days (MAYNE, 2014). Therefore, the next subsections are dedicated to outline the main advances and literature in respect to stability and robustness for deterministic and uncertain systems based on (MAYNE *et al.*, 2000) and (MAYNE, 2014).

Deterministic systems

Here, some formal notations are required in order to facilitate the statement of the main concepts. Let the controlled deterministic, non-linear, discrete-time system be represented by:

$$\begin{aligned} x^+ &= f(x,u) \\ y &= h(x) \end{aligned} \tag{2.26}$$

in which, f is defined by the origination differential set of equations such that $\mathbb{R}^n \times \mathbb{R}^m \rightarrow \mathbb{R}^n$; x^+ is the successor state usually denoted by $x(k+1)$ and y is the output such that $y \in \mathbb{R}^p$. The state and control constraints are to be satisfied, they are represented by $x \in \mathbb{X}$ and $u \in \mathbb{U}$ such that $\mathbb{X}$ and $\mathbb{U}$ are, respectively, a closed subset of $\mathbb{R}^n$ and a compact subset of $\mathbb{R}^m$. Let a finite horizon optimum control problem be denoted by $\mathbb{P}_N(x)$, in which it is solved at each sampling time k resulting in a control sequence denoted by $u = [u(0), u(1), \ldots, u(N-1)]$, such

that:

$$\mathbb{P}_N(x) : V_N^0(x) = \min_u \{V_N(x,u) | u \in \mathcal{U}_N(x)\} \tag{2.27}$$

in which $V_N : \mathbb{R}^n \times \mathbb{U}^N \to \mathbb{R}$ denotes the objective function such that:

$$V_N(x,u) \triangleq V_f(x^u(N;x)) + \sum_{i=0}^{N-1} \ell(x^u(i;x), u(i)) \tag{2.28}$$

and $\mathcal{U}_N(x)$ is the ensemble of possible control sequences that satisfy state, control and terminal constrains all together such that:

$$\mathcal{U}_N(x) \triangleq \{u \in \mathbb{U}^N | x^u(i;x) \in \mathbb{X}, u(i) \in \mathbb{U}, i \in \mathbb{I}_{0:N-1}, x^u(N;x) \in X_f\} \tag{2.29}$$

The feasible set for $\mathbb{P}_N$ is defined as $X_N \triangleq \{x \mid \mathcal{U}_N(x) \neq \varnothing\}$, the solution is $u^0(x) = \{u^0(0;x), u^0(1;x), \ldots, u^0(N-1;x)\}$ and the optimal state sequence is $x^0(x)$. Just the first control action, known as control law, is applied to the system, what characterizes the receding horizon strategy:

$$\kappa_N(x) \triangleq u^0(0;x) \tag{2.30}$$

MAYNE *et al.* (2000) establishes recursively feasibility and stability by the use of a terminal cost $V_f(\cdot)$ and a terminal state constraint set $X_f(\cdot)$. Their use leads to the property that any $x \in X_f \subset \mathbb{X}$ has an associated $u \in \mathbb{U}$ such that $V_f(f(x,u)) \leq V_f(x) - \ell(x,u)$ and $f(x,u) \in X_f$ Therefore, for any $N \in \mathbb{I}_{\geq 0}$, any $x \in X_N$:

$$V_N^0(f(x, \kappa_N(x))) \leq V_N^0(x) - \ell(x, \kappa_N(x)) \tag{2.31}$$

$$V_{N+1}^0(x) \leq V_N^0(x) \tag{2.32}$$

In addition, the function $V_N^0(\cdot)$ satisfies the following statements:

$$V_N^0(x) \in [\alpha_1(|x|), \alpha_2(|x|)] \tag{2.33}$$

$$V_N^0(f(x, \kappa_N(x))) \leq V_N^0(x) - \alpha_1(|x|) \tag{2.34}$$

in which $\alpha_1(\cdot)$ and $\alpha_2(\cdot)$ are $\mathcal{K}_\infty$ functions. If the above considerations are true, so the origin is a stable equilibrium state for the system defined in Equation 2.26 with the region of attraction X_N, $\mathbb{P}_N$ is feasible. MAYNE *et al.* (2000), summarize the stability conditions in four axioms:

$$0 \in X_f \subset \mathbb{X}, \textit{ is closed} \tag{2.35a}$$
$$\kappa_N(x) \in \mathbb{U}, \ \forall x \in X_f \tag{2.35b}$$
$$f(x, \kappa_N(x)) \in X_f, \ \forall x \in X_f \tag{2.35c}$$
$$[\dot{V} + \ell](x, \kappa_N(x)) \leq 0, \ \forall x \in X_f \tag{2.35d}$$

in which $\dot{V}(x, \kappa_N(x)) \triangleq V(f(x, \kappa_N(x))) - V(x)$, is the change in $V(\cdot)$ as the system varies from x to $x^+ = f(x, u)$. It is noteworthy that Equation 2.35d leads to the condition that $V(\cdot)$ is a Lyapunov function for the system represented by Equation 2.26 in the surrounding of the origin. These four axioms, presented in Equation 2.35, establish the stability of the linear, constrained, nominal MPC.

Uncertain systems

According to MAYNE (2014), the topic of robustness in the presence of uncertainty is still a major challenge. Regardless if the uncertainty is in the form of disturbances, inaccurate state estimation or model error, its presence leads to a suboptimal control law resulted from the open-loop optimal control problem since feedback is required (MAYNE, 2014).

Considering that, for treating uncertain systems, the optimization problem continues to have a control sequence as decision variables, two options of strategies may arise. The fist option is to ignore the presence of uncertainty and treat the problem such as in deterministic systems, it is shown that this strategy is robustly stable under specific conditions in a small additive disturbance (MAYNE, 2014). The second option is to consider the disturbance into the system and force all the constraints to be satisfied for every possibility of disturbance sequence (MAYNE, 2014). Taking the second option more deeply, let the system be described for:

$$x^+ = f(x, u, w) \tag{2.36}$$

in which, x and u follow the same definition stated in Section 2.2.5, subjected to the same constraints, and $w \subset \mathbb{W} \in \mathbb{R}^n$ is an additive disturbance. It is required that all possible sequence of disturbance is bounded to a limited subset, $w = \{w(0), w(1), \ldots, w(N-1)\} \in \mathcal{W}_N \triangleq \mathbb{W}^N$.

To guarantee stability, the first studies have applied the Lyapunov theory, such that:

$$V_N^0(f(x, \kappa_N(x), 0)) \leq V_N^0(x) - \alpha_1(|x|) \tag{2.37}$$

$$V_N^0(f(x, \kappa_N(x), w)) \leq V_N^0(x) - \alpha_1(|x|) + \delta(x, w) \tag{2.38}$$

$$\delta(x, w) \triangleq V_N^0(f(x, \kappa_N(x), w)) - V_N^0(f(x, \kappa_N(x), 0)) \tag{2.39}$$

It is shown in KHALIL (2002) that if $\delta(x, w)$ is sufficiently small, then $V_N^0(\cdot)$ is robust, asymptotically stable and positively invariant.

Recent developments of robust MPC have shifted from the Lyapunov approach applied to deterministic systems to the input-to-state stability (ISS) concept. The function $V(\cdot)$ is said to be ISS-Lyapunov for all $x, w \in \mathbb{R}^n$ if the following sentences are satisfied:

$$V(x) \in [\alpha_1(|x|), \alpha_2(|x|)] \tag{2.40}$$

$$V(f(x, w)) - V(x) \leq -\alpha_3(|x|) + \sigma(|w|) \tag{2.41}$$

in which, $\alpha_1(\cdot)$,$\alpha_2(\cdot)$ and $\alpha_3(\cdot)$ are $\mathcal{K}_\infty$ class functions and $\sigma(\cdot)$ is a $\mathcal{K}$ class function. (MAYNE, 2014) makes a deep review of recent studies employing the ISS theory for different applications.

Basically, the stability problem for robust MPC is centred in proving that $\delta(x, w)$ is bounded by a constant (Lyapunov theory) or a class $\mathcal{K}$ function of $|w|$ (ISS theory) (MAYNE, 2014). For that, there are several strategies and a complete literature review would be unpractical, therefore, just two of them are outlined in the following.

One common choice for the cost function is the nominal one, defined bellow:

$$V(x,u) \triangleq V_f(x^{u,0}(N;x)) + \sum_{i=0}^{N-1} \ell(x^{u,0}(i;x), u(i)) \tag{2.42}$$

This strategy's recursive feasibility was firstly obtained by MARRUEDO *et al.* (2002) using a terminal set and a terminal penalty. After this study, the method was extended by GRIMM *et al.* (2007) so that terminal set is not required and then by PIN *et al.* (2009) so that the state constraint sets are computed online, rather then offline as it was done by MARRUEDO *et al.* (2002), what has increased the feasible set of solution of the optimal problem. Detailed discussion of this approach can be found in MAYNE (2014).

Other common choice is the use of a maximum cost, which turns the problem into a min-max optimal control problem, also called min-max approach:

$$V(x,u) \triangleq \max_{w} \left\{ V_f(x^{u,w}(N;x)) + \sum_{i=0}^{N-1} \ell(x^{u,w}(i;x), u(i)) \right\} \mid w \in \mathbb{W}^N \tag{2.43}$$

This approach is rather theoretical then practical due to its computational complexity MAYNE (2014).

2.3 Adaptive Control

A linear model based controller makes use of a linear approximation in order to represent the process around an operation point. However, if the process operation is required to move away from the linearization point, the controller model turns to be a poor approximation and a significant model-plant mismatch may occur. The classical control approach ignores the fact that the process may move away from the operation point and, therefore, the controller model should change so that it could better describe the new operation conditions. Any strategy that automatically changes its parameters in order to diminish model-plant mismatch is an adaptive control (OGUNNAIKE and RAY, 1994).

The difference between the various types of adaptive control strategies lay on the method of controller parameters adjustment (OGUNNAIKE and RAY, 1994). Three methods are noteworthy for their popularity, in which the first one is the focus of present work:

- Scheduled adaptive control;
- Model reference adaptive control;

- Self-tuning controller.

Scheduled adaptive control (SAC) is the main theme of interest of this work. It requires a previous knowledge of the process nonlinearities in order to identify which variables are most responsible for changes in process behaviour, so that the controller can adapt to these changes by adjusting its parameters (OGUNNAIKE and RAY, 1994). Figure 2.2 shows a diagram that illustrates a scheduled adaptive control strategy based on instant measurements of process input and output to evaluate any required adjustment. This method can be as simple as determining various gains for each operation point and run a table look-up procedure based on a set of process information or more complex such as pre-obtaining a desired set of models for each zone of operation and then schedule these models according to instant process information. Commonly, the first method is called gain scheduling, while the second one is model scheduling (OGUNNAIKE and RAY, 1994).

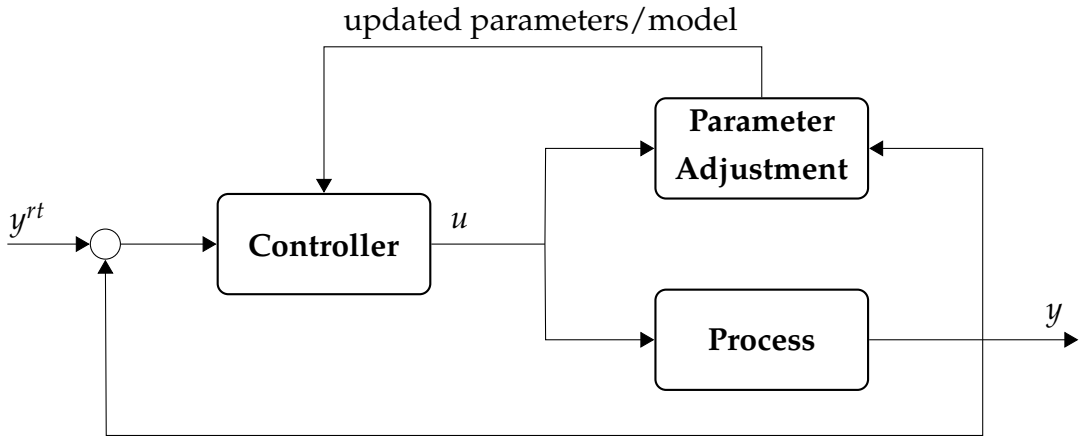

Figure 2.2: Scheduled adaptive control block diagram.

Some recent applications of scheduled adaptive control can be found in literature (FERNANDES *et al.*, 2013; GALLEGO *et al.*, 2019; JIN *et al.*, 2018; LI *et al.*, 2014, 2017; ZHANG *et al.*, 2018b).

The model reference adaptive control (MRAC) differ from the scheduled adaptive control in terms of the adaptation strategy that requires less previous knowledge about the process itself. MRAC strategy reacts to a setpoint change, or reference trajectory change, by comparing the output of a reference model with the actual output measurements so that an observed error (ε_o) is generated. The adaptation scheme would correct some controller parameters by reducing ε_o close to zero. In general, an optimization algorithm is used to minimize the integral squared value of ε_o where the decision variables are the controller parameters themselves (OGUNNAIKE and RAY, 1994). Figure 2.3 illustrates the MRAC block diagram.

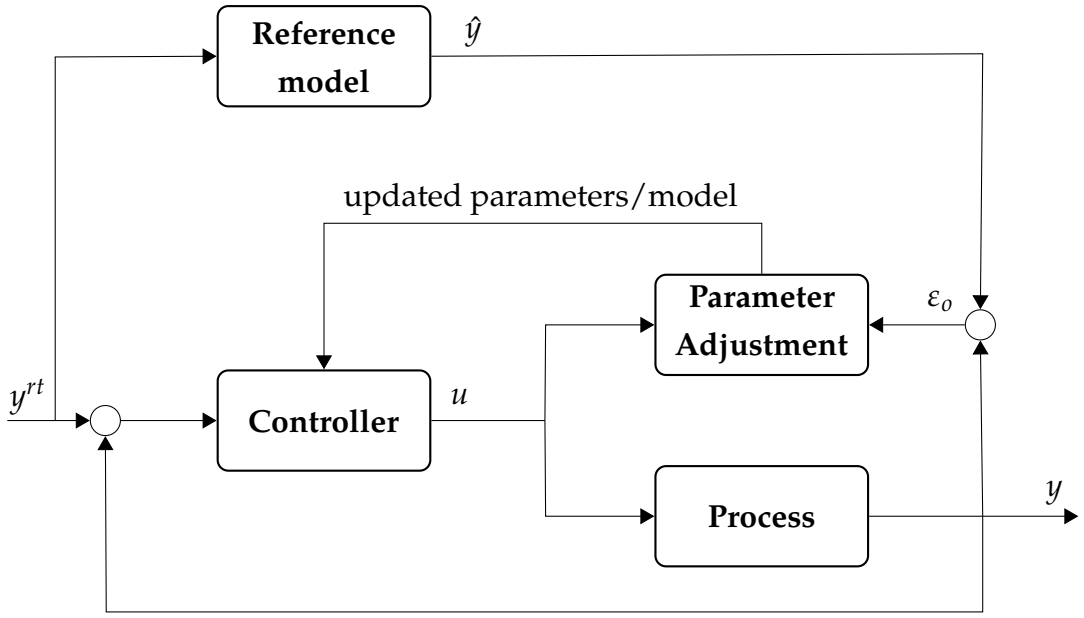

Figure 2.3: Model reference adaptive control block diagram.

MONOPOLI and HSING (1975) report a pioneer work on MRAC schemes for continuous-time MIMO systems with the effective augmented error method, a Lyapunov type design and had the stability analysed by the Meyer-Kalman-Yakubovich lemma. GOODWIN et al. (1980) developed a global stability and error convergence tracking for adaptive control of discrete-time MIMO systems.

The MRAC strategy has a sensible issue in what is related to the control law, depending on its choice it could unstabilize the system or not. One of the most widespread methods is known as "MIT rule", which is a gradient method for minimizing the quadratic error (GONÇALVES, 2017):

$$\frac{d\theta}{dt} = -\gamma\, \varepsilon_o\, \frac{\partial \varepsilon_o}{\partial x} \tag{2.44}$$

Although it has been a very used technique, PARKS and PARKS (1966) have proved that it could unstabilize various systems, including simple ones. To remedy this significant drawback, the author have proposed an alternative method based on the second Lyapunov method that, combined with the Kalman-Yakubovish-Popov Lemma (KHALIL, 2002), it is possible to achieve stability for real positive functions.

Some recent applications of MRAC can be found in literature (BRDYS *et al.*, 2002; DAS *et al.*, 2018; EL-SAMAHY and SHAMSELDIN, 2018; HAN *et al.*, 2017; MUSHIRI *et al.*, 2017; OLTEAN *et al.*, 2016; WANG *et al.*, 2018).

Self-tuning adaptive controller (STAC) makes use of both process input and output in order to estimate the parameters of an approximate linear process

model. This estimation is done every sampling period, on-line and recursively, so that every change on the actual non-linear system, which could be an operation region or even a time change, would be continuously captured by the linear model parameters update procedure. After the parameter estimation, a controller design algorithm uses the linear model so that the new controller parameters or model could be determined (OGUNNAIKE and RAY, 1994). Figure 2.4 illustrates the Self-tuning adaptive controller block diagram.

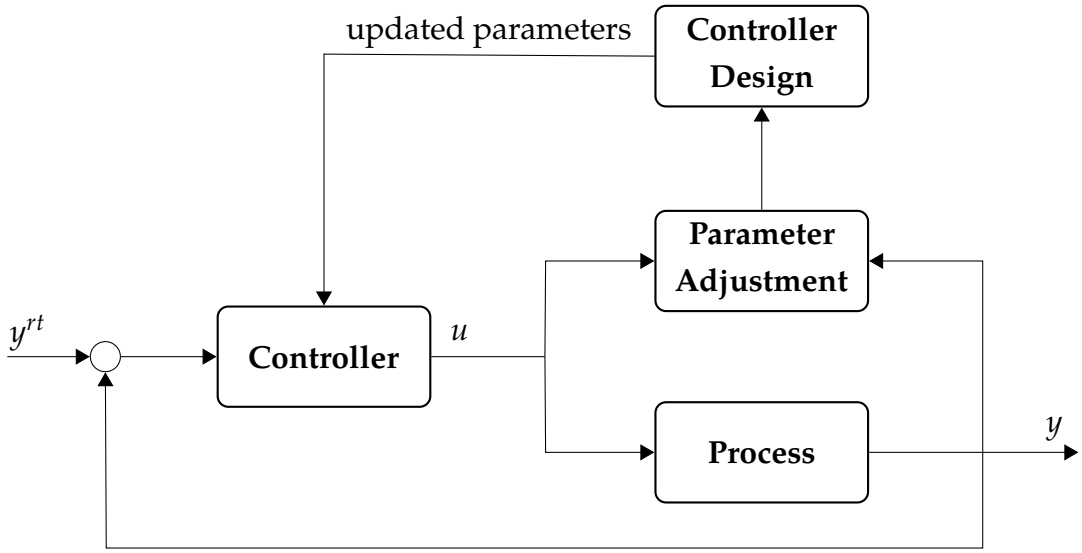

Figure 2.4: Self-tuning adaptive controller block diagram.

It is noteworthy that the STAC does not requires previous knowledge of the process, such as is primordial for scheduled adaptive control and MRAC. However, since the model estimation is the step that determines the controller performance, it is indispensable to have a robust and reliable model identification system to avoid unstable control and process runaway (OGUNNAIKE and RAY, 1994).

Some recent applications of STAC can be found in literature (ASHIDA *et al.*, 2017; BALDI *et al.*, 2018; BIDIKLI and BAYRAK, 2018; JIA *et al.*, 2015; KIM, 2015, 2017; MENDES *et al.*, 2017).

TAO (2014) points out that MRAC and STAC are the most popular adaptive control strategies, highlighting that the study of these methods has influenced each other's development. In literature, it can be noticed that STAC techniques have been applied for stochastic systems with known noise statistical proprieties while MRAC is manly used for deterministic processes with a disturbance type treatment (TAO, 2014).

2.4 State Estimation

State variables are the "minimum set of variables essential for completely describing the internal state (or condition) of a process" (OGUNNAIKE and RAY, 1994). With the information of the initial states and the sequence of entrance variables it is possible to describe the output variables of the system (GONÇALVES, 2017).

State estimation is required when the initial set of state variables is not completely known (GONÇALVES, 2017). Since the early work of KALMAN (1960a) there have been major developments of linear and nonlinear estimators. His work was based on linear systems and constitutes the basis for all posterior developments in this topic, specially when it comes to applications in nonlinear systems, in which many techniques can be found, such as: Extended Kalman filter (EKF), Constrained Kalman filter (CEKF), Moving Horizon Estimators (MHE), Unscented Kalman Filter (UKF), and others. A complete and condensed theory review over these techniques can be found in GONÇALVES (2017). In this section, some aspects of the Kalman Filter and metrics for the estimation performance evaluation are outlined based in SIMON (2006).

Consider the following discrete linear systems where the feedthrough matrix D_k is present:

$$\begin{aligned} x_k &= A_{k-1}x_{k-1} + B_{k-1}u_{k-1} + w_{k-1} \\ y_k &= C_k x_k + D_k u_k + v_k \end{aligned} \tag{2.45}$$

in which, w_k and v_k are white, zero-mean, uncorrelated with known covariance matrices Q_k and R_k:

$$\begin{aligned} w_k &\sim (0, Q_k) \\ v_k &\sim (0, R_k) \end{aligned} \tag{2.46}$$

The cornerstone of the Kalman Filter (KF) is based on the description of how the mean and covariance of the state propagate with time. To do so, two estimations are carried out, the so called *a priori* estimation and the *a posteriori* estimation. The fist is denoted by $\hat{x}^-$ and the second is denoted by $\hat{x}^+$, the superscript "^" denotes that the state is estimated. The *a priori* estimation is carried out before the use of the actual measurements of the outputs, y_k, and the *a posteriori* estimation are done with the information of the actual measurements of the outputs. Hence, when moving from an instant k to $k+1$, the *a posteriori* estimation of instant k is used as the *a priori* estimation for instant $k+1$ and so on.

Let P_k be the covariance of the estimation error, so the *a priori* and the *a posteriori* covariance of the estimation error are:

$$\begin{aligned} P_k^- &= \mathbf{E}\left[(x_k - \hat{x}_k^-)(x_k - \hat{x}_k^-)^T\right] \\ P_k^+ &= \mathbf{E}\left[(x_k - \hat{x}_k^+)(x_k - \hat{x}_k^+)^T\right] \end{aligned} \tag{2.47}$$

The *a priori* estimation consists on the time updating of the states and the covariance of the estimation error, this is done by the following expressions:

$$\hat{x}_k^- = A_{k-1}\hat{x}_{k-1}^+ + B_{k-1}u_{k-1} \tag{2.48}$$

$$\hat{P}_k^- = A_{k-1}P_{k-1}^+A_{k-1}^T + Q_{k-1} \tag{2.49}$$

It is noteworthy that the initial *a posteriori* state estimate, $\hat{x}_0^+$, and the covariance matrix, P_0^+, must be guessed to initialize the filtering procedure. That said, it is possible to state the measurement updating of the *a priori* estimation and this is the end of the filtering procedure:

$$K_k = P_k^-C_k^T(C_kP_k^-C_k^T + R_k)^{-1} \tag{2.50}$$

$$\hat{x}_k^+ = \hat{x}_k^- + K_k(y_k - C_k\hat{x}_k^- - D_ku_k) \tag{2.51}$$

$$P_k^+ = (I - K_kC_k)P_k^- \tag{2.52}$$

2.4.1 Performance Evaluation

It is straight forward that most online applications of KF do not count with the real values of the state variables, so that it could be compared with the state estimate in order to verify whether the filtering performance is reliable.

SIMON (2006) introduces a technique of evaluating the quality of the estimation by analyzing the statistics of the innovations. The innovations, r_k, are the term

that contains the information of the measurement for each instant:

$$r_k = y_k - C_k \hat{x}_k^- - D_k u_k \tag{2.53}$$

It can be showed that the innovation is a zero mean, white noise and has covariance of $(C_k P_k^- C_k^T + R_k)$. During the filter operation, the mean and covariance of the innovations can be computed and compared with their predicted values. SIMON (2006) points out that if any divergence is noted, such as colored, nonzero-mean or wrong covariance innovations, the estimate is not accurate and the most probable reason is due to model error.

2.5 The ESP System

2.5.1 Process Description

In the context of oil production with artificial lift, Electrical Submersible Pump system is one of the available technologies. It consists of multi-stage centrifugal pumps installed in a well located at the sea bed, very distant from the water surface (PAVLOV *et al.*, 2014).

The whole lift system consists of the ESP, the choke valve located at the top of the well and the production manifold. The well scheme can be visualized in Figure 2.5.

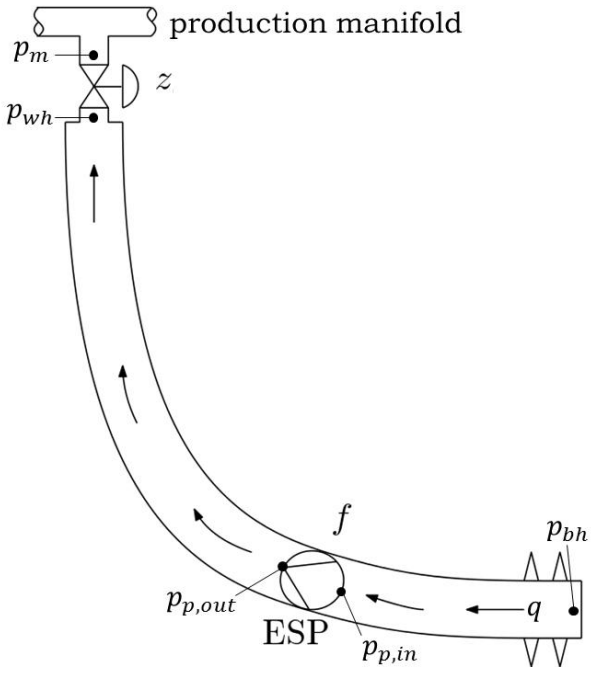

Figure 2.5: Scheme of the artificial oil lift by ESP.

The ESP is responsible for increasing the fluid pressure, so that it could be able to reach the surface with an economical feasible flow rate. In addition, most ESPs are coupled with Variable Speed Drivers (VSDs) which are responsible for driving the pump rotation, enabling the operation to be done in a broader range of conditions (PAVLOV *et al.*, 2014).

The production process is very simple: the fluid flows from the reservoir to the ESP, where its pressure is increased so it reaches the production choke valve at the top of the well. After the valve, the fluid is driven to the production manifold, where it is directed to proper destination.

2.5.2 The ESP Model

The model proposed by PAVLOV *et al.* (2014), and lately improved by BINDER *et al.* (2015), consists on a third-order nonlinear dynamic model. The main hypotheses made to build the model are:

Hypothesis 1 (H1)**.** *Pressure and flow through the system can be modelled by considering it a hydraulic transmission line with pressure loss due to friction along pipes and pressure boost due to the ESP.*

Hypothesis 2 (H2)**.** *The well Productivity Index can be considered constant although it changes along the well lifespan.*

Hypothesis 3 (H3)**.** *There is always a pressure loss across the choke valve, so backflow is not allowed.*

Hypothesis 4 (H4)**.** *The fluid pumped across the ESP is assumed to be incompressible, therefore the affinity laws presented by TAKACS (2011) are valid.*

Hypothesis 5 (H5)**.** *It is assumed that the fluid properties (i.e. density and viscosity) do not changes across the ESP, so the multi-stage pump can be treated as a number of single-stages.*

Hypothesis 6 (H6)**.** *The choice of two control volumes in the two pipes, upstream and downstream of the ESP, is enough to represent the dynamics of the system with sufficient accuracy.*

Hypothesis 7 (H7)**.** *The change of pressure with respect to time in any point of the control volume is equal to the change in average pressure.*

Hypothesis 8 (H8)**.** *The flow rate is constant through the system, which is reasonable for incompressible fluids in steady-state and slow dynamics.*

The model variables and parameters can be visualized in Tables 2.1 and 2.2, respectively.

Table 2.1: ESP Model Variables

Variables	Description	Unit
f	ESP frequency	Hz
z	Production choke valve opening	$-$
p_m	Manifold pressure	Pa
p_{wh}	Wellhead pressure	Pa
$p_{p,out}$	ESP outlet pressure	Pa
$p_{p,in}$	ESP inlet pressure	Pa
Δp_p	Pressure difference across ESP	Pa
p_{bh}	Bottom hole pressure in well	Pa
Δp_f	Frictional pressure drop in the well	Pa
F_1	Frictional pressure drop below ESP	Pa
F_2	Frictional pressure drop above ESP	Pa
q	Average flow rate in well	m^3/s
q_c	Flow rate through production choke	m^3/s
q_r	Inflow from reservoir into well	m^3/s
I	Electric current in ESP motor	A
H	Head developed by ESP	m
P	ESP brake horsepower (BHP)	W

Considering H1, the differential Equations 2.56, 2.57 and 2.58 are derived from the following PDE system:

$$\frac{A}{\beta}\frac{\partial p}{\partial t} = -\frac{\partial q}{\partial x} \tag{2.54}$$

$$\rho\frac{\partial q}{\partial t} = -A\frac{\partial p}{\partial x} + F + A\rho g\frac{dh}{dx} \tag{2.55}$$

in which $p(x,t)$ and $q(x,t)$ are the pressure and flow-rate at position x in time t along the well. A is the cross-section flow area, β is the inverse of the compressibility, ρ is the fluid density, $h(x)$ is the distance from the seabed to x and, finally, F is the pressure variation per unit of length due to friction or to the pump.

Considering H5, H6 and H7 and taking p_{bh} and p_{wh} by the average pressures of the bottom-hole and the well head, respectively, one can derive Equation 2.56

Table 2.2: ESP Model Parameters (BINDER *et al.*, 2015)

Parameter	Description	Value	Unit
g	Gravity constant	9.81	m/s^2
C_c	Choke valve constant	2×10^{-5}	$-$
A_1	Cross-section area of pipe below ESP	0.008107	m^2
A_2	Cross-section area of pipe above ESP	0.008107	m^2
D_1	Pipe diameter below ESP	0.1016	m
D_2	Pipe diameter above ESP	0.1016	m
h_1	Height from reservoir to ESP	200	m
h_w	Total vertical distance in well	1000	m
L_1	Length from reservoir to ESP	500	m
L_2	Length from ESP to choke	1200	m
V_1	Pipe volume below ESP	4.054	m^3
V_2	Pipe volume above ESP	9.729	m^3
f_0	ESP characteristics ref. freq.	60	Hz
I_{np}	ESP motor nominal current	65	A
P_{np}	ESP motor nominal power	1.625×10^5	W
β_1	Bulk modulus below ESP	1.5×10^9	Pa
β_2	Bulk modulus above ESP	1.5×10^9	Pa
M	Fluid inertia parameter	1.992×10^8	kg/m^4
ρ	Density of produced fluid	950	kg/m^3
p_r	Reservoir pressure	1.26×10^7	Pa
PI	Well productivity index	2.32×10^9	$m^3/s/Pa$
μ	Viscosity of produced fluid	0.025	$Pa \times s$

and Equation 2.57 from 2.54. I addition, considering H5, H6 and H8, Equation 2.58 arises from the momentum balance of Equation 2.55, in which $\rho g h_w$ is the hydrostatic pressure difference between well head and bottom, Δp_f is the pressure loss due to friction and Δp_p is the pressure boost due to the ESP.

Therefore, the model is composed by a set of differential-algebraic Equation system. The differential equations can be visualized in the following:

$$\frac{dp_{bh}}{dt} = \frac{1}{V_1}(q_r - q)\beta_1 \tag{2.56}$$

$$\frac{dp_{wh}}{dt} = \frac{1}{V_2}(q - q_c)\beta_2 \tag{2.57}$$

$$\frac{dq}{dt} = \frac{1}{M}(p_{bh} - p_{wh} - \rho g h_w - \Delta p_f + \Delta p_p) \tag{2.58}$$

Equations 2.56, 2.57 and 2.58 are, respectively, the dynamics for the bottom-hole pressure, the well-head pressure and the flow rate.

The inertia parameter M is constant for each system and is calculated by the formula:

$$M = \rho_1 \int_0^{L_1} \frac{1}{A_1} dx + \rho_2 \int_0^{L_2} \frac{1}{A_2} dx \tag{2.59}$$

in which 1 and 2 are indexes for the downstream and upstream pipe sections, respectively, and L_i, A_i and V_i are length, area and volume of section i.

The model for the reservoir inflow is based on H2 and respects a linear inflow performance relation:

$$q_r = PI\ (p_r - p_{bh}) \tag{2.60}$$

The production choke model is derived from the Bernoulli Equation coupled with a characteristic parameter. Assuming H3, the following equations are considered for the flow across the valve:

$$q_c = C_c\ z\ \sqrt{p_{wh} - p_m} \tag{2.61}$$

The pressure drop in pipe section comes from the Darcy-Weisbach considering the Fanning friction factor for smooth pipe and turbulent flow:

$$F_i = 0.158\ \frac{\rho L_i q^2}{D_i A_i^2} \left(\frac{\mu}{\rho D_i q} \right)^{1/4},\ i = 1, 2 \tag{2.62}$$

$$\Delta p_p = \rho g H(q, f, \mu) \tag{2.63}$$

The equations related to the pump are calculated by the affinity laws (TAKACS, 2011) using the pump characteristics provided by the vendor:

$$H = C_H(\mu) H_0(q, f, \mu) \left(\frac{f}{f_0} \right)^2 \tag{2.64}$$

$$q_0 = \frac{q}{C_q(\mu)} \left(\frac{f_0}{f} \right) \tag{2.65}$$

$$P = C_P(\mu) P_0(q, f, \mu) \left(\frac{f}{f_0} \right)^3 \tag{2.66}$$

$$p_{p,in} = p_{bh} - \rho g h_1 - F_1 \tag{2.67}$$

$$I = \frac{I_{np}}{P_{np}} P(q, f, \mu) \tag{2.68}$$

H_0 and P_0 are the head and power characteristic curves, respectively, provided by the ESP vendor. C_q, C_H and C_P are viscosity correction correction factors for flow, head and power. BINDER *et al.* (2015) reported these five functions as polynomial approximations of the type:

$$R(x) = \sum_{i=0}^{4} c_i x^i \tag{2.69}$$

In which $R(x)$ denotes H_0 or P_0 replacing x by q_0, which is the theoretical flow rate at reference frequency, and C_q, C_H or C_P replacing x by μ. Its coefficients can be found in Table 2.3.

Table 2.3: Polynomial coefficients (BINDER *et al.*, 2015)

R	c_4	c_3	c_2	c_1	c_0
H_0	0	0	1.2454×10^6	7.4959×10^3	9.5970×10^2
P_0	0	-2.3599×10^9	-1.8082×10^7	4.3346×10^6	9.4355×10^4
C_q	2.7944	-6.8104	6.0032	-2.6266	1
C_H	0	0	0	-0.03	1
C_P	-4.4376	11.091	-9.9306	3.9042	1

Including the paper that disclosed the previously described model, four works have been published applying the model. PAVLOV *et al.* (2014) proposed this ESP model, an MPC strategy and experimental results of the controller tested in a large scale test facility with a full scale ESP. BINDER *et al.* (2014) implemented an MPC using SEPTIC (Statoil Estimation and Prediction Tool for Identification and Con-

trol) in a PLC. Step response models were used as internal models of the constrained MPC. Desired performance was achieved by tuning of weights and soft constraints penalties. BINDER *et al.* (2015) extended the model to account with ESP characteristics and viscosity correction factors. An MHE was applied to estimate Flow Rate, Viscosity and Production Index in a well using ACADO. The authors reported that the solver performed very fast and so it could be used on an industrial embedded hardware. In KRISHNAMOORTHY *et al.* (2016), the ESP model was used in a high fidelity simulator of an ESP lifted well producing heavy viscous crude oil. The MPC previously proposed was tested with the focus on performance and robustness, which was achieved.

The four works previously described have considered all relevant model variables measurements to be available and only linear MPCs with a single internal model was applied, Table 2.4 summarizes the main aspects of the four works previously cited.

To summarize all dependencies of the vector field of the third order model, it is represented in its nonlinear state space form:

$$\begin{aligned} \frac{dp_{bh}}{dt} &= f_1(p_{bh}, q) \\ \frac{dp_{wh}}{dt} &= f_2(p_{wh}, q, z, p_m) \\ \frac{dq}{dt} &= f_3(p_{bh}, p_{wh}, q, f) \end{aligned} \tag{2.70}$$

In terms of the output variables of interest in this work:

$$\begin{aligned} p_{p,in} &= g_1(q, f) \\ P &= g_2(q, f) \end{aligned} \tag{2.71}$$

Table 2.4: Summary of main aspects of previous literature on the ESP model

Paper[1]	*Strategy*	*Objective*	*Measurements*	*Internal model*	*Model adaption*	*MV*	*Disturbance*
1	MPC (SEPTIC)	SP tracking for $p_{p,in}$, min BHP (by max z) and constraints	$p_{p,in}$, $p_{p,dis}$, $p_w h$, p_m, z, f, I, BHP, v_p (vibration level), $T_{p,m}$ (motor temp.), $T_{p,in}$, $T_{p,dis}$ (fluid intake and discharge temp)	linear SISO, SR, FIR or ARX	Not applied	f and z	p_m
2	MPC (SEPTIC)	SP tracking for $p_{p,in}$, min I (by max z) and constraints	$p_{p,in}$, $p_w h$, p_m, z, f, I, q	linear SISO, SR, FIR or ARX	Not applied	f and z	p_m
3	MHE (ACADO)	Estimate q, μ and PI	$p_{p,in}$, $p_{p,dis}$, $p_w h$, p_m, z, f, I	Nonlinear model	-	f and z	-
4	MPC (SEPTIC)	SP tracking for $p_{p,in}$, min P (by max z) and constraints	$p_{p,in}$, $p_{p,dis}$, $p_w h$, p_m, z, f, I	linear SISO, SR, FIR or ARX	Not applied	f and z	p_m

1 - PAVLOV *et al.* (2014); 2 - BINDER *et al.* (2014); 3 - BINDER *et al.* (2015); 4 - KRISHNAMOORTHY *et al.* (2016).

Chapter 3

Adaptive QDMC with model scheduling strategy

A version of this chapter was presented in 12th IFAC Symposium on Dynamics and Control of Process Systems, including Biosystems (DYCOPS 2019) (DELOU *et al.*, 2019a).

3.1 Introduction

The linear MPC considered by PAVLOV *et al.* (2014), BINDER *et al.* (2015) and KRISHNAMOORTHY *et al.* (2016) has linear models for the entire operating region. When using linear MPC for controlling nonlinear processes, one must ensure that the linear model sufficiently captures the system response over a broad operating range.

KRISHNAMOORTHY *et al.* (2016) showed that for an ESP lifted well, the linear model varies significantly depending on the choke opening. Therefore, in the present paper, we extend the work of PAVLOV *et al.* (2014), BINDER *et al.* (2015) and KRISHNAMOORTHY *et al.* (2016) by considering a linear MPC with model adaptation accounting for process nonlinearity.

Based on the analysis of the process, two linear models were developed, one for operations with large valve openings (low gain) and the other for small valve openings (high gain). It is shown that both models do not work well for the opposite situation of valve opening that they were designed for, therefore, an adaptive strategy was proposed. Moreover, the final MPC strategy had its performance tested within servo and regulatory control approaches resulting in a broader range of operation.

3.2 Methodology

In this chapter, we consider a single ESP lifted well where the objective is to control the inlet pressure $p_{p,in}$ at a desired reference value and to minimize the pump power consumption P, while satisfying the pump and well constraints. The pump frequency f and valve opening z were considered as manipulated variables in order to achieve this objective and the manifold pressure p_m was conservatively considered as an unmeasured disturbance.

All numerical algorithms were developed using MATLAB™.

3.2.1 Model Linearization

Nonlinearities and regions with changes of behavior were investigated by evaluating the effects of changes in the manipulated variables and disturbances in the controlled variables. The linear model for the MPC strategy was developed using Taylor's expansion around a reference point and neglecting the higher order terms. Due to scale difference between state variables and in order to facilitate controller tuning, linearization was performed in terms of relative deviation from the stationary point. More details about the model linearization strategy applied can be found in Appendix A.

3.2.2 MPC Implementation

The MPC problem was implemented as a QDMC algorithm. QDMC is an extended method for the DMC problem consisting of an online QP with rigorous handling of constraints (GARCIA and MORSHEDI, 1986). More details about the implementation of the QDMC algorithm can be found in Section 2.2.3.

In order to implement the control objective, the reference value for power consumption was kept below plant power performance, in an unreachable baseline (setpoint chasing).

The control objectives are prioritized in such a way that the constraints take the highest priority, followed by the setpoint tracking on the pump intake pressure and then the pump power minimization. To reflect this priority order, unbalanced weights were set to the variables in the cost function, namely, 1 and 0.01 to inlet pressure and power, respectively. The weight for suppression of control action was tuned in 10^{-5}, to avoid aggressive MV moves. Moreover, sampling time, prediction horizon and control horizon were set to 1 s, 40 s and 10 s, respectively.

3.2.3 Model Scheduling Strategy

In this chapter, we propose an automatic model adaptive strategy in order to improve the controller performance far from stationary points wherein the linearized models were designed, broadening the operating range. The continuous transition between models was based on the following homotopy:

$$s = \lambda s_1 + (1 - \lambda) s_2 \tag{3.1}$$

in which s is the actual matrix of step response, s_1 and s_2 are the step response matrix of model 1 and 2, respectively, and λ is the continuation parameter. Abrupt model changes in the QDMC structure could cause process instability.

The transition between models is controlled by the instantaneous value of valve opening. In other words, the valve opening is the scheduling variable to switch between two models. If z is lower than a lower bound (l_L), model 2 is purely applied, while for values greater than an upper bound (l_U) model 1 is purely applied. The parameter λ is adjusted according to the actual valve opening and the lower and upper bounds, which can be interpreted as tuning parameters for the adaptive strategy:

$$\lambda = \frac{z - l_L}{l_U - l_L}, \ (l_L \leq z \leq l_U) \tag{3.2}$$

For the case in which the models are abruptly changed, the change is done in a single point denoted by l_C, Equation 3.2 is not valid, and the following logic is applied:

$$\begin{cases} \lambda = 0, & \text{if } z < l_C \\ \lambda = 1, & \text{if } z \geq l_C \end{cases} \tag{3.3}$$

3.3 Results and Discussion

3.3.1 Model Analysis

The stationary values for controlled variables (CV) along the manipulated variable (MV) range are shown in Figure 3.1. As one can see, the behavior of CVs along the frequency range is approximately linear, which suggests that a single linear model can be sufficient for any frequency region. On the other hand, the behavior

of CVs along the production choke valve opening range clearly shows nonlinearities that can be divided into two regions: large production choke valve opening (small variation of CVs as z varies) and low production choke valve opening (high variation of CVs as z varies).

In that manner, two linear models were proposed to represent the plant. The first one (model 1) was linearized around the stationary point obtained for $z = 0.99$ and $f = 58Hz$. The second model (model 2) was linearized around the stationary point obtained for $z = 0.10$ and $f = 35Hz$. The response of the controlled variables obtained for each model and the nonlinear plant can be visualized in Figure 3.2 and Figure 3.3, for a single unit step in the manipulated variables: frequency (f) and choke valve opening (z).

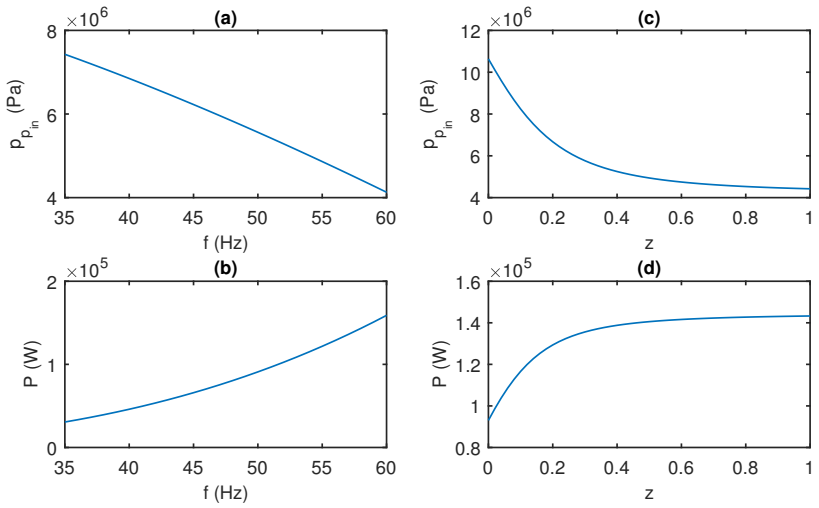

Figure 3.1: Stationary CV varying MV: (a) $p_{p,in}$ steady states for different values of f; (b) P steady states for different values of f; (c) $p_{p,in}$ steady states for different values of z; (d) P steady states for different values of f.

Figure 3.2 shows that for operations where large production choke valve opening position is required, model 1 presents better performance with respect to model 2, especially for a perturbation in the choke valve position, where high nonlinearities were identified.

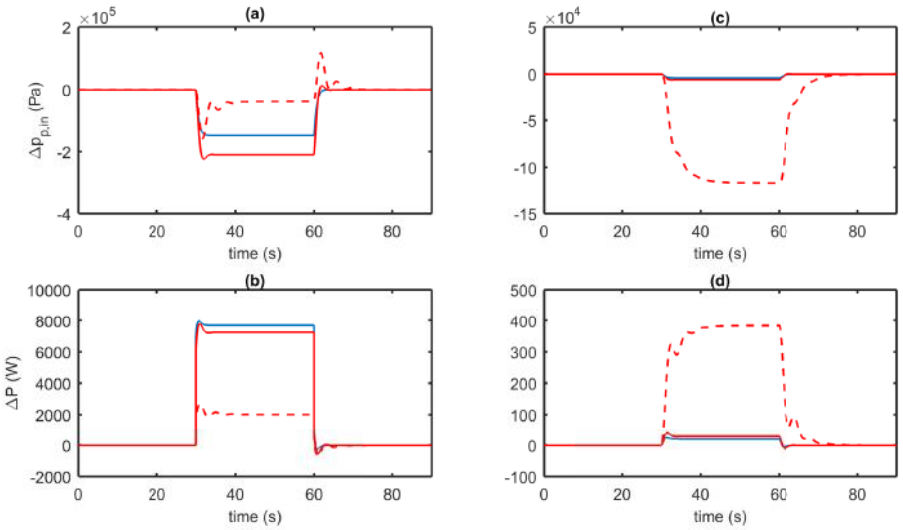

Figure 3.2: Large production choke valve opening: (a) $\Delta p_{p,in}$ response for a unit step in f; (b) ΔP response for a unit step in f; (c) $\Delta p_{p,in}$ response for a unit step in z ; (d) ΔP response for a unit step in z. (——) model 1; (- - - -) model 2; (——) nonlinear model. Steps in $t = 30s$.

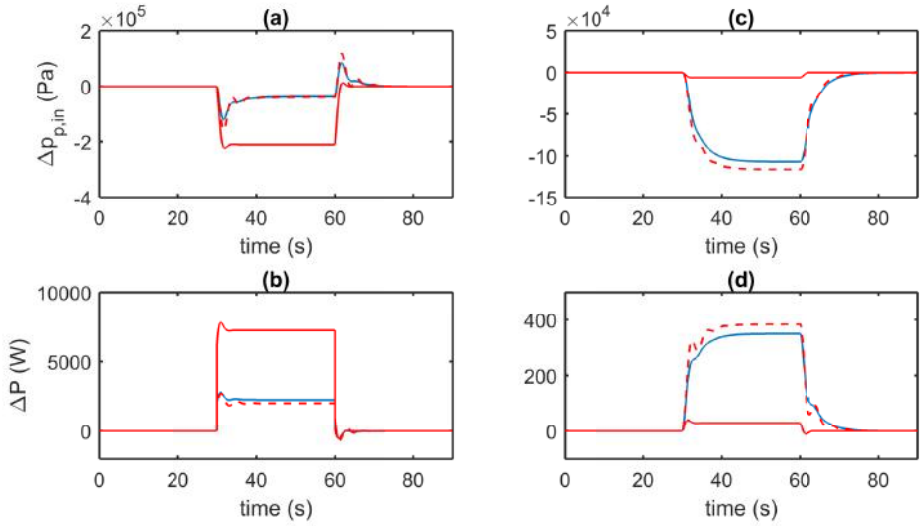

Figure 3.3: Low production choke valve opening: (a) $\Delta p_{p,in}$ response for a unit step in f; (b) ΔP response for a unit step in f; (c) $\Delta p_{p,in}$ response for a unit step in z; (d) ΔP response for a unit step in z. (——) model 1; (- - - -) model 2; (——) nonlinear model. Steps in $t = 30s$.

To sum up, it is shown that both models do not work well for the opposite situation of valve opening that they were designed for. As expected, model 2 deviates from plant performance at the large production choke valve scenario while model 1 fits better. On the side, model 2 provides better response for the low production choke valve scenario, while model 1 is more distant from plant behavior.

3.3.2 Control Performance

The MPC strategy for both models described above had its performance tested. Figure 3.4 shows control actions and system response in terms of non-linear plant controlled variables for three different setpoint values in presence of disturbance (p_m) with model 1 as the only controller's internal model. The manipulated variables adjusted by the MPC are f and z, while p_m is an unmeasured disturbance.

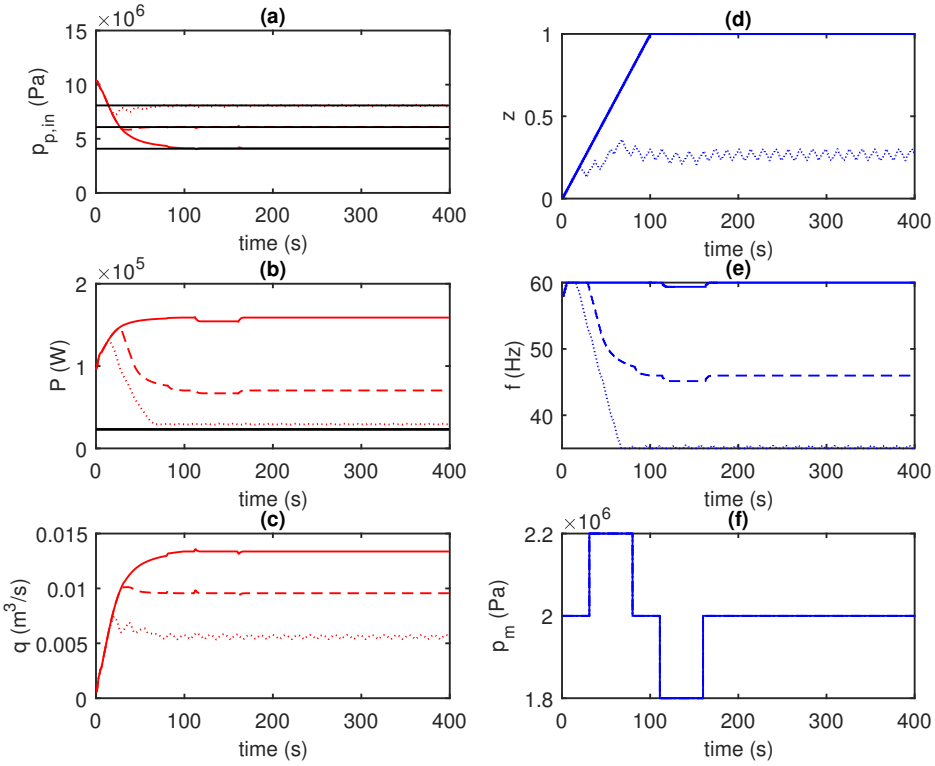

Figure 3.4: Control performance for 3 different setpoints for $p_{p,in}$ subject to p_m disturbances, using Model 1: (a) $p_{p,in}$ responses; (b) P responses; (c) q responses; (d) z manipulations; (e) f manipulations; (f) p_m disturbance. (——) CV for setpoint 1, (- - - -) CV for setpoint 2; (·····) CV for setpoint 3; (——) MV for setpoint 1; (- - - -) MV for setpoint 2; (·····) MV for setpoint 3; (——) desired setpoint.

It can be seen in Figure 3.4 that $p_{p,in}$ responses for setpoints 1 and 2 require an opened valve operation. The MPC strategy to reduce inlet pressure is to increase frequency and open the production choke valve, in order to allow minimum power. These setpoints are achieved in a stable trajectory of control action. On the other hand, setpoint 3 imposes a smaller choke opening operation. In order to keep pressure high with minimum power consumption, pump frequency is reduced and pressure is regulated using the valve. This case leads to oscillatory control actions, which are undesirable for equipment life-time. Analogously, Figure 3.5 shows control actions and system response with model 2 as the internal

model.

For setpoints 1 and 2, the production valve has a large opening, as can be seen in Figure 3.5. In order to keep the pump inlet pressure at its setpoint, pump frequency increases and choke valve opening is maximum to allow minimum flow resistance and thus minimum power consumption. There is also an undesirable offset in pump inlet pressure for setpoints 1 and 2.

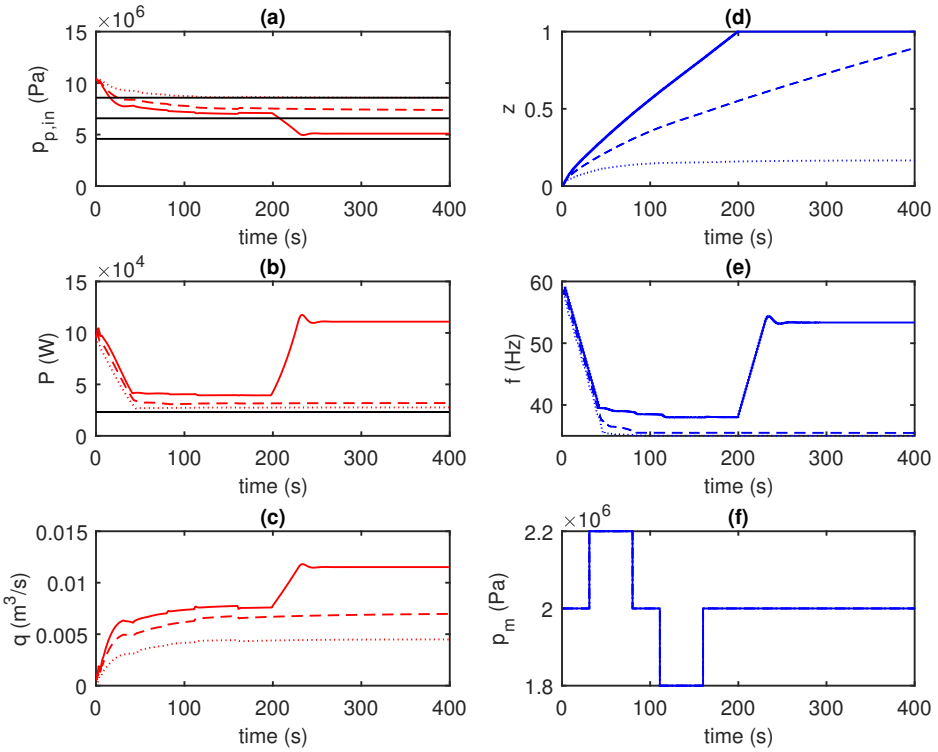

Figure 3.5: Control performance for 3 different setpoints for $p_{p,in}$ subject to p_m disturbances, using Model 2: (a) $p_{p,in}$ responses; (b) P responses; (c) q responses; (d) z manipulations; (e) f manipulations; (f) p_m disturbance. (——) CV for setpoint 1, (- - - -) CV for setpoint 2; (·····) CV for setpoint 3; (——) MV for setpoint 1; (- - - -) MV for setpoint 2; (·····) MV for setpoint 3; (——) desired setpoint.

3.3.3 Model Adaptation

Initially, the parameters l_L and l_U were chosen by investigating the behavior of the adaptive MPC for setpoint changes in the intake pressure. As seen in Section 3.2.3, these parameters are the lower and upper bounds of the valve opening z that define the homotopic change in the internal model. They should be tuned in order to avoid an abrupt change of models. Figure 3.6 illustrates this tuning process, for a setpoint change. It can be seen that, when these parameters are close to each other, an oscillatory behavior is obtained. After this preliminary investigation, these parameters were set to 0.2 and 0.3, respectively.

In the sequence, two simulation cases, transition from low to high and high to low intake pressure setpoint of the adaptive MPC, are shown. During both simulations, control action trajectory shows a short oscillation that does not compromise stability.

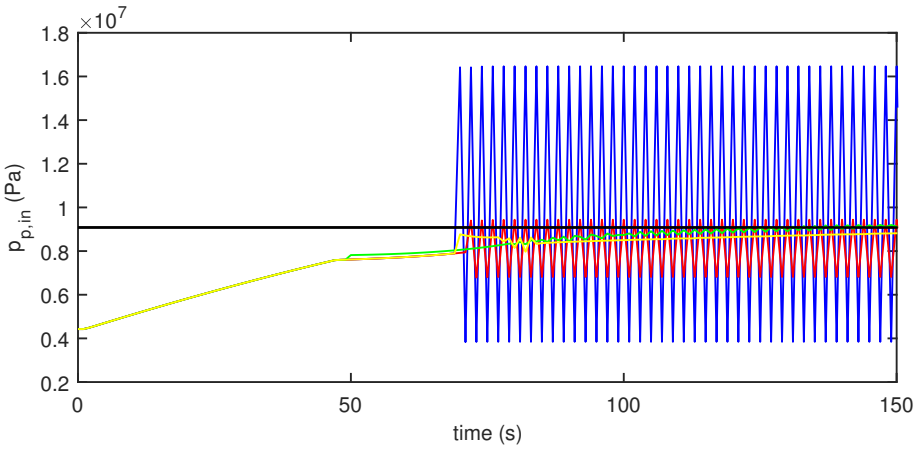

Figure 3.6: Different adaptation tuning. (——) $l_C = 0.3$, (——) $l_L = 0.22$ and $l_U = 0.28$, (——) $l_L = 0.1$ and $l_U = 0.5$, (——) $l_L = 0.2$ and $l_U = 0.3$, which is the chosen tuning in the hybrid model MPC simulations.

Figure 3.7 presents the hybrid model performance in comparison to its individual models when the intake pressure setpoint decreases from 10.1 to 7.0MPa and Figure 3.8 presents the hybrid model performance in comparison to its individual models when the intake pressure setpoint increases from 4.4 to 9.0MPa. The hybrid model in both situations performs well and corrects the problems discussed for each model in the opposite situation of inlet pressure setpoint that they were designed for. It can be seen from Figure 3.7 that the hybrid model MPC does not have an offset from the setpoint unlike model 2, when the valve is fully open. Unlike model 1, the hybrid model MPC does not present continuous oscillation when the valve opening is reduced as seen in Figure 3.8.

When the inlet pressure setpoint changed from 10.1 to 7.0MPa, the hybrid model MPC provides a slower response compared to model 1 individually. However, they reach the setpoint at around the same time as seen in Figure 3.7. Moreover, one can see in Figure 3.8 that the hybrid model MPC presented a fast response when the intake pressure setpoint increases from 4.4 to 9.0MPa and reaches the setpoint before model 2. Therefore, the hybrid model MPC presents a better overall performance with respect to model 1 and 2, individually.

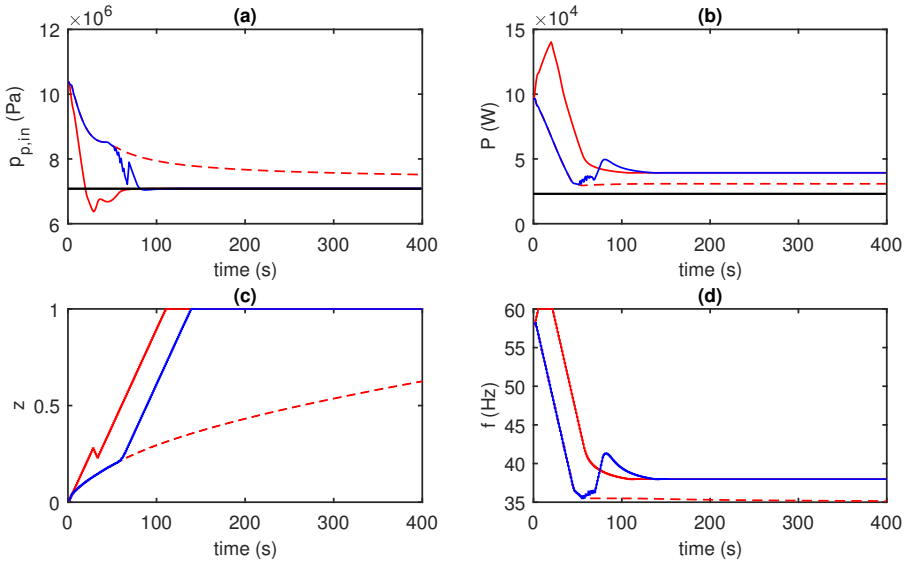

Figure 3.7: Hybrid model performance when $p_{p,in}^{sp} = 7MPa$: (a) $p_{p,in}$ responses; (b) P responses; (c) z manipulations; (d) f manipulations. (——) model 1 MPC, (- - - -) model 2 MPC, (——) hybrid model MPC, (——) desired setpoint.

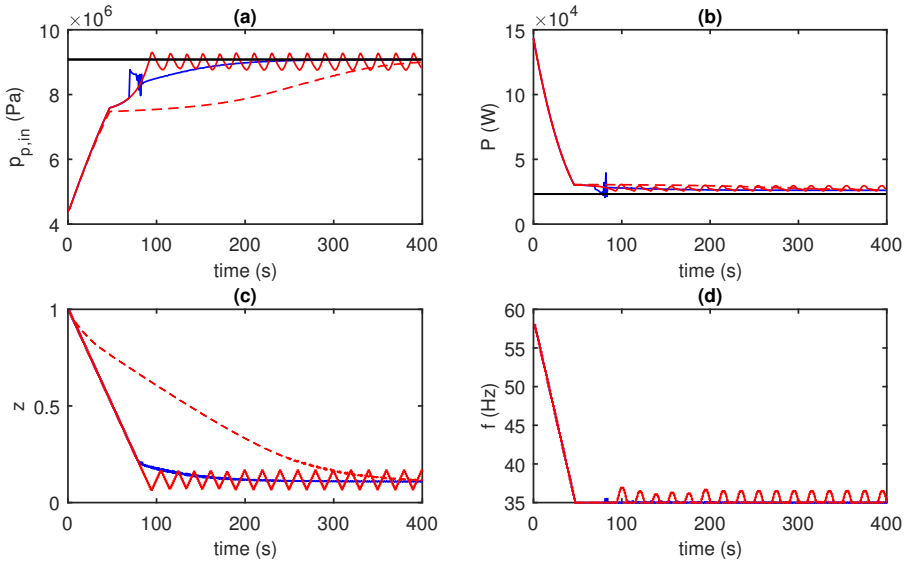

Figure 3.8: Hybrid model performance when $p_{p,in}^{sp} = 9MPa$: (a) $p_{p,in}$ responses; (b) P responses; (c) z manipulations; (d) f manipulations. (——) model 1 MPC, (- - - -) model 2 MPC, (——) hybrid model MPC, (——) desired setpoint.

3.4 Conclusions

The application of MPC with a model adaptive strategy to an oil production well is new, to the best of our knowledge. This strategy was shown to provide a better overall performance compared to MPC based on individual models, as it benefits

from the qualities of the individual models in the regions that they were designed for and suppresses their disadvantages in the regions where each one would not behave as desired.

Chapter 4

Robust Multi-model State-space MPC coupled with Kalman Filter

Some results of this chapter were presented in the I Brazilian Congress on Process Systems Engineering (PSE-BR 2019) (DELOU *et al.*, 2019b).

4.1 Introduction

As a reminder, PAVLOV *et al.* (2014) developed a simple and reliable ESP dynamic model which was employed in a MPC and presented successful tests in a large scale facility. BINDER *et al.* (2014) made use of the model in another MPC application focused on software's development. BINDER *et al.* (2015) extended the model to account with some pump and fluid properties in order to develop a soft sensor to estimate the fluid viscosity and the reservoir production index by the use of a moving horizon estimation technique. KRISHNAMOORTHY *et al.* (2016) focused on developing a MPC strategy to overcome the nonlinearity in the choke opening by using a single internal model identified for a low valve opening, which is the region of higher gain of the system.

The four works previously described, except for BINDER *et al.* (2015), have considered all relevant model variables measurements to be available. In this chapter, we focus on the problem of developing a robust adaptive MPC strategy for a scenario of loss of instrumentation to measure the states variables. For that, we develop an MPC strategy coupled with a Kalman Filter, both using the same strategy to adapt their internal models depending on the instant values of the manipulated variables. Here, we consider important to use the same model adapting strategy both in KF and MPC in order to maintain consistency for the application. We show that a single internal model application, as proposed by KRISHNAMOORTHY *et al.* (2016), and a simple scheduling strategy, as proposed in Chapter 3 of the

present work, lack in performance for the state estimation technique coupled with MPC. To overcome this problem, we propose and compare two model switching strategies based on interpolation of a grid of linear models, previously obtained by linearization or identification. These strategies are also compared to the classical successive linearization strategy used by the EKF technique. Moreover, the optimal grid size and grid points are obtained by solving several optimization problems, the chosen structure is evaluated in terms of state estimation performance by systematically removing a state measurement availability and, in terms of control performance by performing setpoint change tests between high and low intake pressure, what should drive the operation to go through the whole nonlinear region.

4.2 Methodology

In this chapter, as in Chapter 3, we consider a single ESP lifted well where the objective is to control the inlet pressure, $p_{p,in}$, at a desired reference value and to minimize the pump power consumption, P, while satisfying the pump and well constraints. The pump frequency, f, and valve opening, z, were considered as manipulated variables in order to achieve these objectives and the manifold pressure, p_m, was considered as an unmeasured disturbance. The model variables, units and whether the variable measurement are considered available are presented in Table 4.1.

Table 4.1: System Variables in MPC structure

Variable		Unit	Measured
State Variables			
p_{bh}	Bottom hole pressure in well	Pa	no
p_{wh}	Wellhead pressure	Pa	no
q	Average flow rate in well	m^3/s	no
Manipulated Variables			
f	ESP frequency	Hz	yes
z	Production choke valve opening	-	yes
Disturbance			
p_m	Manifold pressure	Pa	no
Controlled Variables			
$p_{p,in}$	ESP inlet pressure	Pa	yes
P	ESP brake horsepower (BHP)	W	yes

To simulate uncertainties in the measurements of the output variables, stochastic white-noise, zero-mean, normally distributed additive disturbances with standard deviation defined in Table 4.2 were considered for each measured variable.

All numerical algorithms were developed using MATLAB™.

Table 4.2: Standard deviation of the white-noise for each variable.

Measurement	p_{bh}	p_{wh}	q	$p_{p,in}$	P
Standard dev.	0.01	0.01	0.01	0.02	0.02

4.2.1 Model Scheduling Strategy

Three scheduling techniques are compared, two interpolation strategies from models previously obtained by identification or linearization and the successive linearization, in which the nonlinear model is linearized around the operational point. Here we will refer to these strategies respectively as:

- SKF1-MPC: The approach making use of the homotopic interpolation proposed in Chapter 3 to obtain the linear model for the Kalman Filter and for the MPC.
- SKF2-MPC: The approach making use of the multivariable linear interpolation, presented by FURLAN *et al.* (2016), to obtain the linear model for the Kalman Filter and for the MPC.
- EKF-MPC: The approach making use of linearization around the operational point, as presented in Appedix A, to obtain the linear model for the Kalman Filter and for the MPC.

In the following we present the formulation of the interpolation strategies.

SKF1: Homotopic Interpolation

The SKF1 strategy for model scheduling was based on homotopic interpolations between local models linearized around a reference steady state. A net of models were generated by arranging some linear models obtained in different combinations of f and z values within the operational range. Figure 4.1 illustrates a 5 by 5 net, where $s_{i,j}$ denotes the linear model obtained by linearization around the stationary point in the node $f = \bar{f}_i$ and $z = \bar{z}_j$, in which $\bar{f}$ and $\bar{z}$ are the vectors of the stationary point nodes for f and z, respectively.

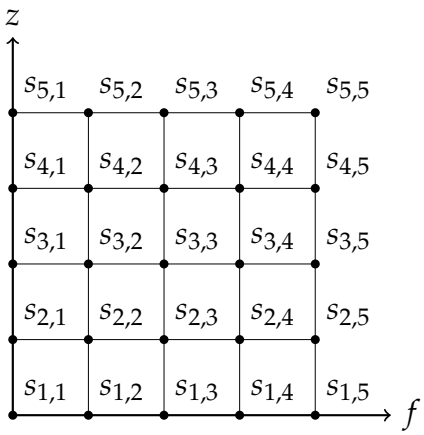

Figure 4.1: Example of a 5 by 5 net of linear models.

In a certain moment of normal operation, f and z are going to assume values inside a quadrant of the net of models, let M denote the active quadrant, which is a square in this 2-dimensional case where the vertices are linear models. The interpolation takes place in a homotopic transition fashion, similarly to Chapter 3 with a parameter for each dimension. The parameters are organized in a matrix, λ, in which each column is for each dimension and each line represent interval between two nodes of the model net. The resultant linear model is obtained by the formulas:

$$s = s_{i+1}\lambda_{i,1} + s_i(1 - \lambda_{i,1}) \tag{4.1}$$

in which, s represents the internal model matrices used for each k instant. Each s_i is calculated by the following formula:

$$s_i = s_{i,j+1}\lambda_{j,2} + s_{i,j}(1 - \lambda_{j,2}) \tag{4.2}$$

Parameters $\lambda_{i,1}$ and $\lambda_{j,2}$ vary according to the instant value of f and z, respectively, by the following logic rules:

$$\lambda_{i,1} = \begin{cases} 1, & \text{if } f_k \geq \bar{f}_{i+1} \\ 0, & \text{if } f_k \leq \bar{f}_i \\ \dfrac{f_k - \bar{f}_{i+1}}{\bar{f}_i - \bar{f}_{i+1}}, & \bar{f}_i \leq f_k \leq \bar{f}_{i+1} \end{cases} \tag{4.3}$$

$$\lambda_{j,2} = \begin{cases} 1, & \text{if } z_k \geq \bar{z}_{j+1} \\ 0, & \text{if } z_k \leq \bar{z}_j \\ \dfrac{z_k - \bar{z}_{j+1}}{\bar{z}_j - \bar{z}_{j+1}}, & \bar{z}_i \leq z_k \leq \bar{z}_{i+1} \end{cases} \tag{4.4}$$

Figure 4.2 illustrates an active square, M, and how the interpolation takes place for this 2-dimensional case.

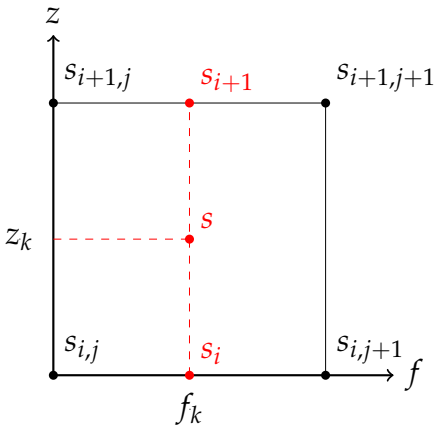

Figure 4.2: Illustration of an active M, intermediate models and interpolated internal model.

SKF2: Multivariable Linear Interpolation

The SKF2 strategy for model scheduling was based on the grid based look-up tables interpolation presented by FURLAN *et al.* (2016). Figure 4.3 illustrates a 2-D grid of models that has to be obtained previously from the studied system.

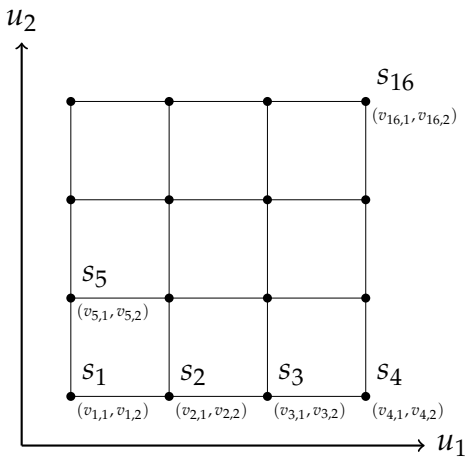

Figure 4.3: Example of a 4 by 4 grid of linear models.

In Figure 4.3, the vector s_i represents the linear model matrices that can be obtained by identification or linearization (A, B, C and D) to be interpolated depending on the actual values of input vector u, v is the matrix in which each row corresponds to a point in the grid and each column corresponds to the value of the k^{th} input variables, $v_{i,k}$.

The output of the interpolation, $\hat{s}$, corresponds to the linear weighted sum of the nearest models, s_i, that are part of the vertices of the smallest cube, M, around the actual input variables. The weights, Φ_i, are the ratio of volumes of each cube with longer diagonal defined by u and the vertex v_j of the opposite M to v_i, in which v_i and v_j corresponds to the longer diagonal of M.

$$\hat{s} = \sum_{i=1}^{M} s_i \, \Phi_i(u, v) \tag{4.5}$$

$$\Phi_i(u, v) = \frac{\prod_{k=1}^{n} |u_k - v_{j,k}|}{\prod_{k=1}^{n} |v_{i,k} - v_{j,k}|} \tag{4.6}$$

$$M = \prod_{k=1}^{n} M_k \tag{4.7}$$

in which, n is the number of input variables and M_k is the number of points in the grid for input k. It is noteworthy that Equation 4.6 is only valid when i is a vertex of M, otherwise Φ_i is null.

4.2.2 Optimal Model Net Structure

Let θ denotes the concatenation of the model net nodes in such a way that $\theta = (\bar{f}^T, \bar{z}^T)^T$. In order to determine the optimal nodes structure and points, an optimization problem was constructed to minimize the normalized sum of the squared errors (SSE) from the nonlinear model static outputs and the response of

the resultant linear model static outputs, such that:

$$\min_{\theta} \sum_{j=1}^{N_f} \sum_{i=1}^{p} \left(\frac{y_i^{NL}(f_j,z) - y_i^{L}(f_j,z)}{y_i^{NL}(f_j,z)} \right)^2 \Bigg|_{z=0.99} + \sum_{j=1}^{N_z} \sum_{i=1}^{p} \left(\frac{y_i^{NL}(f,z_j) - y_i^{L}(f,z_j)}{y_i^{NL}(f,z_j)} \right)^2 \Bigg|_{f=58} \tag{4.8a}$$

s.t.

$$x^L(f,z) = (I - A(f,z))^{-1} B(f,z)u \tag{4.8b}$$

$$y^L(f,z) = C(f,z)x^L(f,z) + D(f,z)u \tag{4.8c}$$

$$x^{NL}(f,z) = F(f,z) \tag{4.8d}$$

$$y^{NL}(f,z) = G(x^{NL},f,z) \tag{4.8e}$$

$$35 \leq f \leq 60 \tag{4.8f}$$

$$0 \leq z \leq 1 \tag{4.8g}$$

in which, x^L and y^L are the static states and outputs from the linearization strategy, x^{NL} and y^{NL} are the static states and outputs from the nonlinear model, denoted by F and G.

In order to obtain the optimal structure, ten different structures were subjected to the above optimization problem, which were all combinations from a 2 by 2 to a 5 by 5 structure, in which the dimension in $\bar{z}$ is greater than the dimension in $\bar{f}$. The best structure was chosen by comparing their performances in a MPC coupled with SKF setpoint tracking test. To do so, the following reference trajectory was imposed and two indicators were observed: the mean of the innovation of the filter and the SSE of the estimated outputs in relation to the real ones (supposing that they were known).

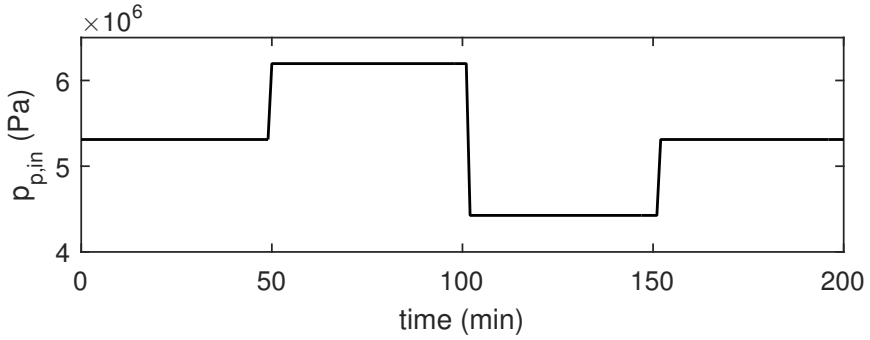

Figure 4.4: Reference trajectory subjected to $p_{p,in}$ in the model net validation.

4.2.3 MPC Implementation

The MPC strategy was implemented as an on-line nonlinear program (NLP), solved by an interior-point solver (WÄCHTER and BIEGLER, 2006), coupled with an observer to estimate the unmeasured states. The internal model was developed as a linear discrete state-space formulation with an adaptive strategy based on the manipulated variables values at the beginning of the prediction horizon. The control law was determined in a receding horizon manner by the solution of the following optimization problem at each sampling time.

$$\min_{\Delta u} \sum_{i=1}^{L} \left\| y_{k+i} - y_{k+i}^{rt} \right\|_{W_y}^2 + \sum_{i=0}^{N-1} \left[\left\| u_{k+i} - u_{k+i}^{rt} \right\|_{W_u}^2 + \left\| \Delta u_{k+i} \right\|_{W_{\Delta u}}^2 \right] \tag{4.9a}$$

s.t. $\forall k \in [0, L]$, in which L is the prediction horizon

$$x(k+1) = A(u(0))x(k) + B(u(0))u(k) \tag{4.9b}$$

$$y(k) = C(u(0))\hat{x}(k) + D(u(0))u(k) \tag{4.9c}$$

$$\hat{x}(k+1) = A(u(0))x(k+1) + B(u(0))u(k) + K\left(y^m(0) - C(u(0))x(0) - D(u(0))u(0)\right) \tag{4.9d}$$

$$x(0) = \hat{x}(0) \tag{4.9e}$$

$$x^{lb} \leq \hat{x} \leq x^{ub} \tag{4.9f}$$

$$u^{lb} \leq u(k) \leq u^{ub} \tag{4.9g}$$

$$\Delta u^{lb} \leq \Delta u(k) \leq \Delta u^{ub} \tag{4.9h}$$

More information about the MPC implementation details can be found in Appendix B and the observer theory is explored in Section 2.4.

The control objectives are prioritized in such a way that the constraints take the highest priority, followed by the setpoint tracking on the pump intake pressure and then the pump power minimization. To do so, cost function weight matrix were selected properly, in which weights for inlet pressure and power were 400 and 0.02, respectively, weights for inputs were settled to zero and for the rate of change of inputs were equal to 0.01. The sampling time, the prediction horizon and the control horizon were set to $1s$, $100s$ and $5s$, respectively. It is important to note that internal models were modelled in a relative deviation manner, as described in Appendix A, so the previous numbers are applied to the normalized variables. Next section describe how the evaluation of the control performance was carried out.

4.2.4 Control Performance

In order to evaluate the control performance, two setpoint tracking problems were subjected to the two proposed SKF coupled with MPC schemes and compared to the classical EKF-MPC. The first test is a low to high intake pressure, from 4.4 MPa to 9 MPa, and the second is a high to low intake pressure, from 9 MPa to 4.4 MPa. These tests force the system from a situation of high choke valve opening to a low choke valve opening and from a low choke valve opening to a high choke valve opening, passing through the whole nonlinear region of the operational range. So the performance of the adaptive scheme can be validated in these tests.

In order to soften these transitions, aiming to avoid discontinuities and aggressiveness from the step disturbance, the following regularization function of a unit step was used to condition the transition between the two intake pressure operation points:

$$y(t) = \frac{1 + \tanh\left(\epsilon(t - t_0)\right)}{2} \tag{4.10}$$

in which, ϵ is a tuning parameter of the regularization function and t_0 is the step disturbance time. The setpoint of the pump power was kept lower than a realizable value, in order to guarantee the minimum power consumption in the operation.

4.3 Results and Discussion

In this section, we compare the both proposed interpolation strategies with the successive linearization, and in both we keep the model used in the Kalman Filter as the same used in the MPC in order to hold methodology consistency.

4.3.1 Optimal Model Net Structure

The optimal structures obtained from different number of nodes from a 2 by 2 to a 5 by 5 structure can be visualized in Table 4.3. It can be highlighted that the result of the optimization problem for all structures followed a reasonable trend, which was more or less uniformly distributed for the frequency and greater number of nodes concentration in the low choke opening region. This is very straight forward considering that the outputs are almost linear in relation to the frequency and present a high gain in the region of low choke opening. In addition, it is noteworthy that both interpolation strategies resulted in the same optimal model net structure.

Table 4.3: Optimal nodes for different model net structures.

	Nodes	
Structure	f_n	z_n
2 by 2	$[56.51, 42.7]^T$	$[0.69, 0.22]^T$
2 by 3	$[56.47, 42.15]^T$	$[0.82, 0.35, 0.13]^T$
2 by 4	$[56.36, 41.86]^T$	$[1, 0.46, 0.24, 0.1]^T$
2 by 5	$[56.62, 41.93]^T$	$[1, 0.51, 0.3, 0.18, 0.07]^T$
3 by 3	$[57.08, 47.93, 39.81]^T$	$[0.8, 0.35, 0.13]^T$
3 by 4	$[56.89, 47.41, 39.23]^T$	$[1, 0.48, 0.25, 0.1]^T$
3 by 5	$[57.24, 47.61, 39.31]^T$	$[1, 0.54, 0.33, 0.19, 0.08]^T$
4 by 4	$[58.63, 51.44, 44.76, 38.68]^T$	$[0.84, 0.46, 0.25, 0.1]^T$
4 by 5	$[58.5, 51.12, 44.42, 38.42]^T$	$[0.89, 0.54, 0.34, 0.2, 0.08]^T$
5 by 5	$[58.92, 53.75, 48, 42.7, 37.82]^T$	$[0.89, 0.54, 0.33, 0.19, 0.08]^T$

All structures generated stable models for the whole operational range, that is all eigenvalue of the Jacobian matrix remained inside the unit circle in the complex plane. The SSE for each input-output combination of the structures can be visualized in Table 4.4.

Table 4.4: SSE for different model net structures.

	$p_{p,in}$		P	
Structure	f	z	f	z
2 by 2	1.07E+12	1.47E+13	3.20E+08	1.67E+09
2 by 3	4.57E+11	2.69E+12	3.05E+08	5.25E+08
2 by 4	4.28E+11	7.31E+11	2.99E+08	3.16E+08
2 by 5	4.27E+11	2.44E+11	3.18E+08	1.60E+08
3 by 3	2.43E+11	2.73E+12	6.10E+07	4.08E+08
3 by 4	1.27E+11	8.30E+11	5.57E+07	2.22E+08
3 by 5	1.18E+11	2.94E+11	5.83E+07	8.70E+07
4 by 4	8.91E+10	9.38E+11	2.49E+07	8.57E+07
4 by 5	5.75E+10	3.98E+11	2.30E+07	3.43E+07
5 by 5	3.71E+10	3.93E+11	9.44E+06	3.50E+07

As expected, as the size of the model net increases, the higher is the interpolation strategy fidelity compared to the nonlinear model, that can be observed by the decrease of the SSE. It would be desired to have the best model net possible. However, it comes with the cost of having to identify more models. So, the analysis of the SSE between the nonlinear model and the interpolation strategy is not

enough in order to determine the best net structure, for that would also be interesting to evaluate the Kalman Filter performance for each model net structure.

The setpoint tracking test, as described in Section 4.2.2, was carried out for each model net structure. In order to be more conservative, all state measures were considered unknown. The SSE and the mean of the innovation for each test can be visualized in Tables 4.5 and 4.6.

Table 4.5: SSE in Kalman Filter performance test.

Structure	p_{bh}	p_{wh}	q	$p_{p,in}$	P
2 by 2	4.84E+12	1.28E+12	3.93E-05	7.32E+12	7.74E+09
2 by 3	2.33E+12	1.28E+11	2.52E-05	3.55E+12	7.38E+09
2 by 4	2.05E+12	1.12E+12	2.36E-05	3.04E+12	6.85E+09
2 by 5	2.05E+12	8.37E+11	2.36E-05	3.06E+12	7.3E+09
3 by 3	2.27E+12	1.55E+11	2.63E-05	3.31E+12	4.76E+09
3 by 4	2.06E+12	8.41E+11	2.48E-05	2.98E+12	4.57E+09
3 by 5	2.08E+12	5.55E+11	2.50E-05	3.02E+12	4.78E+09
4 by 4	2.26E+12	1.39E+11	2.66E-05	3.25E+12	4.68E+09
4 by 5	2.25E+12	1.01E+11	2.62E-05	3.26E+12	4.63E+09
5 by 5	2.30E+12	1.08E+11	2.67E-05	3.31E+12	4.77E+09

Table 4.5 shows that the minimum SSE in Kalman Filter performance test is obtained for p_{bh} and q was achieved by structures 2 by 4 and 2 by 5, for p_{wh} was achieved by structure 4 by 5, for $p_{p,in}$ and P was achieved by structure 3 by 4.

Table 4.6: Mean of the innovation in Kalman Filter performance test.

Structure	p_{bh}	p_{wh}	q	$p_{p,in}$	P
2 by 2	1.53E-02	2.57E-02	-2.67E-02	2.97E-02	-4.00E-02
2 by 3	6.00E-03	-3.22E-03	-1.08E-02	1.39E-02	-3.79E-02
2 by 4	7.57E-04	-2.70E-02	-2.59E-03	4.64E-03	-3.46E-02
2 by 5	1.06E-03	-2.35E-02	-3.12E-03	5.20E-03	-3.67E-02
3 by 3	5.24E-03	1.52E-03	-9.77E-03	1.19E-02	-1.78E-02
3 by 4	-4.76E-04	-2.29E-02	-5.16E-04	1.86E-03	-1.49E-02
3 by 5	-2.38E-04	-1.86E-02	-9.99E-04	2.27E-03	-1.64E-02
4 by 4	1.64E-03	2.54E-04	-4.29E-03	5.07E-03	-5.68E-03
4 by 5	2.12E-04	-1.60E-03	-2.02E-03	2.57E-03	-6.74E-03
5 by 5	3.21E-04	-1.55E-03	-2.20E-03	2.76E-03	-6.88E-03

As pointed out in Section 2.4.1, it is desirable that the mean of the innovation, represented by Equation 2.53, is as near as zero as possible, so it could be con-

sidered accurate. As shown in Table 4.6, the values nearest to zero for variable p_{bh} was structure 4 by 5, for p_{wh} and P was structure 4 by 4 and for q and $p_{p,in}$ was structure 3 by 4. In order to balance between the three indicators previously presented in Tables 4.4, 4.5 and 4.6, structure 4 by 5 was chosen to have the best balance between model fidelity, number of models to identify and filter performance.

The proposed model scheduling strategies produced a high accurate dynamic representation of the nonlinear system, as can be observed in Figure 4.5.

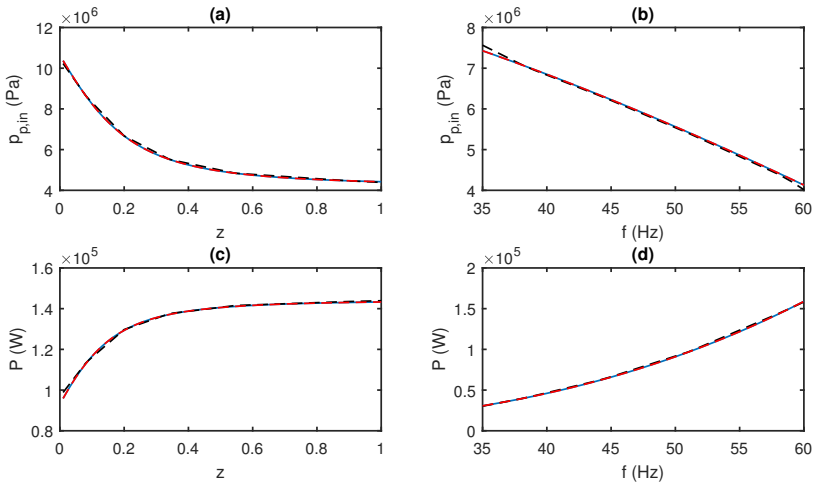

Figure 4.5: Static outputs versus inputs: (a) $p_{p,in}$ versus z; (b) $p_{p,in}$ versus f; (c) P versus z; (d) P versus f. (——) nonlinear model response, (- - - -) 4 by 5 interpolation response, (- - - -) Successive linearization response.

Figures 4.6 and 4.7 show the eigenvalues for the whole operational range of f and z in both interpolation and successive linearization approaches.

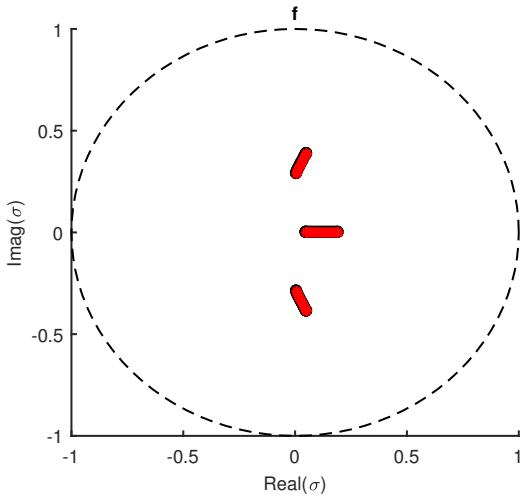

Figure 4.6: Internal model stability analysis over the range of f. (- - - -) unit circle, ($\circ\ \circ\ \circ$) scheduled eigenvalues, ($*\ *\ *$) nonlinear eigenvalues.

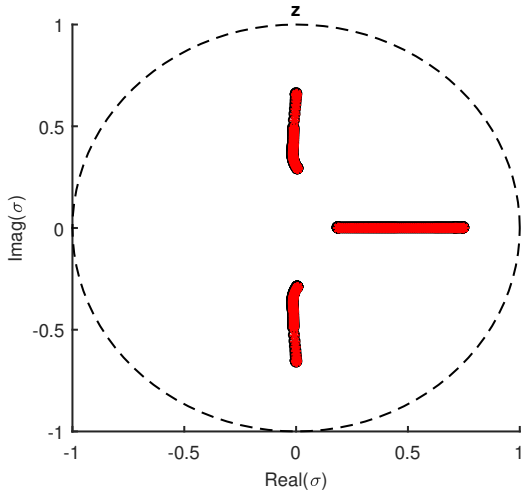

Figure 4.7: Internal model stability analysis over the range of z. (- - - -) unit circle, ($\circ \circ \circ$) scheduled eigenvalues, ($* * *$) nonlinear eigenvalues.

It can be seen that all models resulted from the scheduling strategies are stable, since their eigenvalues remain inside the unit circle for the whole operational range. Moreover, it can be seen that the eigenvalues of the nonlinear model and the scheduling strategy match.

Figures related to the Kalman Filter performance tests are shown in Section 4.3.2.

4.3.2 State Estimation Performance

Although a single internal model strategy might produce a robust MPC due to feedback, as proposed by KRISHNAMOORTHY *et al.* (2016), it lacks in quality when a single model Kalman Filter is applied as demonstrated in Figure 4.8. The same result is obtained for the model scheduling strategy presented in Chapter 3, since a single model is applied for a large operational range. Since the internal model is linear, local and there is no adaptive strategy in both MPC and KF schemes, the observer fails in estimating the unmeasured states, resulting in an offset between real and the estimated outputs what leads to poor MPC performance as it directs the estimated output to the reference trajectory, not the real outputs themselves. KRISHNAMOORTHY *et al.* (2016) suggest the use of a single model obtained in the region of higher gain, that is the region of small valve opening. However, if that would be applied in a KF scheme the offset between real and estimated outputs would be even larger, as most of the operation occurs in the region of high valve opening. Therefore, for a linear MPC scheme to work properly together with a KF scheme applied to a nonlinear system, an adaptive strategy must be carried out in order to obtain the best local models for each sampling instant.

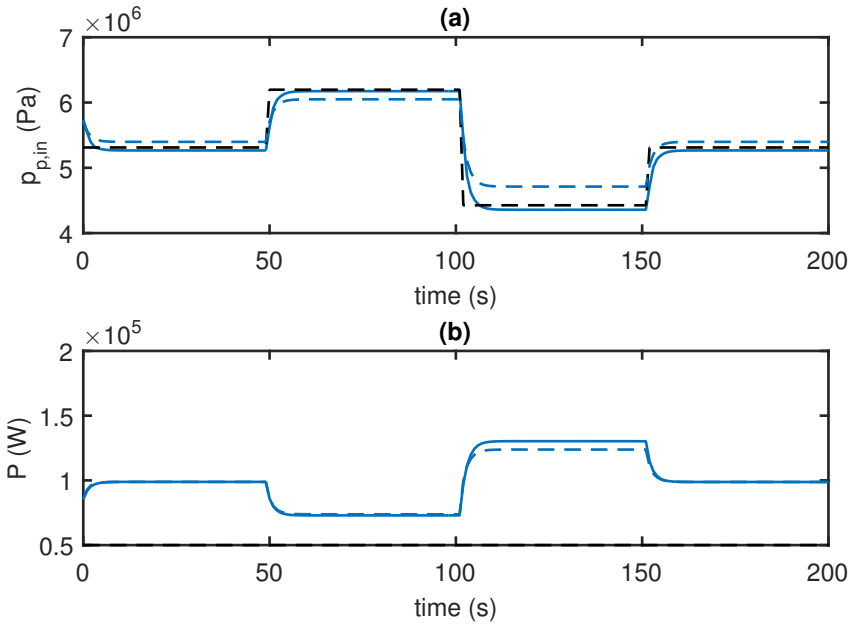

Figure 4.8: Outputs - filter performance test - single model: (a) $p_{p,in}$; (b) P. (- - - -) reference trajectory, (- - - -) real system trajectory, (——) estimated trajectory.

The most common strategy is the one applied in EKF, in which the nonlinear model is needed in order to obtain a linearization every sampling instant. As an alternative, Figure 4.9 shows the performance of the proposed SKF1-MPC and SKF2-MPC compared to the EKF-MPC strategy for the output variables.

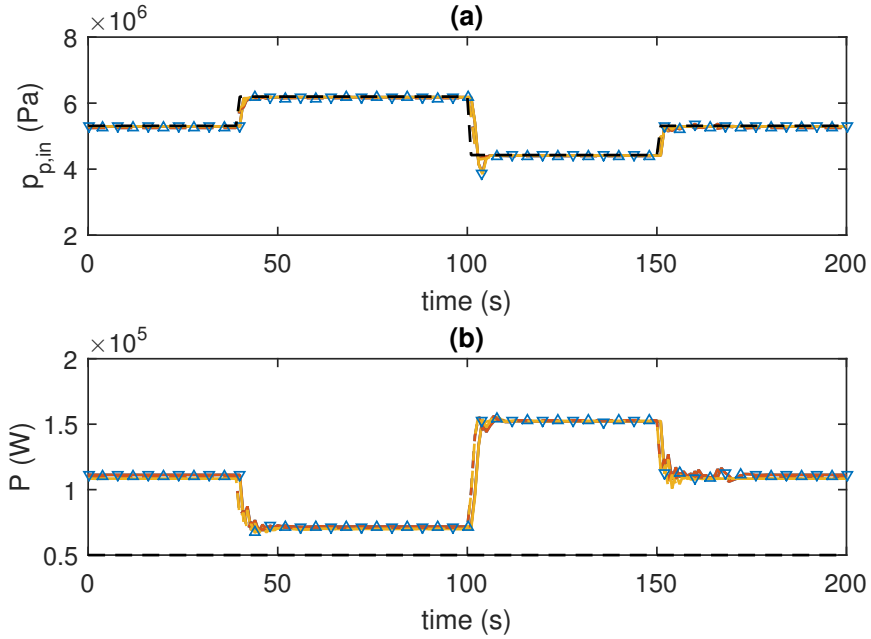

Figure 4.9: Outputs - filter performance test: (a) $p_{p,in}$; (b) P. (- - - -) reference trajectory, (- △ -) SKF1-MPC real system trajectory, (—▽—) SKF1-MPC estimated trajectory, (- - - -) SKF2-MPC real system trajectory, (——) SKF2-MPC estimated trajectory, (- - - -) EKF-MPC real system trajectory, (——) EKF-MPC estimated.

As one can seen, the three strategies presented a very similar performance with an accurate estimation of the states, resulting in an offset free inlet pressure and a minimum pump power consumption. The scheduling strategies present the advantages of not requiring the availability of a nonlinear model to proceed the every sampling time linearization and the fact that its models can be developed with identification techniques from real data of the process, while it presents the disadvantage of the so called "curse of dimensionality" (BELLMAN, 1957), in which the number of models needed to represent the nonlinear system grows significantly with the size of the system.

Figure 4.10 shows the states estimated by the three strategies.

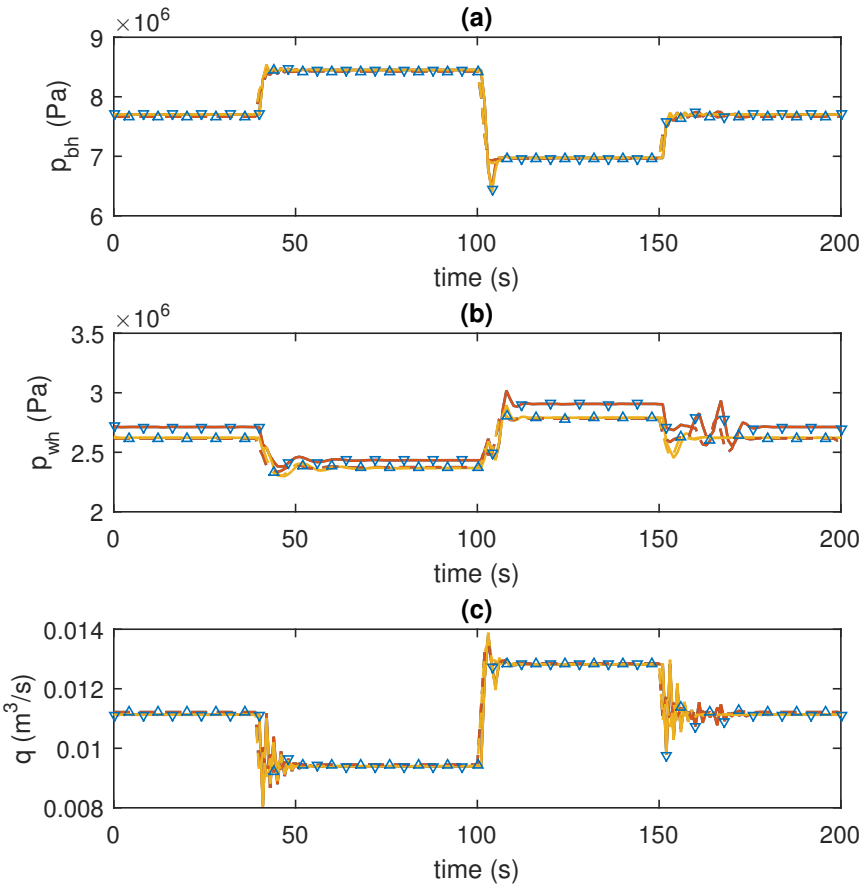

Figure 4.10: States - filter performance test: (a) p_{bh}; (b) p_{wh}; (c) q. (- - - -) reference trajectory, (- △ -) SKF1-MPC real system trajectory, (—▽—) SKF1-MPC estimated trajectory, (- - - -) SKF2-MPC real system trajectory, (——) SKF2-MPC estimated trajectory, (- - - -) EKF-MPC real system trajectory, (——) EKF-MPC estimated trajectory.

All the states were well represented compared to the real system, only for p_{wh} the scheduling techniques left a slight offset between real system and estimated values, this estimation offset is an indicative that the model net applied is not as accurate as the successive linearization, but this difference has not produced any

effect in the controlled and manipulated variables, as one can see in Figure 4.11.

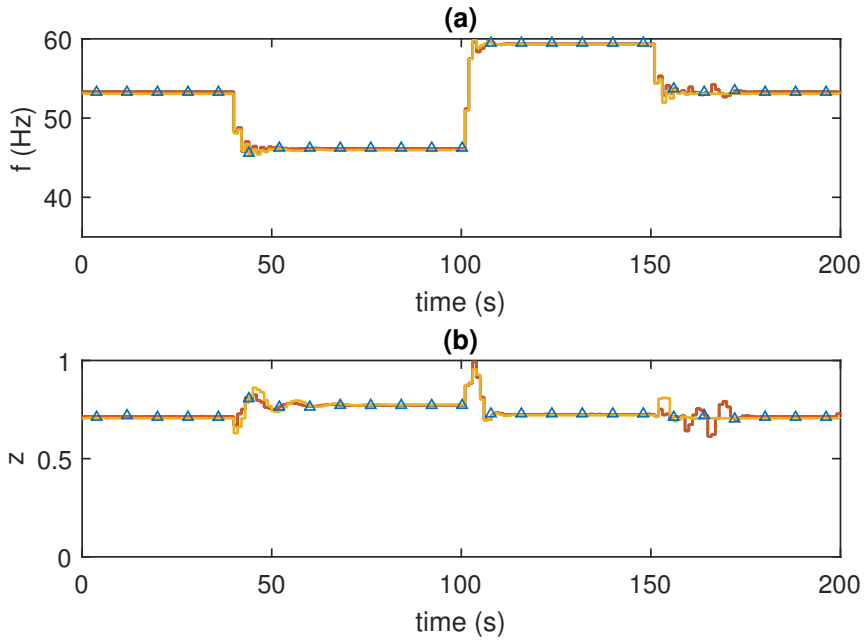

Figure 4.11: Inputs - filter performance test: (a) f; (b) z. (—△—) SKF1-MPC trajectory, (——) SKF2-MPC trajectory, (——) EKF-MPC trajectory.

The previous tests proved that the Kalman Filter scheme presents a great performance estimating the states variables, even though no state measurement is available. To evaluate the performance of the estimation while each state measurement is lost, Table 4.7 shows the SSE between the estimation and the real trajectories for all possible combinations of state measurement availability. The performance test carried out was the same setpoint tracking test presented in Section 4.2.2.

Table 4.7: SSE in SKF1-MPC performance test for different state measurement availability.

Measurements	p_{bh}	p_{wh}	q	$p_{p,in}$	P
all	2.25E+12	1.01E+11	2.62E-05	3.26E+12	4.63E+09
p_{wh} and q	2.25E+12	1.01E+11	2.62E-05	3.26E+12	4.62E+09
p_{bh} and q	2.25E+12	1.06E+11	2.66E-05	3.26E+12	4.68E+09
p_{wh} and p_{bh}	2.24E+12	1.03E+11	2.68E-05	3.25E+12	4.64E+09
p_{bh}	2.24E+12	1.04E+11	2.69E-05	3.25E+12	4.66E+09
q	2.25E+12	1.06E+11	2.66E-05	3.26E+12	4.68E+09
p_{wh}	2.24E+12	1.02E+11	2.68E-05	3.25E+12	4.64E+09
none	2.23E+12	1.04E+11	2.70E-05	3.25E+12	4.66E+09

As expected the SSE decreases in the direction of more available measurements for most estimated variables, indicating a better filtering performance when more

measures are available. However, this difference can be practically neglected, as the distance when all measures are available to none is very small, resulting in a very similar performance. It is also important to highlight that the previous results presented for the interpolation strategies were precisely equivalent.

4.3.3 Control Performance

Figures 4.12, 4.13 and 4.14 show the control performance in a low to high intake pressure setpoint change test, respectively to, output, input and state variables. In Figure 4.12 one can see that for both output variables, $p_{p,in}$ and P, the SKF1-MPC and SKF2-MPC presented an equivalent response and similar to the EKF-MPC in terms of estimated and real system trajectories. The only deviation were between 20 and 30 seconds, in which the real system goes to the opposite direction of what the estimation predicts for the three strategies, that may be due to the saturation of the pump frequency in the lower bound, which can be observed in Figure 4.13(a). In spite of that, all strategies were able to direct the real system to the high intake pressure setpoint without leaving an offset between real and estimated outputs keeping the lower power consumption possible.

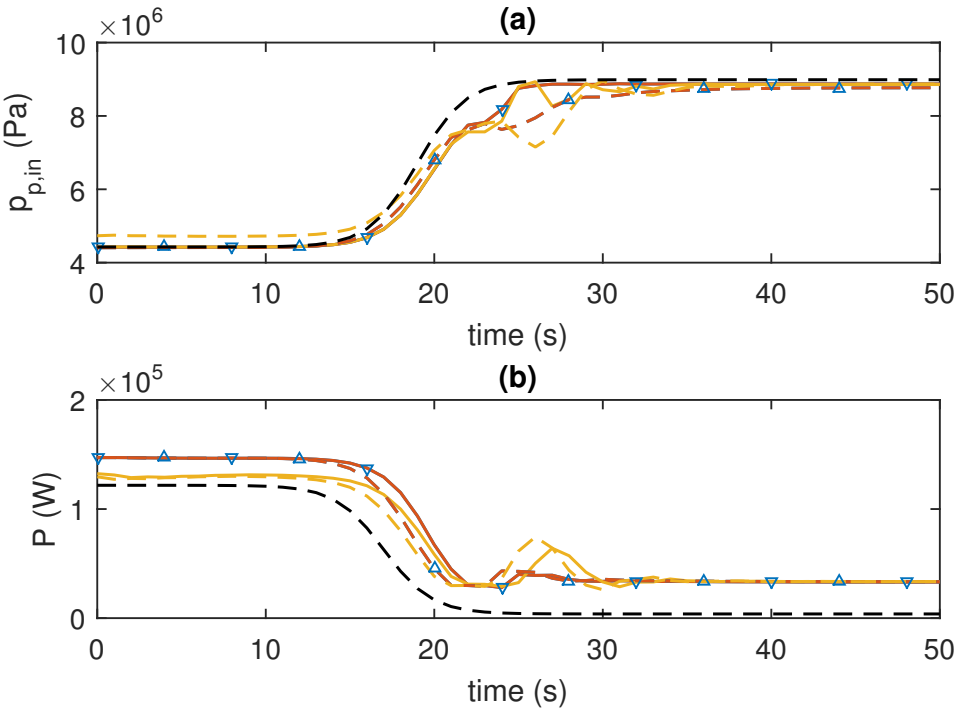

Figure 4.12: Outputs - control performance test - low to high intake pressure setpoint change: (a) $p_{p,in}$; (b) P. (- - - -) reference trajectory, (-△- -) SKF1-MPC real system trajectory, (—▽—) SKF1-MPC estimated trajectory, (- - - -) SKF2-MPC real system trajectory, (——) SKF2-MPC estimated trajectory, (- - - -) EKF-MPC real system trajectory, (——) EKF-MPC estimated trajectory.

Figure 4.13 presents the trend of the input variables, we can see that both inputs goes from a near upper bound value to a near lower bound value, what can be expected from the characteristics of the carried out test. It is noteworthy that the frequency saturates around 23 minutes in the lower bound, what is undesired since there is the loss of this degree of freedom to the MPC scheme to keep control of the system, therefore the intake pressure setpoint transition might be softened or the MPC must be better tuned to present a less aggressive behavior.

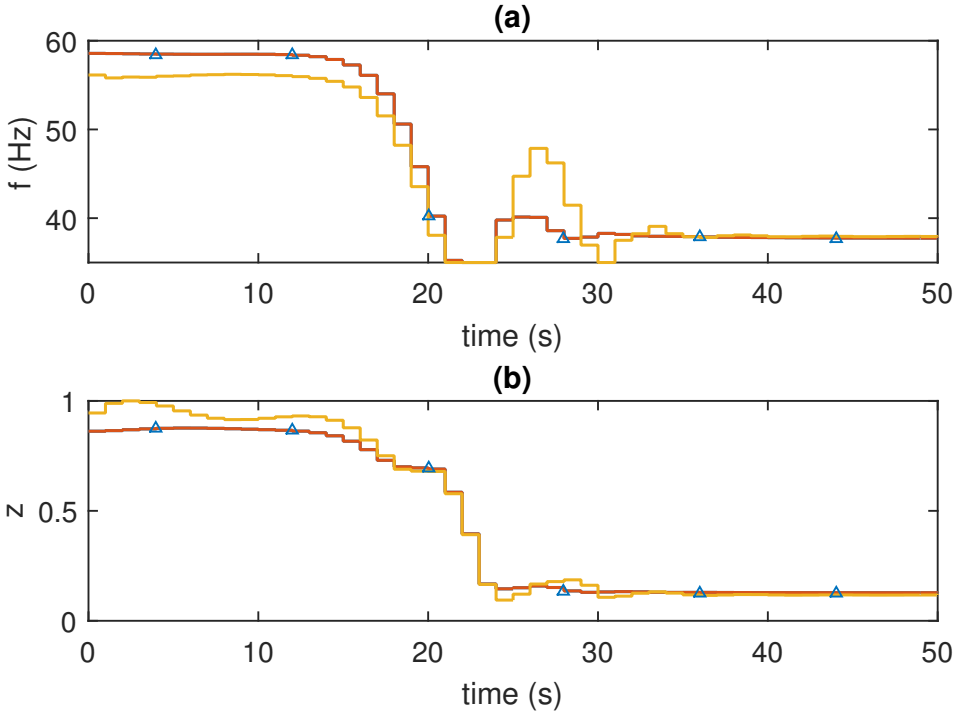

Figure 4.13: Inputs - control performance test - low to high intake pressure setpoint change: (a) f; (b) z. (—△—) SKF1-MPC trajectory, (——) SKF2-MPC trajectory, (——) EKF-MPC trajectory.

Figure 4.14 presents the behavior of the state variables. One can see that the three approaches were able to predict the state variables without leaving an offset between the real system and the estimation, what is a great benefit since these variables were considered unmeasured for the control and filter schemes. The only divergence was around the minute 25, already discussed before, when the frequency saturates in the lower bound.

All the results presented a reasonable profile, since the performance test was to increase the pump intake pressure, it is expected to also increase the bottom hole and the well head pressures, reduce the choke opening, what would lead to a decrease in the fluid flow rate, and therefore the pump frequency and the pump power would also decrease.

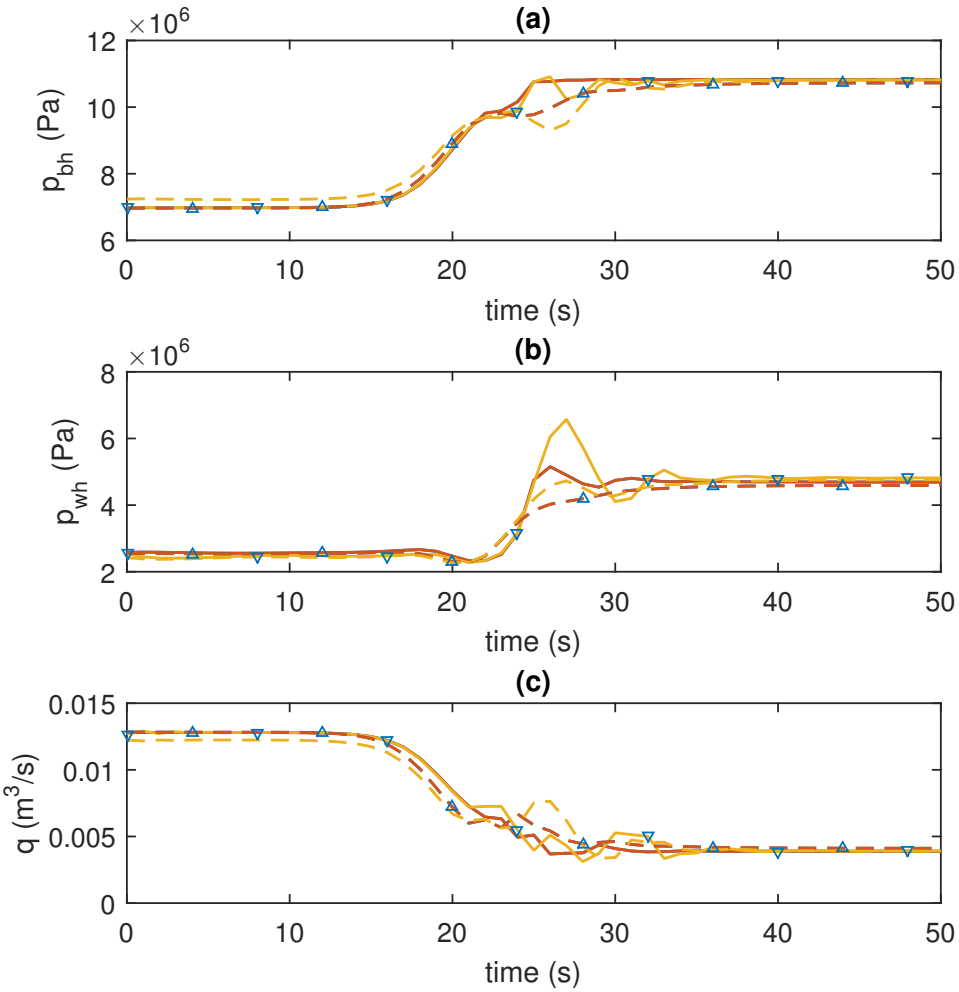

Figure 4.14: States - control performance test - low to high intake pressure setpoint change: (a) p_{bh}; (b) p_{wh}; (c) q. (- - - -) reference trajectory, (-△-) SKF1-MPC real system trajectory, (—▽—) SKF1-MPC estimated trajectory, (- - - -) SKF2-MPC real system trajectory, (——) SKF2-MPC estimated trajectory, (- - - -) EKF-MPC real system trajectory, (——) EKF-MPC estimated trajectory.

Figures 4.15, 4.16 and 4.17 show the control performance in a high to low intake pressure setpoint change test, respectively, to output, input and state variables.

In Figure 4.15 one can see that for both output variables, $p_{p,in}$ and P, the SKF1-MPC and the SKF2-MPC presented an equivalent response, similar to the EKF-MPC trajectory in terms of the real system and the estimated trajectories. All strategies were able to direct the real system to the low intake pressure setpoint without leaving an offset between real and estimated outputs and keeping the lower power consumption possible. It is important to highlight that the EKF-MPC presented a slightly different trajectory for the pump power consumption in comparison to the interpolation strategies. That can be explained by observing, in Figure 4.16, that in this scheme the input variables also took different trajectories, what led to different power consumption.

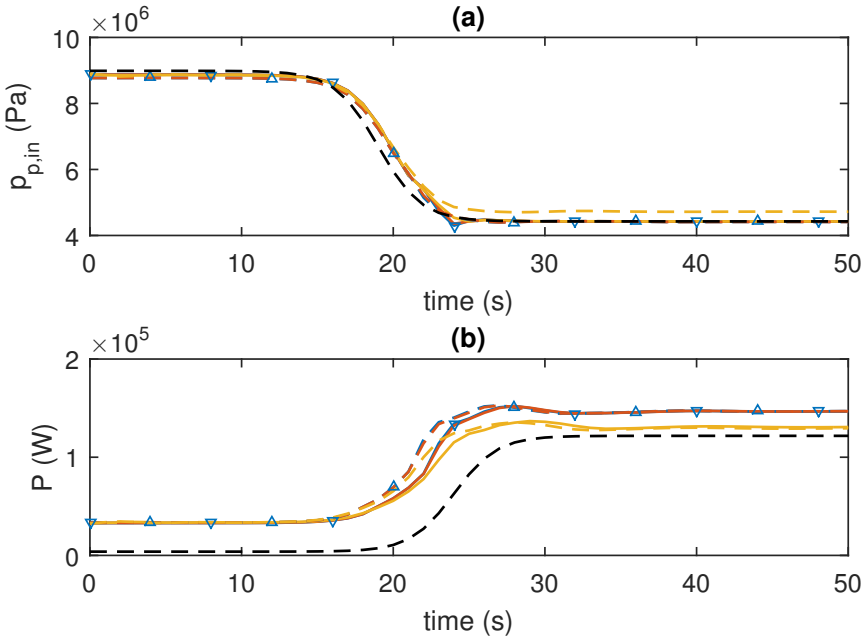

Figure 4.15: Outputs - control performance test - high to low intake pressure setpoint change: (a) $p_{p,in}$; (b) P. (- - - -) reference trajectory, (-△-) SKF1-MPC real system trajectory, (—▽—) SKF1-MPC estimated trajectory, (- - - -) SKF2-MPC real system trajectory, (——) SKF2-MPC estimated trajectory, (- - - -) EKF-MPC real system trajectory, (——) EKF-MPC estimated trajectory.

Figure 4.16 shows the trend of the input variables, we can see that both inputs go from a near lower bound value to a near upper bound value, what can be expected from the characteristics of the carried out test.

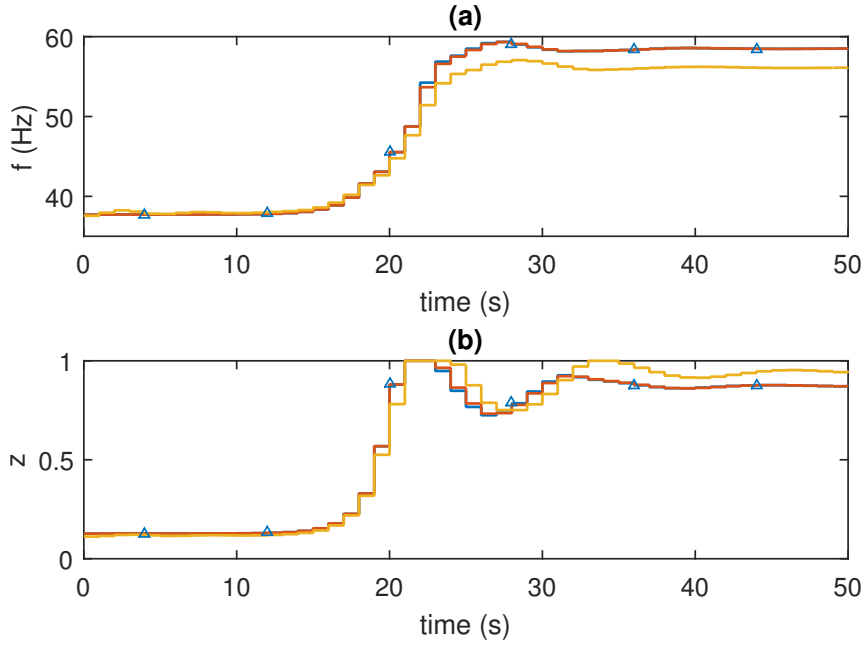

Figure 4.16: Inputs - control performance test - high to low intake pressure setpoint change: (a) f; (b) z. (—△—) SKF1-MPC trajectory, (——) SKF2-MPC trajectory, (——) EKF-MPC trajectory.

Here we can see that the frequency has not saturated for any case but the choke opening has saturated around 23 and 35 minutes in the upper bound, what is undesired due to loss of degrees of freedom, as previously pointed out. In spite of that, the choke saturation have not produced a performance problem in the output or state variables.

Figure 4.17 presents the behavior of the state variables. One can see that both SKF strategies and EKF were able to predict the state variables without offset to the real system, what is a great benefit since these variables were considered unmeasured for the control and filter schemes.

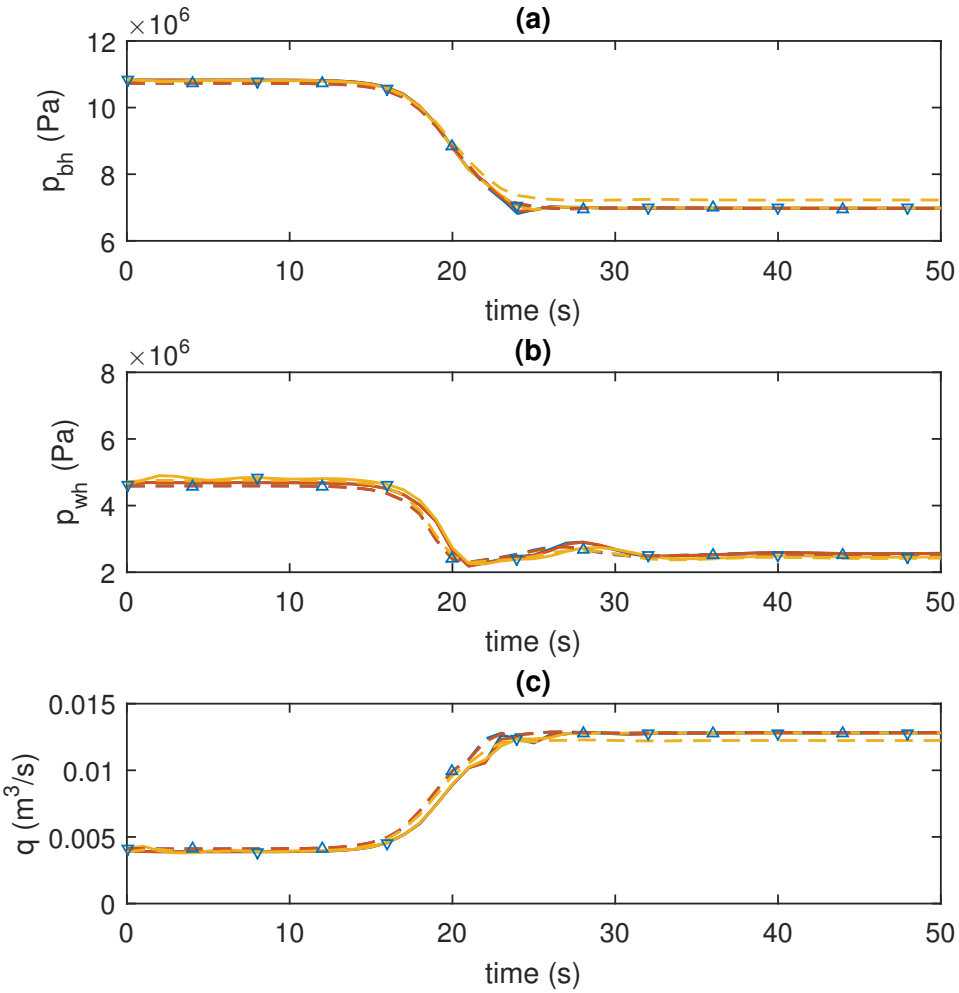

Figure 4.17: States - control performance test - high to low intake pressure setpoint change: (a) p_{bh}; (b) p_{wh}; (c) q. (- - - -) reference trajectory, (-△-) SKF1-MPC real system trajectory, (—▽—) SKF1-MPC estimated trajectory, (- - - -) SKF2-MPC real system trajectory, (——) SKF2-MPC estimated trajectory, (- - - -) EKF-MPC real system trajectory, (——) EKF-MPC estimated trajectory.

All the results presented a reasonable profile, since the performance test was to decrease the pump intake pressure, it is expected to also decrease the bottom hole and the well head pressures and so, the increase in the choke opening is

also expected. With that, the fluid flow rate would also increase, increasing the pump frequency and so the pump power. One can observe a slightly oscillatory behaviour in the well head pressure, that might be explained due to the oscillatory behavior of the choke opening presented in Figure 4.16(b).

It is important to highlight that for all previous results showed, both interpolation strategies produced equivalent responses in the tests for SKF1-MPC and SKF2-MPC. Even though, the multivariable homotopy is not a linear strategy due to the arise of higher order terms, it presented equivalent results compared to the linear interpolation strategy. One advantage of using multivariable homotopy is in terms of code implementation, it is very straightforward and does not requires a previous search algorithm to locate the active region where the interpolation takes place. In the other hand, it is very difficult to generalize it in mathematical notation and the arise of higher order terms can be a problem in bigger nets when compared to the multivariable linear interpolation.

4.3.4 Model Structural Uncertainty Problem

The present chapter addresses the problem of uncertainty in measurements, but nothing is done about model structural uncertainty, that is the uncertainty in the parameters or equations of the model. A common problem in the regard of ESP systems is the unknown viscosity of the fluid as introduced by BINDER *et al.* (2015). In all results previously presented, the viscosity is considered a known and unchanged parameter, however it might suffer disturbances due to increase of water flow in the well, as discussed in KRISHNAMOORTHY *et al.* (2016). Figure 4.18 shows a simple disturbance in the viscosity value, that is a step from the oil production directly to water production.

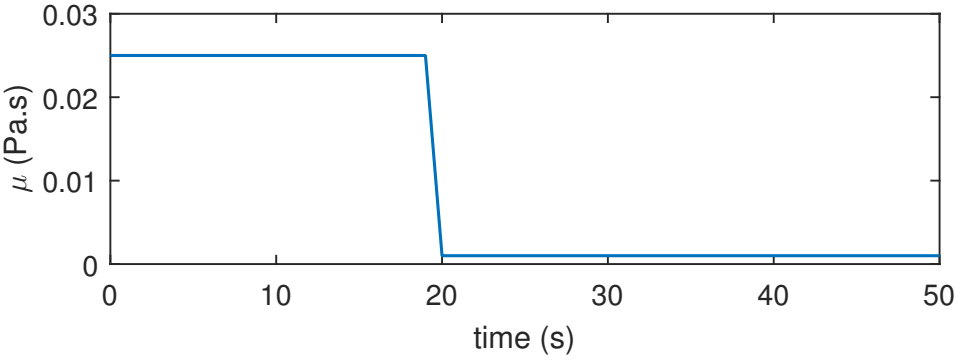

Figure 4.18: Simple disturbance in viscosity from oil production directly to water production.

This profile has not the real dynamics of the disturbance, as it neglects the emulsion formation, but it serves to illustrates the problems with the presented

approach if this model uncertainty is present.

Figure 4.19 shows the result of the viscosity disturbance in the output variables. One can see that the control scheme does not feel the viscosity change and does not act over it. Since the Kalman Filter strategy is not able to predict its variation what is observed is a great offset between predicted and real outputs. That is because the viscosity is not considered in the linear model. Next chapter is dedicated to overcome this issue in the proposed strategy keeping the interpolations proposition in a parameter estimation scheme.

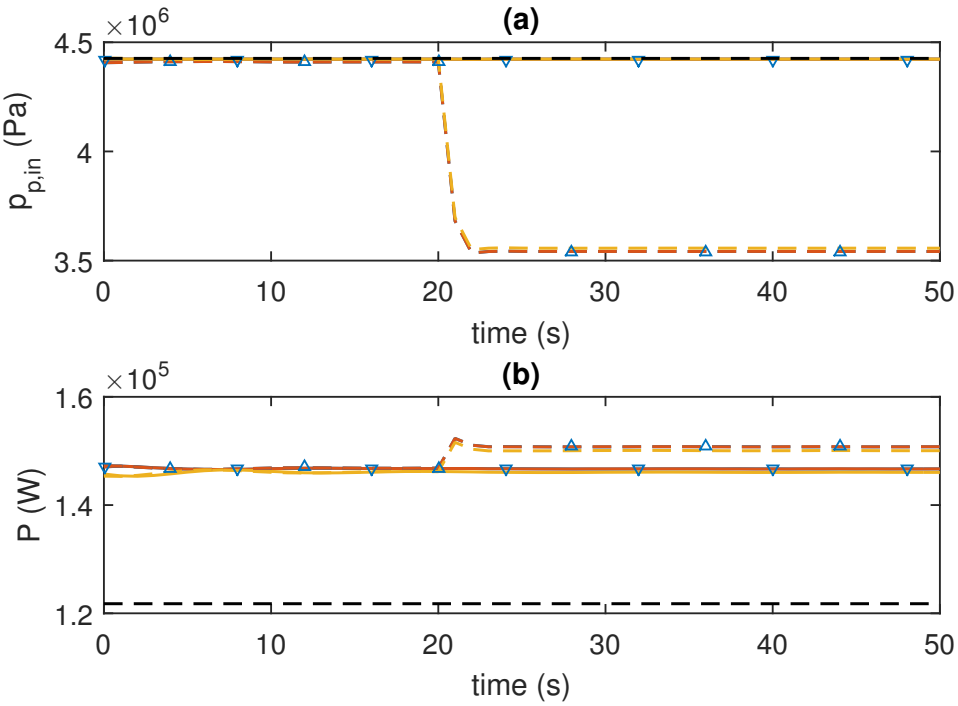

Figure 4.19: Outputs - proposed schemes performance over a disturbance in viscosity: (a) $p_{p,in}$; (b) P. (----) reference trajectory, (-△-) SKF1-MPC real system trajectory, (—▽—) SKF1-MPC estimated trajectory, (----) SKF2-MPC real system trajectory, (——) SKF2-MPC estimated trajectory, (----) EKF-MPC real system trajectory, (——) EKF-MPC estimated trajectory.

4.4 Conclusions

In this chapter, the problem of lack of measurements of the state variables due to the extreme subsea environment is addressed. A single linear model strategy was proved to be insufficient in a MPC coupled with a KF and two multi-model techniques based on model net interpolations were successfully applied to an adaptive MPC coupled with SKF, they presented an equivalent performance between each other and a similar performance compared to the EKF strategy. The main advantage of the SKF schemes over the EKF is not needing an available nonlinear model to proceed linearization. The proposed schemes presented a high accurate state

estimation capability with a great performance over the whole nonlinear range of operation. However, the schemes proved to be insufficient to overcome model structural uncertainty, as introduced by a fluid viscosity disturbance. Therefore, more sophisticated parameter estimation technique must be coupled to the SKF-MPC strategies to overcome this issue.

Chapter 5

Robust Multi-model State-space MPC for Measurement and Model Uncertainty

5.1 Introduction

This chapter presents a methodology to enhance the algorithm presented in Chapter 4 in order to cope with model structural uncertainty in a Robust MPC scheme. This is done by developing a parameter estimation strategy to estimate the viscosity based on the output measurements. As in Chapter 4, all state measurements are considered to be unavailable, so only the measurements of the outputs are used in order to observe the states and the parameter values.

BINDER *et al.* (2015) introduce the problem of uncertainty in the flow rate measurement and in viscosity and PI parameters. They propose a nonlinear MHE to estimate these variables based on the measurements of the output variables and the bottom hole and well pressures. However, the control performance coupled with the proposed soft-sensor methodology is not presented. Hence, in this chapter we propose a parameter estimation strategy based on the maximization of the probability of occurrence of the linear model, using the parameter as a degree of freedom, in a Kalman Filter scheme. A soft-sensor of the parameter is proposed to be coupled with a Kalman Filter to estimate the states and filter the output measurements, so that this information is used to select the proper linear model from the interpolation strategy of the model net and the linear MPC is fed with the model and the actual states in order to provide the control action.

The methodology presented in this chapter is able to produce a robust linear MPC that can deal with process nonlinearity, measurement uncertainty and model structural uncertainty with no requirement of having a phenomenologi-

cal modeling of the process. The methodology is an alternative to more complex and CPU intensive algorithms such as NMPC, set-based estimation techniques (GONÇALVES *et al.*, 2016) or scenario tree estimation in a min-max apporach (IVO, 2018).

5.2 Methodology

5.2.1 Model Scheduling Strategy

The strategy for model scheduling was the same as proposed in Chapter 4, but to take the viscosity into account, the model net was expanded in the direction of the viscosity. Figure 5.1 illustrates a 3-D net of linear models.

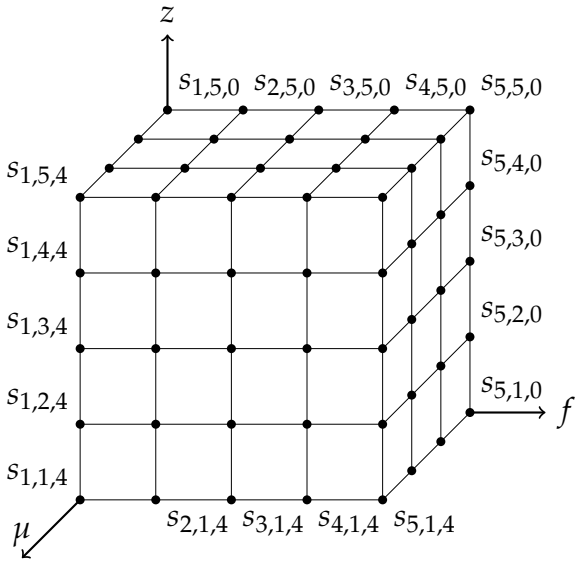

Figure 5.1: Example of a 3-D net of linear models.

As in Chapter 4, each node of the 3-D model net represents a linear model obtained for different operational points in different values of f, z and μ. The same scheduling strategies are applied, here we will refer to these strategies, respectively, as:

- SKF1-MPC: The approach making use of the homotopic interpolation to obtain the linear model for the Kalman Filter and for the MPC.
- SKF2-MPC: The approach making use of the multivariable linear interpolation to obtain the linear model for the Kalman Filter and for the MPC.
- EKF-MPC: The approach making use of linearization around the operational point, as presented in Appedix A, to obtain the linear model for the Kalman Filter and for the MPC.

More details about the formulation of the interpolations can be found in Section 4.2.1.

5.2.2 Optimal Model Net Structure

To determine the optimal nodes of the model net in the dimension of the parameter, an extension of the structure obtained in Section 4.2.2 is proposed. So, from the elected 2-D model net structure in Section 4.3.1, the net was expanded in the direction of the parameter from two to six nodes. Let θ denotes the concatenation of the model net nodes, such that $\theta = (\bar{f}^T, \bar{z}^T, \bar{\mu}^T)^T$, the metric to determine the optimal structure was the SSE from the nonlinear model and the response of the model net. The optimal nodes for the parameter was obtained from the following optimization problem:

$$\begin{aligned}\min_{\theta} \sum_{j=1}^{N_f}\sum_{i=1}^{p}\left(\frac{y_i^{NL}(f_j,z,\mu)-y_i^{L}(f_j,z,\mu)}{y_i^{NL}(f_j,z,\mu)}\right)^2\Bigg|_{z=0.99,\mu=0.025} + \\ \sum_{j=1}^{N_z}\sum_{i=1}^{p}\left(\frac{y_i^{NL}(f,z_j,\mu)-y_i^{L}(f,z_j,\mu)}{y_i^{NL}(f,z_j,\mu)}\right)^2\Bigg|_{f=58,\mu=0.025} + \\ \sum_{j=1}^{N_\mu}\sum_{i=1}^{p}\left(\frac{y_i^{NL}(f,z,\mu_j)-y_i^{L}(f,z,\mu_j)}{y_i^{NL}(f,z,\mu_j)}\right)^2\Bigg|_{f=58,z=0.99}\end{aligned} \tag{5.1a}$$

s.t.

$$x^L(f,z,\mu) = (I - A(f,z,\mu))^{-1}B(f,z,\mu)u \tag{5.1b}$$

$$y^L(f,z,\mu) = C(f,z,\mu)x^L(f,z,\mu) + D(f,z,\mu)u \tag{5.1c}$$

$$x^{NL}(f,z,\mu) = F(f,z,\mu) \tag{5.1d}$$

$$y^{NL}(f,z,\mu) = G(x^{NL},f,z,\mu) \tag{5.1e}$$

$$\bar{f} = [58.5, 51.12, 44.42, 38.42]^T \tag{5.1f}$$

$$\bar{z} = [0.89, 0.54, 0.34, 0.2, 0.08]^T \tag{5.1g}$$

$$35 \leq f \leq 60 \tag{5.1h}$$

$$0 \leq z \leq 1 \tag{5.1i}$$

$$0 \leq \mu \leq 0.5 \tag{5.1j}$$

in which, x^L and y^L are the static states and outputs from the linearization strategy, x^{NL} and y^{NL} are the static states and outputs from the nonlinear model, denoted by F and G.

5.2.3 Parameter Estimation Strategy

The parameter estimation strategy proposed is based on a discrete multi-model estimation technique presented in SIMON (2006). The main difference is that the author presented a strategy for the case in which the parameter can only assume some values in a limited scenario of possibilities. Here we present an extension of that strategy for the case in which the parameter can assume any value in a continuous bounded range.

The main idea is to maximize the probability of occurrence of the linear model by having the parameter as a degree of freedom and giving that a measurement of the system is obtained for the previous sampling time. To begin the formulation, one must remember the Bayes' rule and some proprieties of probability:

$$\Pr(x|y) = \frac{\Pr(y|x)\Pr(x)}{\Pr(y)} \tag{5.2}$$

That is, the probability of occurrence of an event x given the fact that an event y has occurred is equal to the probability of occurrence of an event y given the fact that an event x has occurred times the probability of occurrence of an event x over the probability of occurrence of an event y. If the event x can assume any value value in a continuous bounded range (x_i, x_s), then the pdf of occurrence of an event y can be written as:

$$\text{pdf}(y) = \int_{x_i}^{x_s} \text{pdf}(y|x)\text{pdf}(x)dx \tag{5.3}$$

Since now we are dealing with continuous range, the probability of a single value does not play any role, therefore the discussion is carried out in terms of a probability density function (pdf). Hence, Equation 5.2 can be rewritten as:

$$\text{pdf}(x|y) = \frac{\text{pdf}(y|x)\text{pdf}(x)}{\int_{x_i}^{x_s} \text{pdf}(y|x)\text{pdf}(x)dx} \tag{5.4}$$

To put it in context, let q denotes the set of matrices that define the linear state-space model (A, B, C, D, Q, R) that is a function of parameter μ, which can vary in the range (μ_i, μ_s). Now, let the events be the occurrence of a model $q(\mu)$ giving

the fact that a measurement y_k is available, so the pdf can be written as:

$$\text{pdf}(q(\mu)|y_k) = \frac{\text{pdf}(y_k|q(\mu))\text{pdf}(q(\mu))}{\int_{\mu_i}^{\mu_s} \text{pdf}(y_k|q(\mu))\text{pdf}(q(\mu))d\mu} \tag{5.5}$$

Now, we shall discuss each element of Equation 5.5 in order to come to a final formulation. If $\mu = \hat{\mu}$, then $q(\mu) = q(\hat{\mu})$ and a Kalman Filter can be carried out for this model, if the estimation is accurate then the real state variable $x_k \approx \hat{x}_k^-$ and the measured output will approximate the value predicted by the model $y_k \approx C\hat{x}_k^- + Du_k + v_k$, so the $\text{pdf}(y_k|q(\hat{\mu})) \approx \text{pdf}(y_k|\hat{x}_k^-) = \text{pdf}(y_k - C\hat{x}_k^- - Du_k) = \text{pdf}(r_k)$. Therefore, if w_k, v_k and x_0 are Gaussian, then the filter residue, r_k, is also Gaussian and it can be showed that:

$$\text{pdf}(y_k|q(\hat{\mu})) = \frac{\exp(-r_k^T S_k^{-1} r_k/2)}{(2\pi)^{p/2}|S_k|^{1/2}} \tag{5.6}$$

in which, p is the number of measured outputs and S_k is the covariance matrix of the Kalman Filter.

Also from Bayes' rule, one can write the pdf of $q(\mu) = q(\hat{\mu})$ giving the fact that the measurement of the previous sampling time, y_{k-1} is observed:

$$\text{pdf}(q(\hat{\mu})|y_{k-1}) = \frac{\text{pdf}(y_{k-1}|q(\hat{\mu}))\text{pdf}(q(\hat{\mu}))}{\text{pdf}(y_{k-1})} \tag{5.7}$$

Considering the fact that at a time k the measurement y_k is already given, so $\text{pdf}(y_{k-1}) = \text{pdf}(y_{k-1}|q(\hat{\mu})) = 1$ and Equation 5.7 is reduced to:

$$\text{pdf}(q(\hat{\mu})|y_{k-1}) = \text{pdf}(q(\hat{\mu})) \tag{5.8}$$

Finally, Equation 5.5 can be modified, based on previous comments, to its final form:

$$\text{pdf}(q(\hat{\mu})|y_k) = \frac{\text{pdf}(y_k|q(\hat{\mu}))\text{pdf}(q(\hat{\mu})|y_{k-1})}{\int_{\mu_i}^{\mu_s} \text{pdf}(y_k|q(\hat{\mu}))\text{pdf}(q(\hat{\mu})|y_{k-1})d\mu} \tag{5.9}$$

Equation 5.9 shows that it is possible to obtain the pdf of occurrence of the model given the actual measurement by having the pdf of occurrence of the ac-

tual measurement given the model, which can be calculated by Equation 5.6, and the pdf of occurrence of the model given the last measurement. In order to enable this calculation process, the pdf can be parameterized in order to pass the pdf from an iteration to the next. Here, the assumption made is that the pdf of occurrence of the model given the actual measurement is a Gaussian shaped distribution, so in each sampling time, one must just estimate the mean and the variance of the distribution to obtain the full pdf and pass them to the next iteration. In addition, the mean is the most probable occurrence of the model in a Gaussian distribution, and therefore the most probable value for the parameter can be obtained by maximizing the pdf in Equation 5.9. The Gaussian shape distribution is an assumption, but even if the real distribution is in fact Gaussian, the fact that the search space is bounded creates non-modelled regions, in which there will be no distribution at all, so the methods to obtain the mean and the variance of the pdf were estimated by formulating two optimization problems. The mean is obtained by the following:

$$\hat{\mu}_k = \arg\max_{\hat{\mu}} \text{pdf}(q(\hat{\mu})|y_k) \tag{5.10a}$$

$$\text{s.t. } 0 \leq \hat{\mu} \leq 0.5 \tag{5.10b}$$

As in a Gaussian distribution three standard deviations from the mean corresponds to an area of 49.86% of the area of the distribution, the following optimization is proposed to obtain an auxiliary value of parameter that corresponds to the area of three standard deviations:

$$\hat{\mu}_k^{aux} = \arg\min_{\hat{\mu}} \left(0.4986 - \int_{\mu_k}^{\hat{\mu}} \text{pdf}(q(\mu)|y_k)d\mu\right)^2 \tag{5.11a}$$

$$\text{s.t. } 0 \leq \hat{\mu} \leq 0.5 \tag{5.11b}$$

After obtaining $\hat{\mu}_k^{aux}$ it is possible to model the distribution variance:

$$\sigma_k^2 = \left(\alpha \frac{\hat{\mu}_k^{aux} - \hat{\mu}_k}{3}\right)^2 \tag{5.12}$$

in which, α is a scaling factor, settled to 2.5, in order not to let the variance be too small so that the strategy cannot return from different values of the parameter

after a long period of stability. With that said, it is possible to model the pdf of the model given the measurement as a Gaussian distribution:

$$\text{pdf}(q(\hat{\mu})|y_k) = \mathcal{N}(\hat{\mu}_k, \sigma_k^2) \tag{5.13}$$

5.2.4 MPC Implementation

The MPC strategy was implemented as an on-line nonlinear program (NLP), solved by an interior-point solver, coupled with an observer to estimate the unmeasured states and a parameter estimation strategy to estimate the fluid viscosity. This methodology is illustrated in Section 5.2.5. As in Chapter 4, the internal model is a linear discrete state-space with an adaptive strategy based on the manipulated variables and parameter values at the beginning of the prediction horizon. The control law is determined in a receding horizon manner by the solution of the following optimization problem at each sampling time.

$$\min_{\Delta u} \sum_{i=1}^{L} \left\| y_{k+i} - y_{k+i}^{rt} \right\|_{W_y}^2 + \sum_{i=0}^{N} \left[\left\| u_{k+i} - u_{k+i}^{rt} \right\|_{W_u}^2 + \left\| \Delta u_{k+i} \right\|_{W_{\Delta u}}^2 \right] \tag{5.14a}$$

s.t. $\forall k \in [0, L]$, in which L is the prediction horizon

$$x(k+1) = A(u(0), \hat{\mu})x(k) + B(u(0), \hat{\mu})u(k) \tag{5.14b}$$

$$y(k) = C(u(0), \hat{\mu})\hat{x}(k) + D(u(0), \hat{\mu})u(k) \tag{5.14c}$$

$$\begin{aligned} \hat{x}(k+1) = {} & A(u(0), \hat{\mu})x(k+1) + B(u(0), \hat{\mu})u(k) + \\ & K\left(y^m(0) - C(u(0), \hat{\mu})x(0) - D(u(0), \hat{\mu})u(0)\right) \end{aligned} \tag{5.14d}$$

$$x(0) = \hat{x}(0) \tag{5.14e}$$

$$x^{lb} \leq \hat{x}(k) \leq x^{ub} \tag{5.14f}$$

$$u^{lb} \leq u(k) \leq u^{ub} \tag{5.14g}$$

$$\Delta u^{lb} \leq \Delta u(k) \leq \Delta u^{ub} \tag{5.14h}$$

in which, $\hat{\mu}$ is the estimated value of the fluid viscosity by the estimator described in Section 5.2.5. More information about the MPC implementation details can be found in Appendix B and the observer theory is explored in Section 2.4.

Control objectives remain the same introduced in Chapter 3 and Chapter 4, that consist in keeping ESP inlet pressure at a desirable setpoint within the minimum pump power consumption. The objective priorities also remain the same, in order from higher to lower priority, they are constraints satisfaction, intake pressure setpoint tracking and pump power minimization.

The cost function weight matrices were selected properly to respect the control priority, in which weights for inlet pressure and power are 400 and 0.02, respectively, weights for inputs were set to zero and for the rate of change of inputs were equal to 5 for pump frequency and 0.5 for choke opening. The sampling time, the prediction horizon and the control horizon were set at $1s$, $100s$ and $5s$, respectively. It is important to note that internal models were modelled in a relative deviation manner, as described in Appendix A, so the previous numbers are applied to the normalized variables.

5.2.5 Algorithm Scheme

Appendix 5.2 illustrates the algorithm scheme of the proposed methodology.

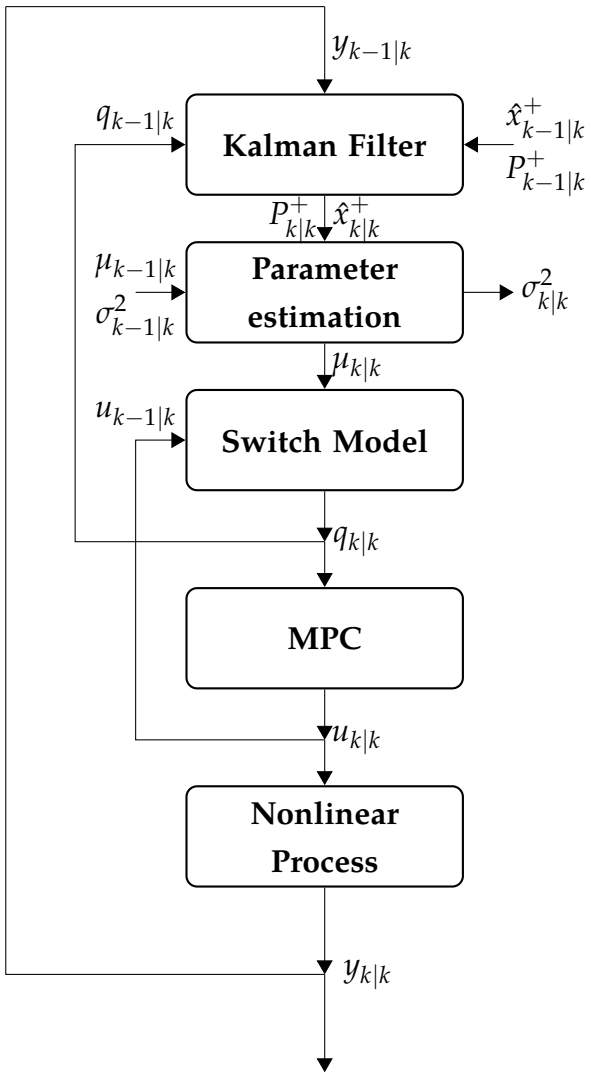

Figure 5.2: Algorithm scheme of the parameter estimation coupled with the KF-MPC

The iteration k begins with a Kalman Filter algorithm, making use of the infor-

mation obtained in the previous iteration $k-1$, they are the output measurements, $y_{k-1|k}$, the *a posteriori* error covariance matrix, $P^{+}_{k-1|k}$, the *a posteriori* state estimate, $\hat{x}^{+}_{k-1|k}$, and the linear model from the model switching strategy of the previous iteration, $q_{k-1|k}$, which in the SKF approaches are the interpolation strategies described in Section 5.2.1. In the EKF approach, it is the classical linearization from the nonlinear model around the operation point.

The Kalman Filter provides the actual *a posteriori* error covariance matrix, $P^{+}_{k|k}$, and the *a posteriori* state estimate, $\hat{x}^{+}_{k|k}$, to the Parameter Estimation routine, which solves the two optimization problems introduced in Section 5.2.5. This step assumes that the pdf of occurrence of the internal model is a Gaussian-shaped distribution and uses the uncertain parameter as a degree of freedom in order to obtain the parameter value in which the pdf reaches its maximum, which is in the average value, $\mu_{k|k}$. To do so, the routine receives the mean, $\mu_{k-1|k}$, and covariance, $\sigma^2_{k-1|k}$, estimated in the previous iteration and provides parameter value to the model switching strategy.

In the Model Switching block, the internal model is obtained by using the information of the inputs from the previous iteration, $u_{k-1|k}$, and the parameter which has been estimated in order to provide the set of matrices that define the linear model, here denoted by $q_{k|k}$, to the MPC scheme. This block makes use of two strategies depending on the approach, the proposed interpolations between models obtained in different points of operation, these strategies are being called as SKF, and the successive linearization from the nonlinear model, which is a consolidated technique that is being used in order to validate the proposed interpolation strategy, here mentioned as EKF.

The MPC routine runs the optimization problem, described in Section 5.2.4, in a receding horizon manner making use of the linear model provided by the switching model strategy in order to provide the control law, $u_{k|k}$, to be implemented in the system. More details about the MPC algorithm can be found in Appendix B. After implementing the control law in the nonlinear system, a new measurement is available and the algorithm returns to its initial point.

5.2.6 Control and Parameter Estimation Performance

The control performance is evaluated, as in Chapter 4, by two setpoint tracking problems subjected to the two proposed SKF coupled with MPC schemes and compared to the classical EKF-MPC. The first test is a low to high intake pressure, from 5.7 MPa to 8.1 MPa, and the second one is a high to low intake pressure, from 9 MPa to 5.7 MPa. These tests force the system from a situation of high choke valve opening to a low choke valve opening and from a low choke valve opening

to a high choke valve opening, passing through the whole nonlinear region of the operational range. So the performance of the adaptive scheme can be validated while the parameter is being estimated. In these tests, as the focus is to test the control performance, it is supposed that the parameter estimator starts from the real value of the system.

In order to make these transitions softened the same step regularization function of Section 4.2.4 was used. The setpoint of the pump power was kept lower than a realizable value, in order to guarantee the minimum power consumption in the operation.

Two test were carried out in order to test the parameter estimation performance. The first one initiates the algorithm from a distant value of the parameter to check if it is able to drive the estimated value to the real one. To do so, the initial estimated value of the parameter is 0.01 $Pa \cdot s$, which is very distant from the actual system value, 0.15 $Pa \cdot s$. The second one is a disturbance in the viscosity due to the increase of watercut in the produced oil. This disturbance was introduced by KRISHNAMOORTHY *et al.* (2016) and consists of the continuous increase of the water-cut in the flow, forming an emulsion due to the mixing of water and oil. The formation of the emulsion is responsible for an exponential growth in viscosity until almost 4 times the initial viscosity of the oil in a period of 70 seconds. While the watercut increases and the viscosity reaches its critical point, the emulsion breaks down in an inversion point in which the viscosity of the fluid suddenly decreases to the water viscosity. Figure 5.3 illustrates the disturbance introduced by KRISHNAMOORTHY *et al.* (2016), however in a smaller time scale.

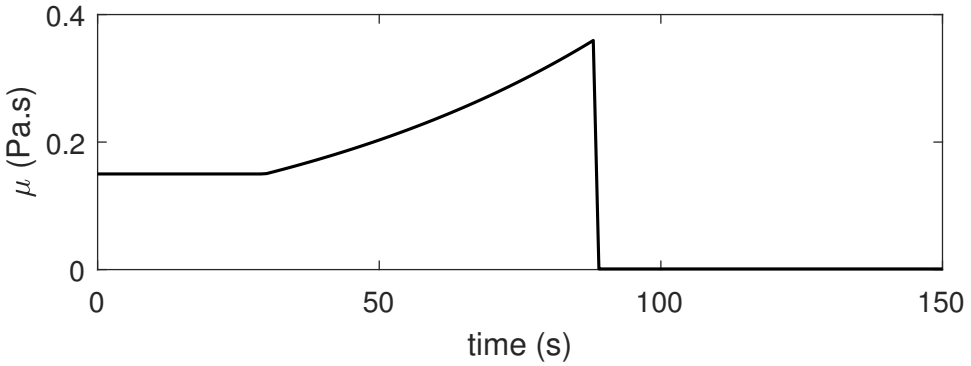

Figure 5.3: Viscosity disturbance as the watercut in the flow increases.

5.3 Results and Discussion

In this section, we compare both proposed interpolation strategies with the successive linearization in the algorithm scheme proposed in Section 5.2.

5.3.1 Optimal Model Net Structure

The optimal nodes for μ in the expansion of the 2-D, 4 by 5 net proposed in Section 4.3.1, as it grows in size from 2 to 6 nodes as a result of the optimization problem described in Section 5.2.2, can be visualized in Table 5.1.

Table 5.1: Optimal μ nodes for different net sizes from the 4 by 5 net selected in Chapter 4.

	Nodes
Size	μ_n
2	$[0.307, 0.024]^T$
3	$[0.401, 0.128, 0.019]^T$
4	$[0.416, 0.151, 0.026, 0.002]^T$
5	$[0.458, 0.231, 0.089, 0.021, 0.001]^T$
6	$[0.478, 0.286, 0.161, 0.071, 0.026, 0.0016]^T$

The results of the optimal nodes in the direction of μ seam very reasonably in the sense that the more concentrated number of point is in the region of higher gain, that is the lower viscosity values, as shown in Figure 5.4.

Table 5.2 shows the SSE between the static responses from the nonlinear model and from the interpolation strategy while each input is varied. As one can see, the overall SSE decreases while the size of the model net increases. However, as pointed out in Chapter 4, the increase of the model net comes with the drawback of increasing the number of models that has to be obtained. In the context of the parameter, this is even more dramatic as each node increased requires the number of models in the inputs net to be added. For instance, as the input net is 4 by 5, it has 20 models, so each node in the parameter direction increases 20 more models to the net. And, as one can see in Table 5.2, the increase in number of nodes enhances the model net accuracy to the nonlinear model. Therefore, a limited size must be arbitrarily imposed in order to avoid an unpractical number of models to be obtained. Here, we will consider the model size of 6 nodes in the parameter dimension.

Table 5.2: SSE for different net size from the 4 by 5 net selected in Chapter 4.

	$p_{p,in}$			P		
Size	f	z	μ	f	z	μ
2	3.48E+11	7.02E+10	3.57E+12	3.64E+07	2.44E+07	1.60E+08
3	3.06E+11	1.40E+11	1.17E+12	4.39E+07	2.92E+07	5.89E+07
4	3.26E+11	8.09E+10	5.15E+11	3.70E+07	2.53E+07	4.55E+07
5	3.24E+11	8.20E+10	2.11E+11	3.74E+07	2.54E+07	2.84E+07
6	3.38E+11	7.48E+10	1.43E+11	3.63E+07	2.48E+07	2.26E+07

Figure 5.4 shows the static responses of the nonlinear model, compared to the model net interpolation strategy and the successive linearization as the inputs and the viscosity varies. As one can see, both interpolation strategy and successive linearization produced a very accurate profile compared to the nonlinear system.

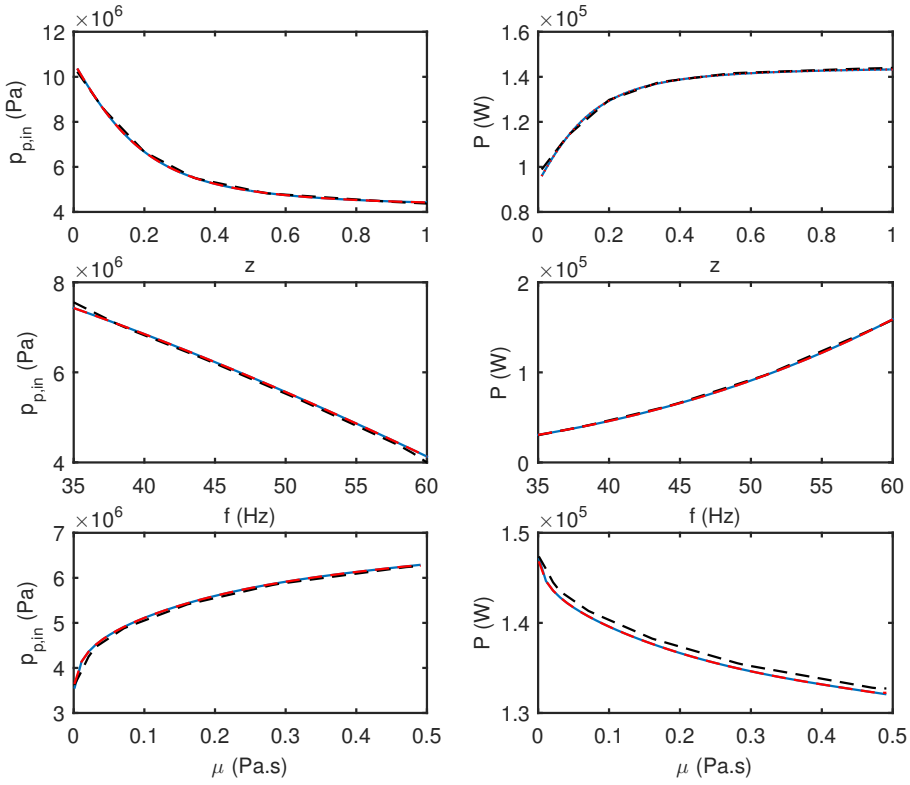

Figure 5.4: Static outputs versus inputs: (a) $p_{p,in}$ versus z; (b) $p_{p,in}$ versus f; (c) P versus z; (d) P versus f. (——) nonlinear model response, (- - - -) 4 by 5 by 6 interpolation response, (- - - -) successive linearization response.

Figure 5.5 shows the eigenvalues of the models resulting from the interpolation strategy and from the nonlinear model as f varies from the lower bound to the upper bound of the operational range.

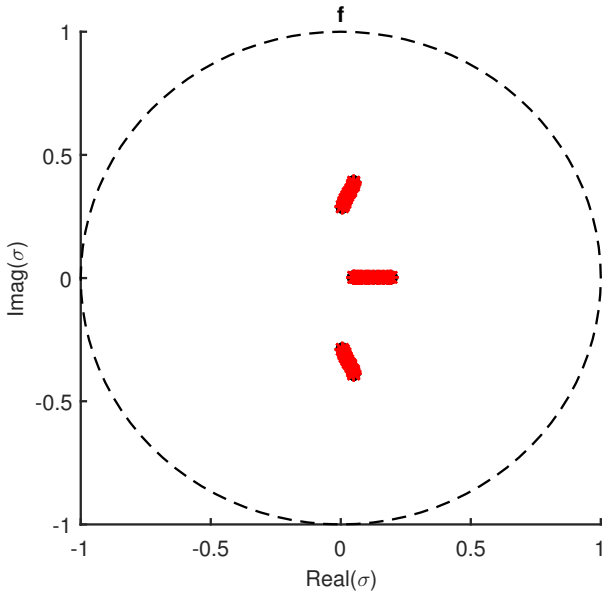

Figure 5.5: Internal model stability analysis over the range of f. (- - - -) unit circle, ($\circ\ \circ\ \circ$) scheduled eigenvalues, ($*\ *\ *$) nonlinear eigenvalues.

Figure 5.6 shows the eigenvalues of the models resulting from the interpolation strategy and from the nonlinear model as z varies from the lower bound to the upper bound of the operational range.

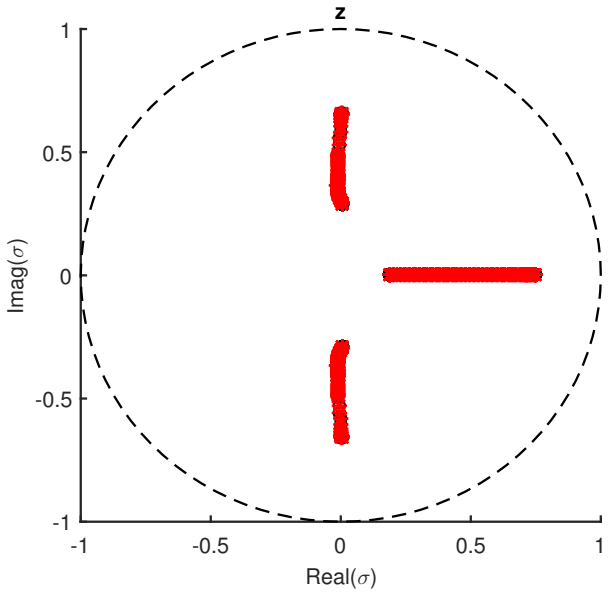

Figure 5.6: Internal model stability analysis over the range of z. (- - - -) unit circle, ($\circ\ \circ\ \circ$) scheduled eigenvalues, ($*\ *\ *$) nonlinear eigenvalues.

Figure 5.7 shows the eigenvalues of the models resulting from the interpolation strategy and from the nonlinear model as μ varies from the lower bound to the upper bound of the operational range.

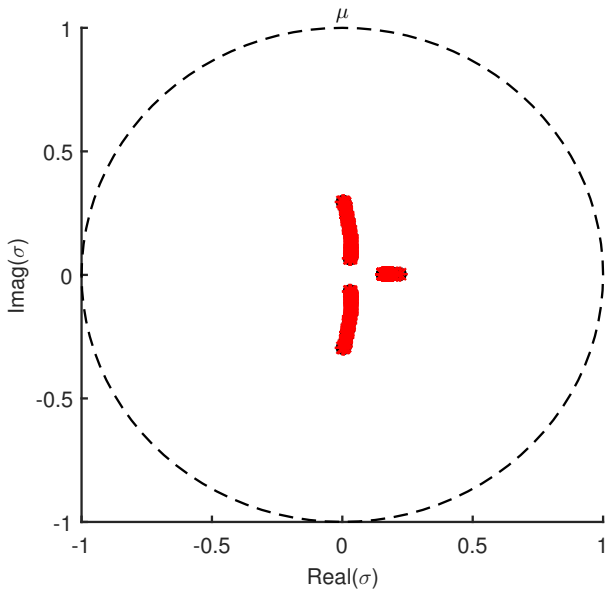

Figure 5.7: Internal model stability analysis over the range of μ. (- - - -) unit circle, ($\circ\ \circ\ \circ$) scheduled eigenvalues, ($*\ *\ *$) nonlinear eigenvalues.

In addition, no model resulting from the model net interpolation strategy presented unstable dynamics, as one can see in Figures 5.5, 5.6 and 5.7. On the contrary, these figures show that the eigenvalues of the nonlinear model match the model net interpolation strategies and none remained outside the unit circle. It is noteworthy that both interpolation strategies resulted in the same results previously labeled as "model net interpolation strategy".

5.3.2 State Estimation Performance

To evaluate the state estimation performance, all state variables were considered to be unavailable and a setpoint change in inlet pressure from a baseline to an upper baseline and then to a lower baseline was assumed. In addition, the initial viscosity value were considered to be known.

Figure 5.8 showd the output variables. One can see that all the strategies produced a similar trajectory, validating the interpolation strategies as an alternatives to the traditional successive linearization strategy. It is important to highlight that there is a slight difference in the response of the SKF1-MPC and the SKF2-MPC. Also, there is a small disturbance in the power consumption around 125 seconds, that might be explained by Figures 5.8, 5.9, 5.10 and 5.11, specially the inputs and the estimated viscosity.

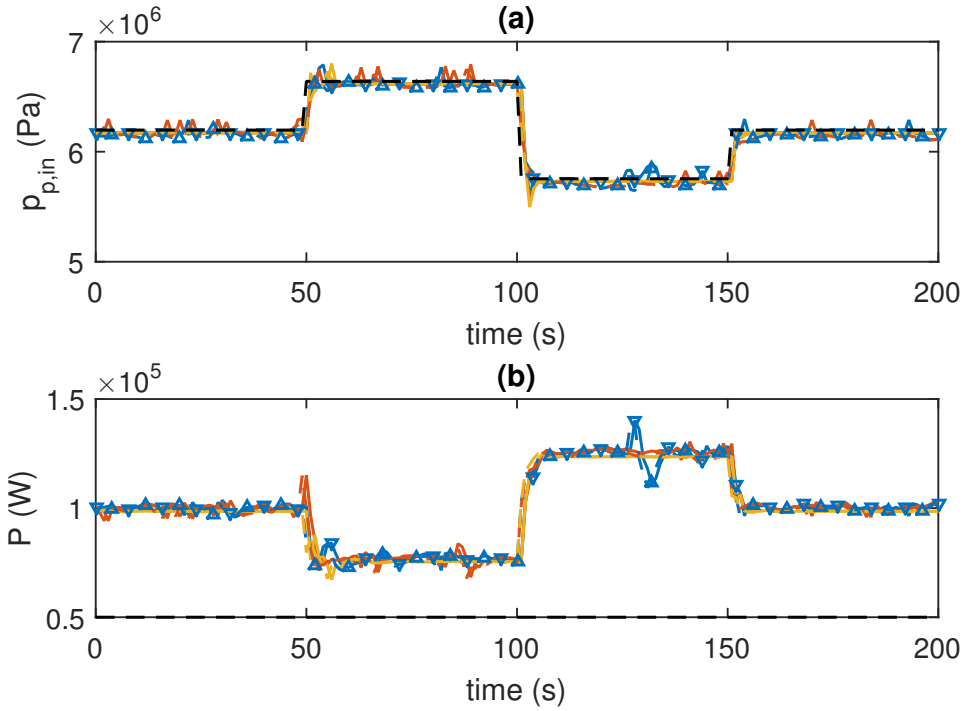

Figure 5.8: Outputs - filter performance test: (a) $p_{p,in}$; (b) P. (----) reference trajectory, (-△-) SKF1-MPC real system trajectory, (—▽—) SKF1-MPC estimated trajectory, (----) SKF2-MPC real system trajectory, (——) SKF2-MPC estimated trajectory, (----) EKF-MPC real system trajectory, (——) EKF-MPC estimated trajectory.

Figure 5.9 shows the result of the parameter estimation strategy, it can be noticed that the algorithm was successful for all approaches. The fact that the estimated value does not stabilize in a single value, instead it remains around the real values, might be explained due to the fact that the viscosity is a degree of freedom to shape the most probable model, so other model uncertainties might be added to the parameter value.

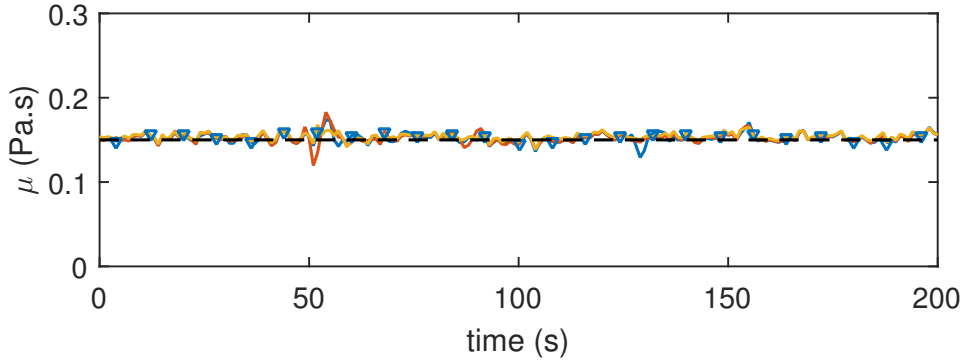

Figure 5.9: Viscosity - filter performance test. (----) real system trajectory, (—▽—) SKF1-MPC estimated trajectory, (——) SKF2-MPC estimated trajectory, (----) EKF-MPC real system trajectory

Figure 5.10 shows the input values. It can be observed that in the choke valve

opening around the second 125 there is an undesirable oscillation in the approach SKF1-MPC in a region that it should not occur. That may be explained by bad tuning of the MPC or the Kalman Filter matrices, since all approaches presented an oscillatory behavior, but it was more aggressive in the SKF1-MPC and in the SKF2-MPC.

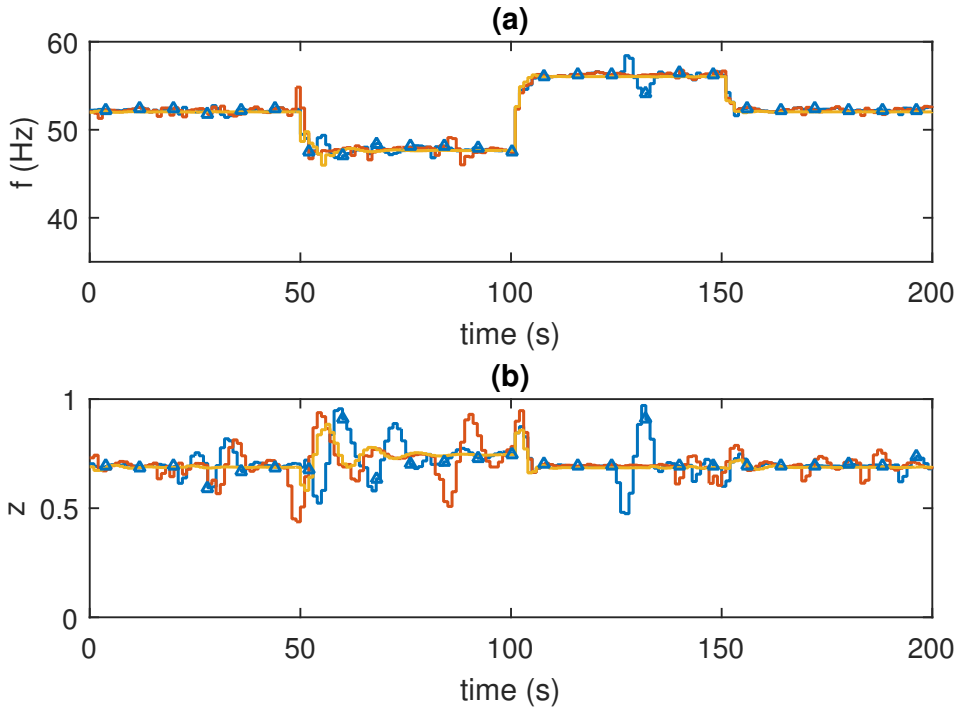

Figure 5.10: Inputs - filter performance test: (a) f; (b) z. (—△—) SKF1-MPC trajectory, (——) SKF2-MPC trajectory, (——) EKF-MPC trajectory.

Figure 5.11 shows the state variables. It can be verified that all approaches presented a very good state estimation resulting from the good accuracy of the linear model selected in each time instant. For the well head pressure we can observe a strong oscillatory response that is a result of the choke opening and the estimated viscosity.

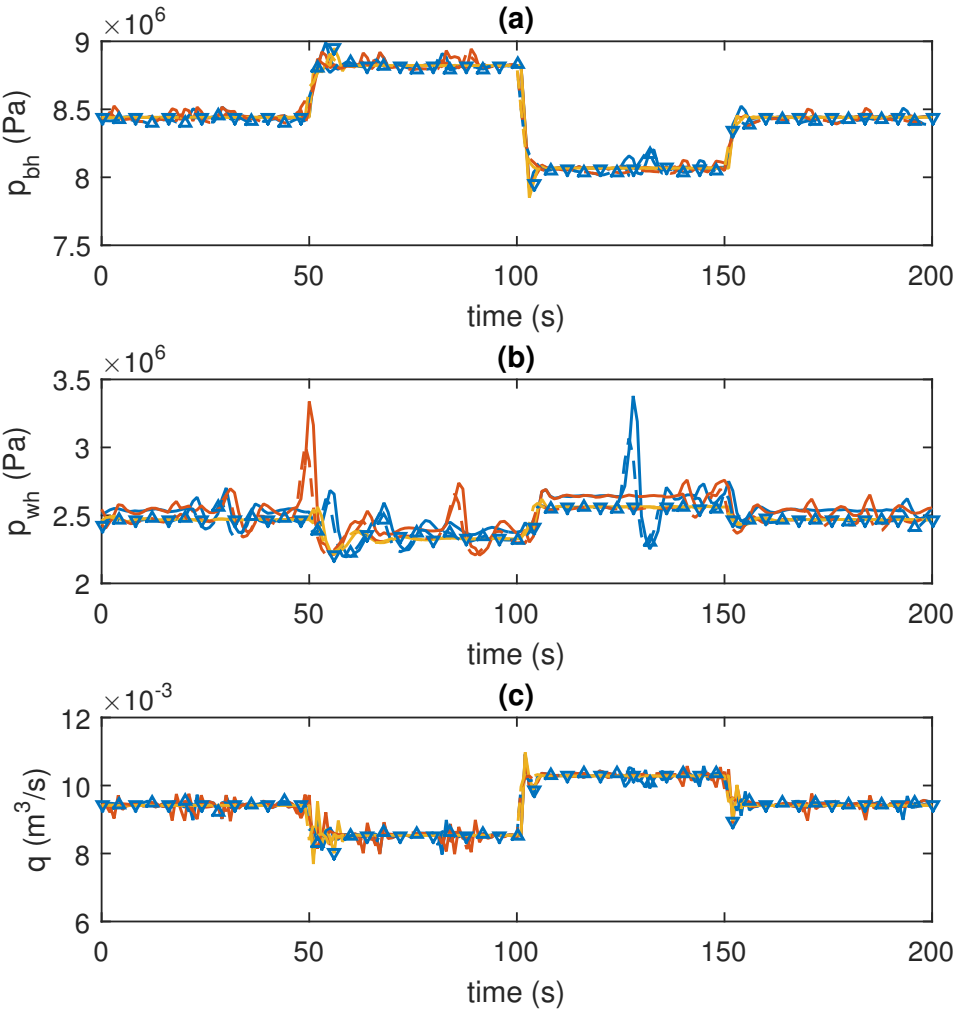

Figure 5.11: States - filter performance test: (a) p_{bh}; (b) p_{wh}; (c) q. (- - - -) reference trajectory, (- △ -) SKF1-MPC real system trajectory, (—▽—) SKF1-MPC estimated trajectory, (- - - -) SKF2-MPC real system trajectory, (——) SKF2-MPC estimated trajectory, (- - - -) EKF-MPC real system trajectory, (——) EKF-MPC estimated trajectory.

5.3.3 Control Performance

This section presents the results related to the validation of the control performance in the scheme in which the Parameter Estimation Algorithm is responsible to estimate the parameter value that is used, together with the input variables, to select the most probable model to take place in the linear MPC coupled with a Kalman Filter.

Figures 5.12, 5.13, 5.14 and 5.15 are related to the setpoint change test from a low to high intake pressure aiming to force the system through the whole nonlinear region of choke opening in the direction of a high to a low choke opening.

Figure 5.12 shows the trajectory of the output variables. Its is possible to see that all approaches presented a soft transition in the intake pressure trajectory,

with an accurate estimation of the real value of the variable with no offset in the low neither in the high pressure regions. The same is observed in the pump power consumption, except for an oscillatory moment after the high intake pressure stabilization. That might be explained due to an oscillatory behaviour in pump frequency as can be observed in Figure 5.14. This issue might be tackled by fine adjustment in MPC and KF tuning.

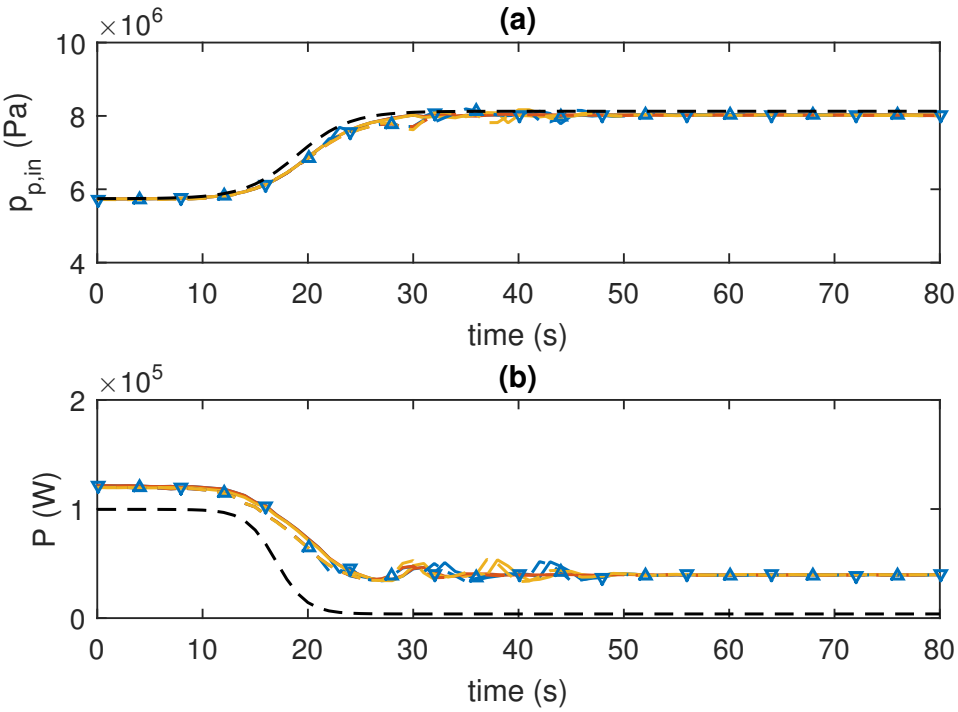

Figure 5.12: Outputs - control performance test - high to low intake pressure setpoint change: (a) $p_{p,in}$; (b) P. (- - - -) reference trajectory, (-△-) SKF1-MPC real system trajectory, (—▽—) SKF1-MPC estimated trajectory, (- - - -) SKF2-MPC real system trajectory, (——) SKF2-MPC estimated trajectory, (- - - -) EKF-MPC real system trajectory, (——) EKF-MPC estimated trajectory.

Figure 5.13 depicts the estimated viscosity. The three approaches started from the real value of the parameter, 0.150 $Pa \cdot s$, and presented an accurate performance in the region of low intake pressure setpoint. However, in the transition of setpoints and even a bit longer after the high intake pressure stabilization it is possible to see an oscillatory behaviour with different dynamics, even for the two interpolation approaches, SKF1-MPC and SKF2-MPC. This difference was not observed in the results of Chapter 4 and it is important to highlight that, after the transition period, both strategies converged to the same profile of estimation. However, differently from what was observed in the EKF-MPC approach, this profile presented a considerable offset between the estimated and the real value. Moreover, the SKF1-MPC responds more aggressively than the SKF2-MPC, this behaviour will be also observed in the next results.

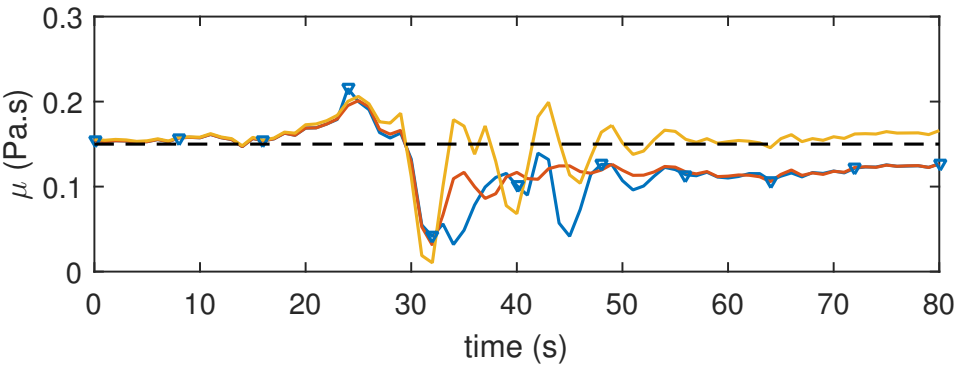

Figure 5.13: Viscosity - control performance test - high to low intake pressure setpoint change. (- - - -) real system trajectory, (—▽—) SKF1-MPC estimated trajectory, (——) SKF2-MPC estimated trajectory, (- - - -) EKF-MPC real system trajectory

Input variables are illustrated in Figure 5.14. The oscillatory behaviour can be observed in both variables after the high intake pressure setpoint stabilization. However, it is more evident in pump frequency, what has a direct effect in pump power consumption. Although the three approaches present slightly different dynamics, their overall behaviour and static stabilization values are the same.

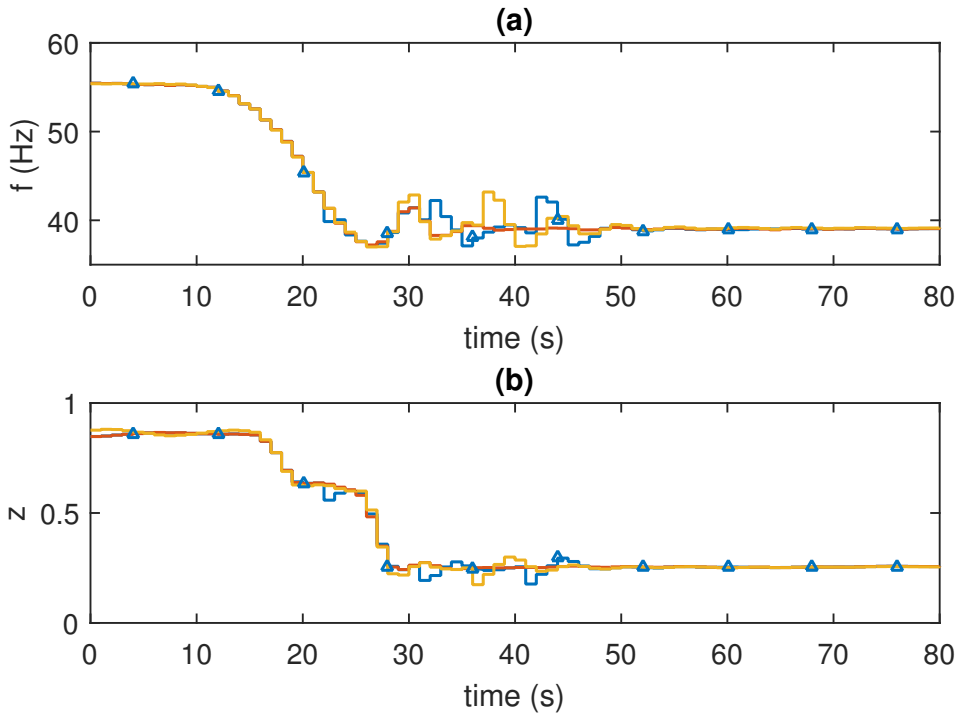

Figure 5.14: Inputs - control performance test - high to low intake pressure setpoint change: (a) f; (b) z. (—△—) SKF1-MPC trajectory, (——) SKF2-MPC trajectory, (——) EKF-MPC trajectory.

The state variables are presented in Figure 5.15. The same similar overall behaviour is observed in the three approaches. The most evident differences can

be observed in the well head pressure, both interpolation approaches have left a small offset after the high intake pressure setpoint stabilization. In addition, the SKF2-MPC approach presented the less aggressive behaviour.

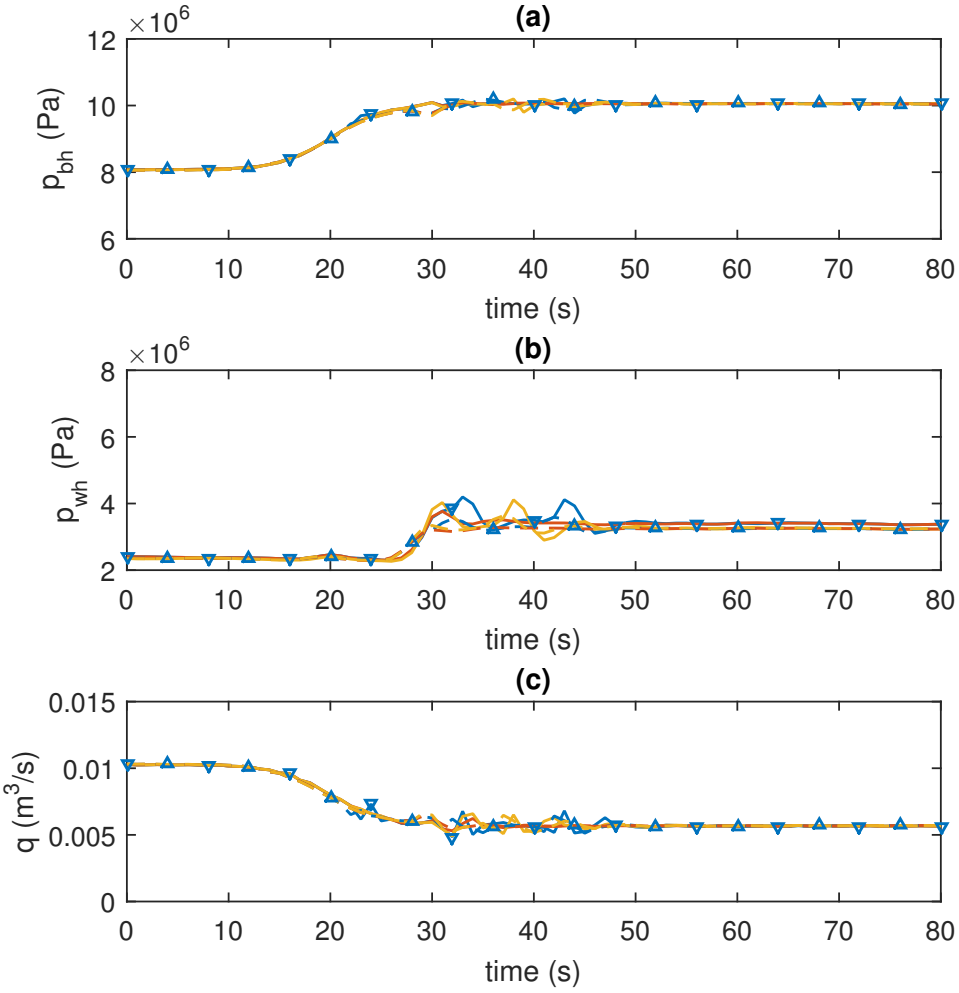

Figure 5.15: States - control performance test - high to low intake pressure setpoint change: (a) p_{bh}; (b) p_{wh}; (c) q. (- - - -) reference trajectory, (-△-) SKF1-MPC real system trajectory, (—▽—) SKF1-MPC estimated trajectory, (- - - -) SKF2-MPC real system trajectory, (——) SKF2-MPC estimated trajectory, (- - - -) EKF-MPC real system trajectory, (——) EKF-MPC estimated trajectory.

Figures 5.16, 5.17, 5.18 and 5.19 are related to the setpoint change test from a high to low intake pressure aiming to force the system through the whole nonlinear region of choke opening in the direction of a low to a high choke opening.

Figure 5.16 shows the trajectory of the output variables. Its is possible to see that all approaches presented a soft transition in the intake pressure trajectory, with an accurate estimation of the real value of the variable with no offset in the high neither in the low pressure regions, as in the previous test. The same is observed in the pump power consumption, it is important to note that for this test this variable did not present an oscillatory behaviour, as observed in the previous

test.

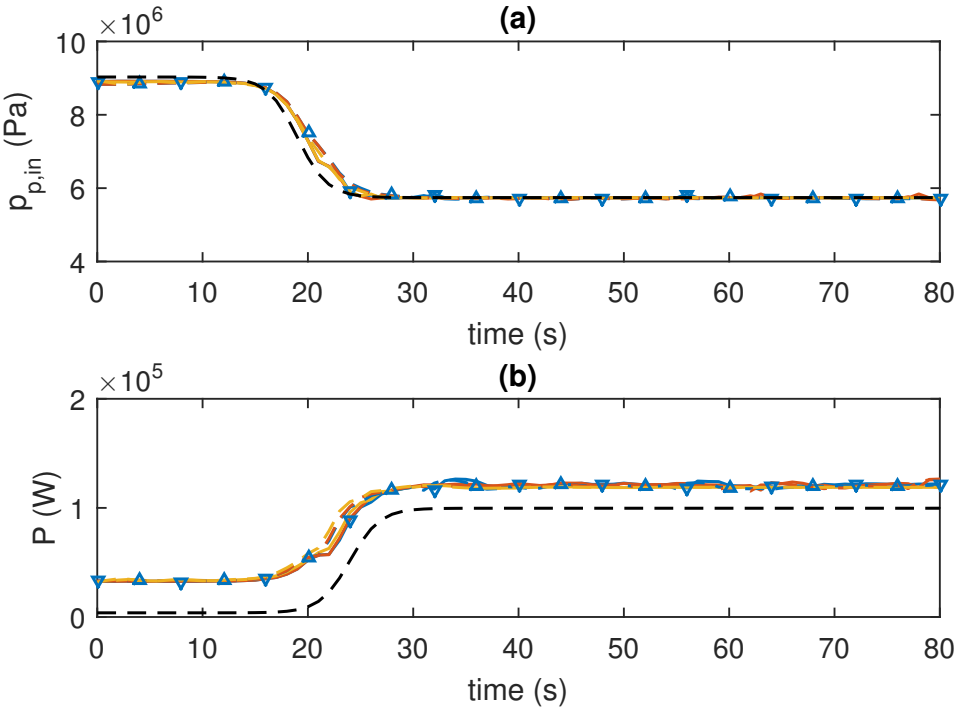

Figure 5.16: Outputs - control performance test - low to high intake pressure setpoint change: (a) $p_{p,in}$; (b) P. (----) reference trajectory, (-△-) SKF1-MPC real system trajectory, (—▽—) SKF1-MPC estimated trajectory, (----) SKF2-MPC real system trajectory, (——) SKF2-MPC estimated trajectory, (----) EKF-MPC real system trajectory, (——) EKF-MPC estimated trajectory.

The estimated viscosity can be observed in Figure 5.17. The three approaches started from the real value of the parameter, 0.150 $Pa \cdot s$, and presented an accurate performance in the region of low intake pressure setpoint. However, in the transition region and in the high intake pressure setpoint, all approaches struggled to find an estimated viscosity near to the real value. The EKF-MPC presented the best response, in spite of the oscillatory behaviour, it presented a mean value near to the real and the picks tended to decrease. On the other hand, both interpolation strategies failed to find and accurate value of the parameter. However, that have not reflected in the state estimation performance, leading to the conclusion that there are more uncertainties in the region of high intake pressure for the interpolation in the net of linear models. Hence, the parameter value is used to find the most probable model so that the estimated states and outputs can be trusted, but it does not reflect the same trust in the estimated parameter value.

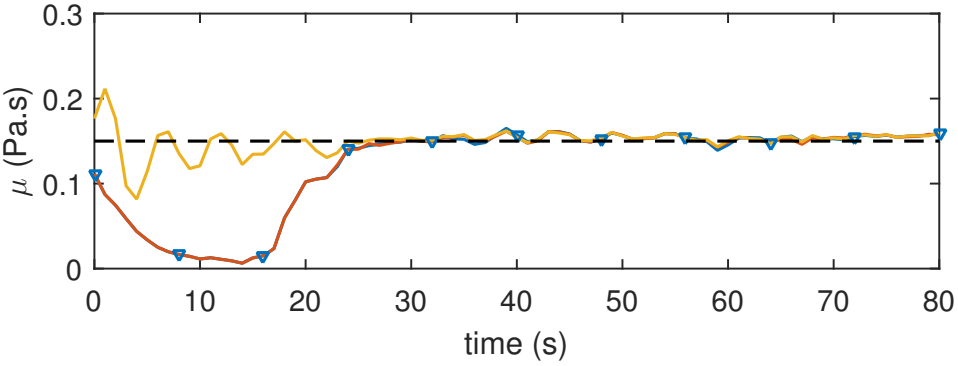

Figure 5.17: Viscosity - control performance test - low to high intake pressure setpoint change. (- - - -) real system trajectory, (—▽—) SKF1-MPC estimated trajectory, (——) SKF2-MPC estimated trajectory, (- - - -) EKF-MPC real system trajectory

Input variables are illustrated in Figure 5.18. A small oscillatory behaviour can be observed in both variables after the low intake pressure setpoint stabilization. However, it was more evident in the choke opening for the interpolation approaches. Although the three approaches present slightly different dynamics, their overall behaviour and static stabilization values are the same.

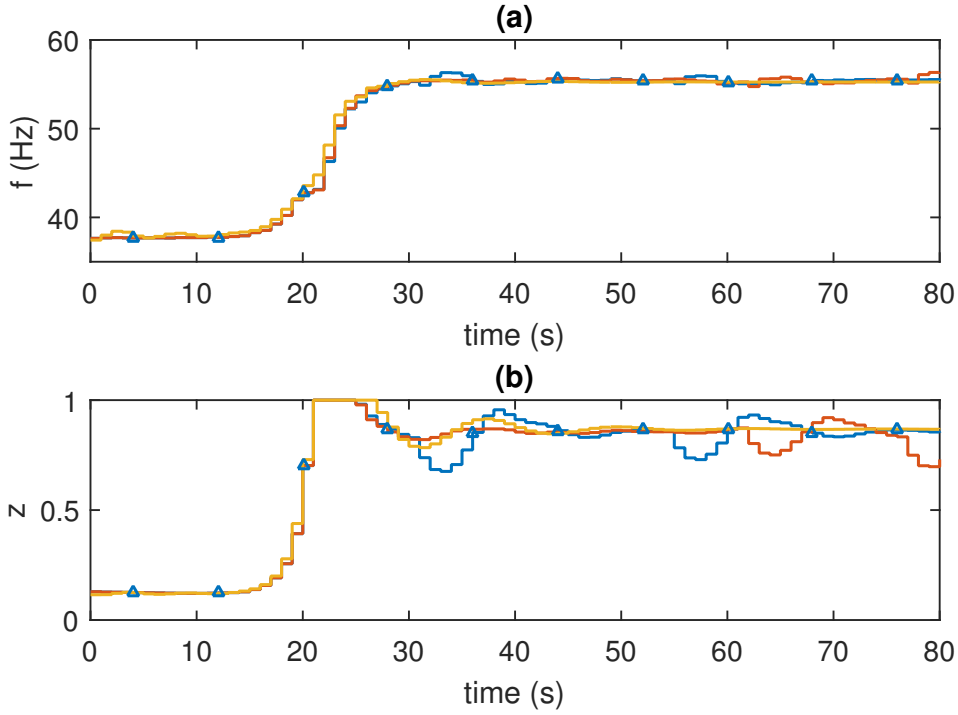

Figure 5.18: Inputs - control performance test - low to high intake pressure setpoint change: (a) f; (b) z. (—△—) SKF1-MPC trajectory, (——) SKF2-MPC trajectory, (——) EKF-MPC trajectory.

The state variables are presented in Figure 5.19. The same similar overall behaviour is observed in the three approaches. The most evident differences can

be observed in the well head pressure, both interpolation approaches have left a small offset in the region of high intake pressure setpoint. That result can be explained for the greater uncertainties in this region.

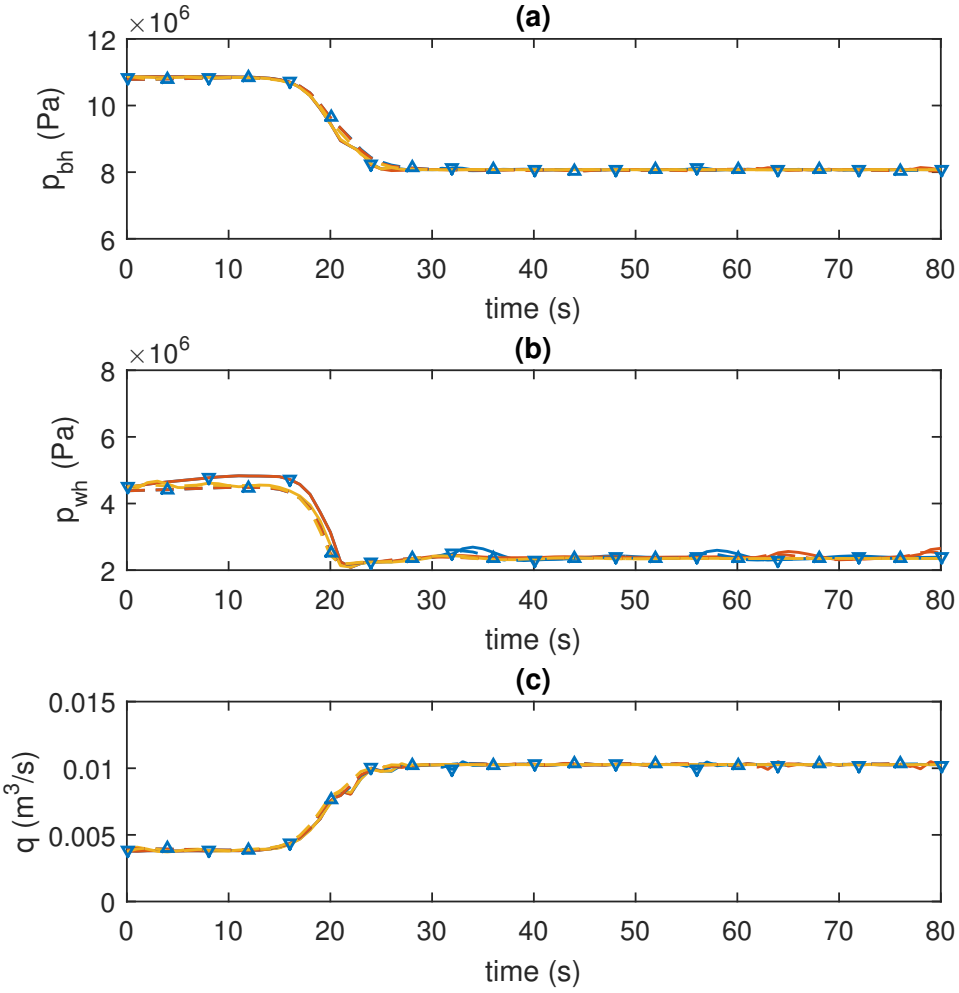

Figure 5.19: States - control performance test - low to high intake pressure setpoint change: (a) p_{bh}; (b) p_{wh}; (c) q. (- - - -) reference trajectory, (-△-) SKF1-MPC real system trajectory, (—▽—) SKF1-MPC estimated trajectory, (- - - -) SKF2-MPC real system trajectory, (——) SKF2-MPC estimated trajectory, (- - - -) EKF-MPC real system trajectory, (——) EKF-MPC estimated trajectory.

5.3.4 Parameter Estimation Performance

The first Parameter Estimation Performance test consisted in a stable operation with constant intake pressure setpoint and unknown starting viscosity value. Figure 5.20 illustrates the outputs in this test, it is possible to see that all approaches presented a high quality state estimation performance and stable control performance.

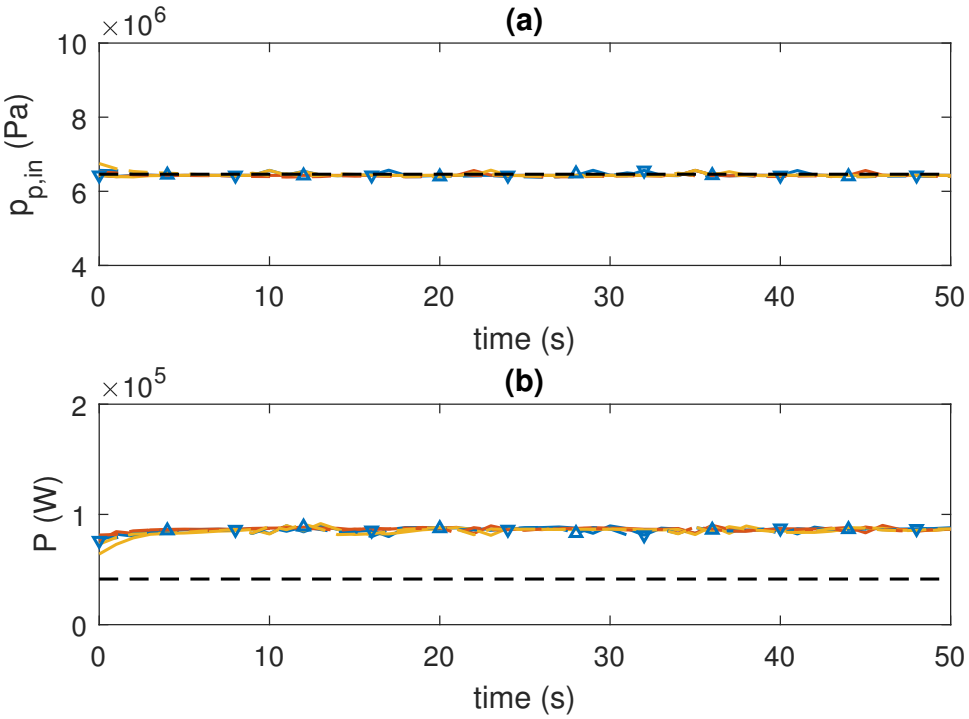

Figure 5.20: Outputs - viscosity estimation performance test from unknown initial value: (a) $p_{p,in}$; (b) P. (- - - -) reference trajectory, (-△-) SKF1-MPC real system trajectory, (—▽—) SKF1-MPC estimated trajectory, (- - - -) SKF2-MPC real system trajectory, (——) SKF2-MPC estimated trajectory, (- - - -) EKF-MPC real system trajectory, (——) EKF-MPC estimated trajectory.

Figure 5.21 shows the parameter estimation trajectory, from a wrong initial guess of 0.01 $Pa \cdot s$ to the real value of the system of 0.15 $Pa \cdot s$. All approaches were able to estimate the real value of the viscosity. The SKF2-MPC was the fastest one, while The EKF-MPC was the slowest.

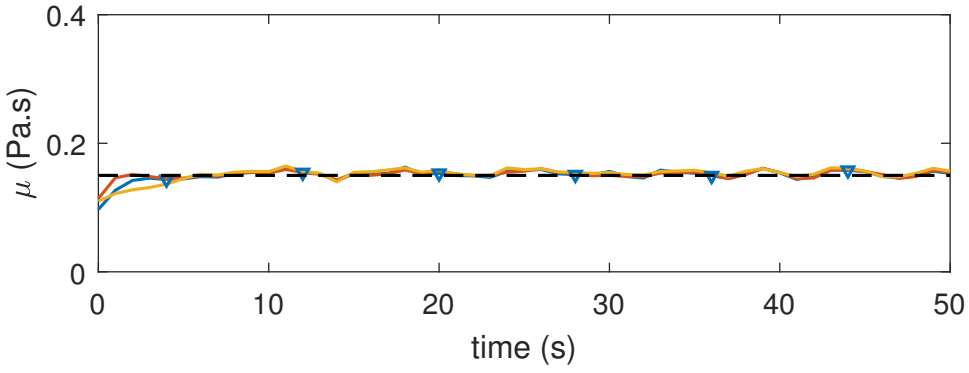

Figure 5.21: Viscosity - viscosity estimation performance test from unknown initial value. (- - - -) real system trajectory, (—▽—) SKF1-MPC estimated trajectory, (——) SKF2-MPC estimated trajectory, (——) EKF-MPC estimated trajectory

The manipulated variables trajectories can be visualized in Figure 5.22. The pump frequency presented a stable value, but the choke opening presented a

slightly aggressive behaviour, exhibiting oscillatory modules. The both interpolation approaches, SKF1-MPC and SKF2-MPC, showing a similar behaviour in terms of aggressiveness, while the EKF-MPC was a little more aggressive, displaying higher values of the peak of the oscillations.

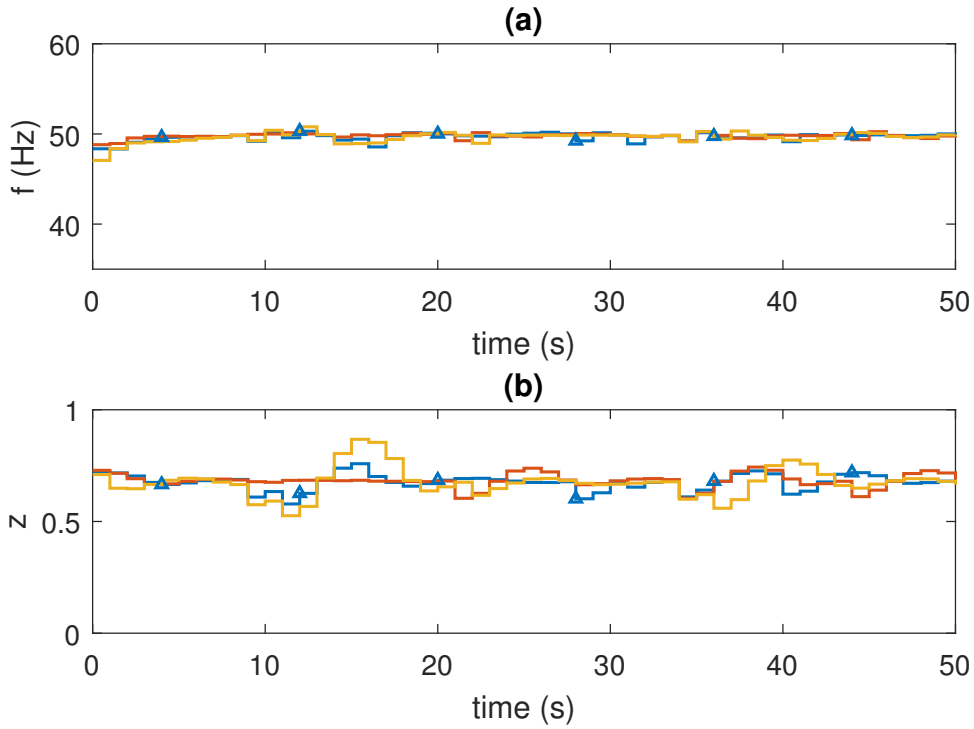

Figure 5.22: Inputs - viscosity estimation performance test from unknown initial value: (a) f; (b) z. (—△—) SKF1-MPC trajectory, (——) SKF2-MPC trajectory, (——) EKF-MPC trajectory.

The states trajectories can be visualized in Figure 5.23. Its is possible to realize that all approaches presented a high quality state estimation, keeping all variables in a stable behaviour and without leaving offset between the real system trajectory and the estimated trajectory.

The next figures present the result of the real disturbance in the viscosity as described in Section 5.2.6. Similarly good performances were obtained for all approaches while estimating the viscosity during the MPC algorithm. These results prove the robustness of the proposed methodology to measurement and model structural uncertainties.

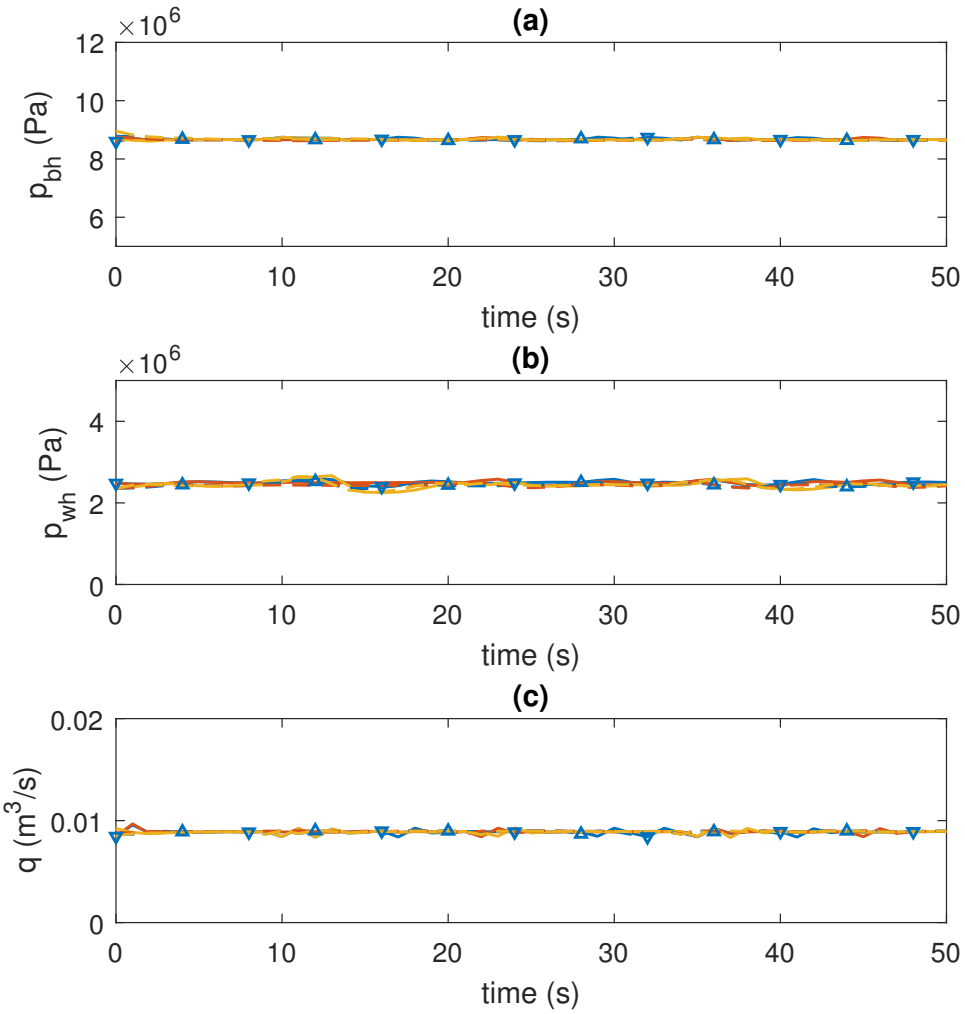

Figure 5.23: States - viscosity estimation performance test from unknown initial value: (a) p_{bh}; (b) p_{wh}; (c) q. (- - - -) reference trajectory, (-△-) SKF1-MPC real system trajectory, (—▽—) SKF1-MPC estimated trajectory, (- - - -) SKF2-MPC real system trajectory, (——) SKF2-MPC estimated trajectory, (- - - -) EKF-MPC real system trajectory, (——) EKF-MPC estimated trajectory.

Figure 5.24 shows the output trajectories. All approaches were able to keep the intake pressure in the desired setpoint in the whole dynamics due to the viscosity increase and its subsequent decrease decrease. It is important to highlight that around the second 90, all the real system trajectories present a valley due to delay in the viscosity estimation. In Figure 5.25 it is possible to see that there is a delay in the viscosity estimation, during this delay the real system viscosity is 0.001 $Pa \cdot s$ while the estimator has not detected this decrease yet, so the state estimation fails to capture the real system trajectory and the MPC does not realize this sudden change. However, as soon as the estimator is able to update the viscosity estimation and reach the real value of the system, the state estimator captures the real system trajectory and the MPC is able to drive the system back to the intake pressure setpoint.

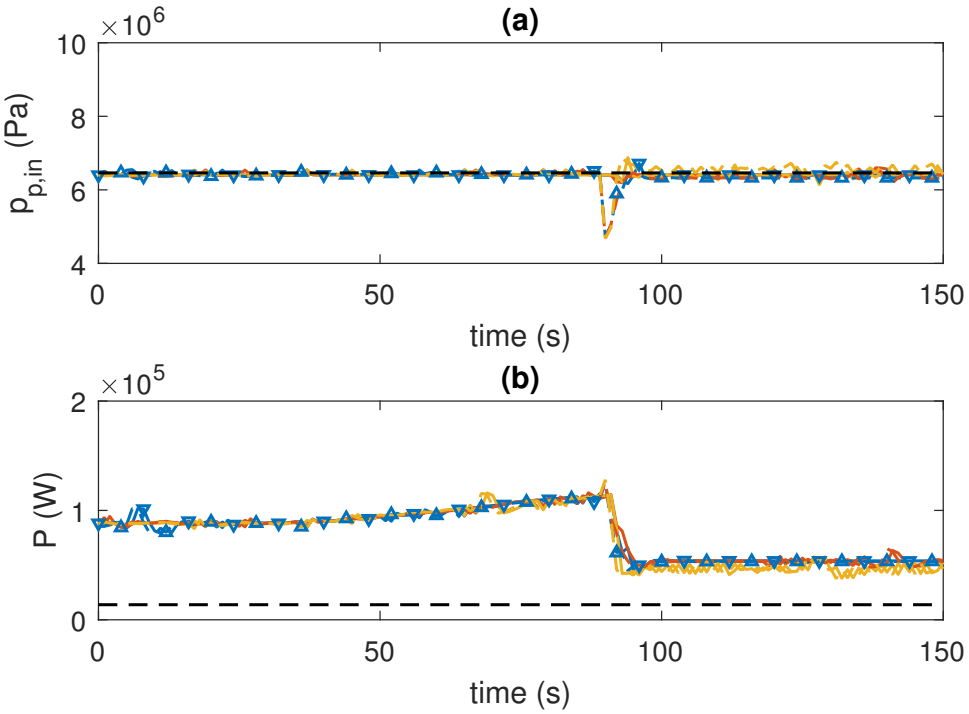

Figure 5.24: Outputs - viscosity estimation performance test for viscosity disturbance: (a) $p_{p,in}$; (b) P. (- - - -) reference trajectory, (-△-) SKF1-MPC real system trajectory, (—▽—) SKF1-MPC estimated trajectory, (- - - -) SKF2-MPC real system trajectory, (——) SKF2-MPC estimated trajectory, (- - - -) EKF-MPC real system trajectory, (——) EKF-MPC estimated trajectory.

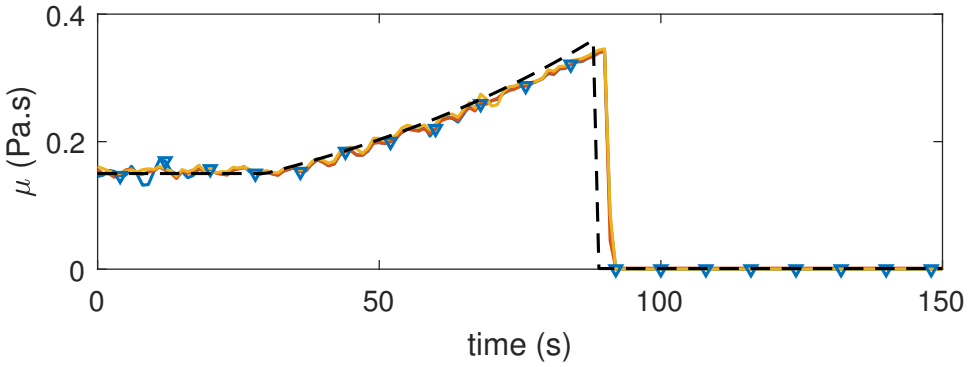

Figure 5.25: Viscosity - viscosity estimation performance test for viscosity disturbance. (- - - -) real system trajectory, (—▽—) SKF1-MPC estimated trajectory, (——) SKF2-MPC estimated trajectory, (——) EKF-MPC estimated trajectory.

It can also be seen Figure 5.24 that the pump power consumption decreases with the viscosity, that is because the decrease in viscosity produces a decrease in pump frequency, what can be observed in Figure 5.26. It is also noteworthy that the approach EKF-MPC presented an oscillatory behaviour with respect to the pump frequency after the emulsion collapse, that can be improved with better tuning. Additionally, during the whole operation, the choke opening presented some undesired oscillations that might be overcome with tuning improvement.

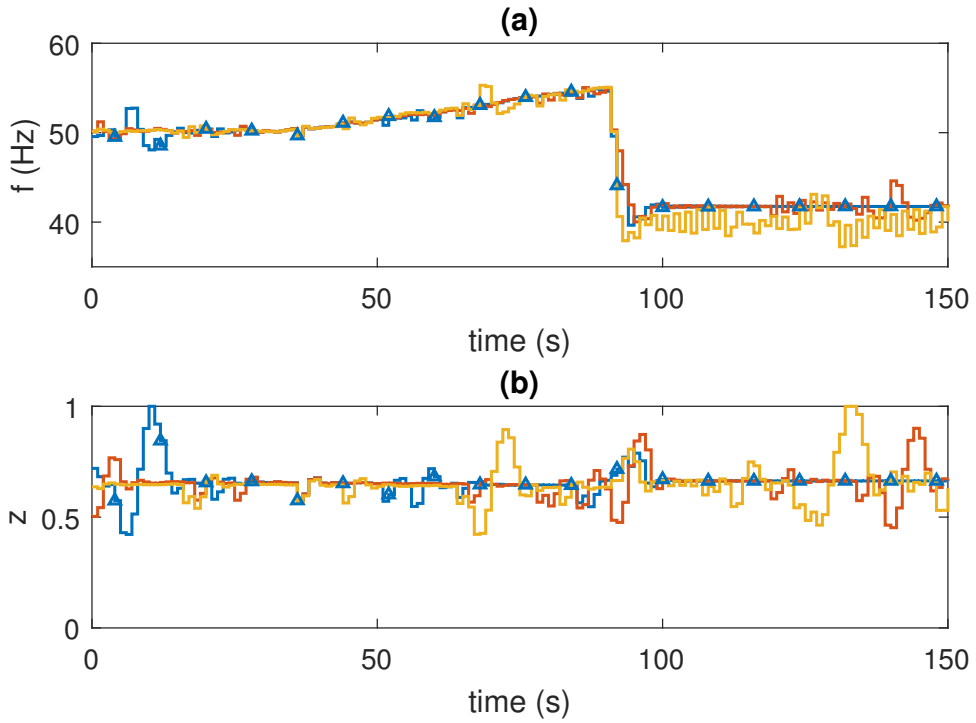

Figure 5.26: Inputs - viscosity estimation performance test for viscosity disturbance: (a) f; (b) z. (—△—) SKF1-MPC trajectory, (——) SKF2-MPC trajectory, (——) EKF-MPC trajectory.

The states trajectory can be visualized in Figure 5.27. The same estimation problem previously reported in the time instant of 90 seconds occurs for the three states due to the delay in the parameter estimation in all approaches. The undesired oscillations in the choke opening reflect in the behavior of the well head pressure, so oscillations in this variables are observed in the same periods that oscillation occurs in the choke opening. In the EKF-MPC, after the collapse of the emulsion and abrupt decrease of the fluid viscosity, an oscillatory behavior in the pump frequency appeared, as already pointed out. This behavior is responsible for the same profile in the fluid flow rate. Above all, all the approaches presented a great performance during the disturbance evaluation, not only from the state and parameter estimation point of view, but also from the control point of view.

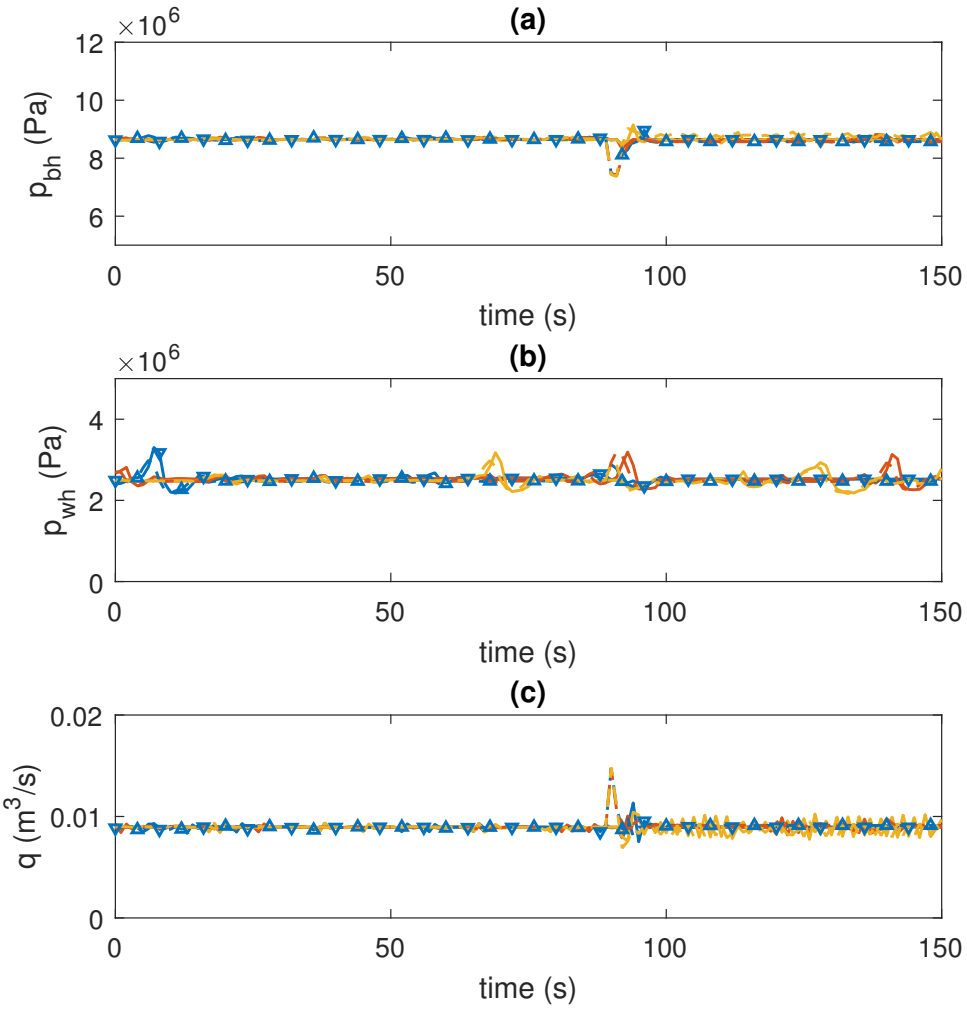

Figure 5.27: States - viscosity estimation performance test for viscosity disturbance: (a) p_{bh}; (b) p_{wh}; (c) q. (- - - -) reference trajectory, (-△-) SKF1-MPC real system trajectory, (—▽—) SKF1-MPC estimated trajectory, (- - - -) SKF2-MPC real system trajectory, (——) SKF2-MPC estimated trajectory, (- - - -) EKF-MPC real system trajectory, (——) EKF-MPC estimated trajectory.

5.4 Variance Scaling Factor

The propose of the variance scaling factor, introduced in Section 5.2.3, is not to let the fitted normal distribution bell to close, leading the distribution to approximate to an impulse. After a period of satisfactory performance, the variance would of the pdf would decrease due to the coincidence of the estimated and the real value. If a disturbance is subjected to the real parameter in this condition, the algorithm would not be able to correctly estimate the parameter. Therefore, the scaling factor is proposed to overcome this issue.

In the results previously presented, the scaling factor was set to 2.5. In this section we show the effect of three values, 1, 2.5 and 5, in the EKF-MPC scheme as shown in Figure 5.28.

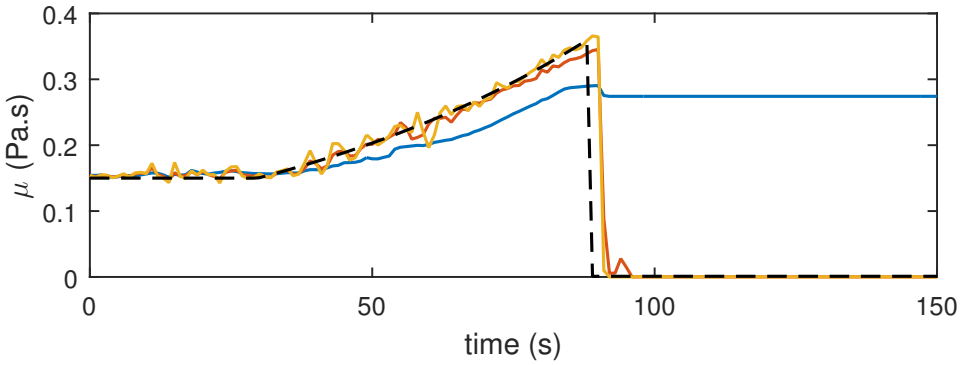

Figure 5.28: Viscosity for different variance scaling factors in the EKF-MPC scheme. (- - - -) real system trajectory, (——) $\alpha = 1$ estimated trajectory, (——) $\alpha = 2.5$ estimated trajectory, (——) $\alpha = 5$ estimated trajectory.

The variance for each scaling factor value can be visualized in Figure 5.29. For the case in which $\alpha = 1$ the parameter is poorly estimated due to the low estimated variance and the fact that after the sudden decrease of the viscosity, the variance goes to zero and the algorithm is not able to estimate the real value of the parameter. On the other hand, for cases $\alpha = 2.5$ and $\alpha = 5$ the parameter is satisfactorily estimated due to greater value of the variance. So, $\alpha = 2.5$ was chosen to be applied because the case in which $\alpha = 5$ presented higher noise.

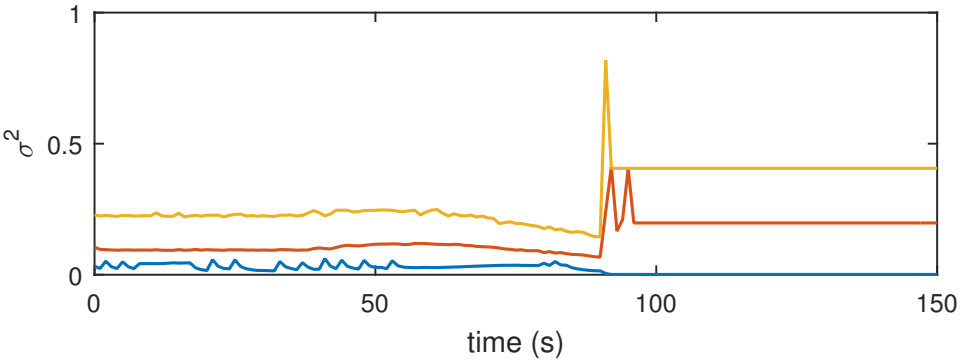

Figure 5.29: Estimated variance for different variance scaling factors in the EKF-MPC scheme. (——) $\alpha = 1$, (——) $\alpha = 2.5$, (——) $\alpha = 5$.

5.5 Conclusions

This chapter presents a methodology that fulfills all objectives of the present dissertation. Two proposed interpolations between a set of linear models previously obtained by linearization or identification proved to be as efficient as the classical successive linearization in order to deal with system nonlinearities in an adaptive linear MPC scheme. An adaptive linear Kalman filter is proposed, using the same interpolation strategies, in order to overcome measurement uncertainties for a white, unbiased and normally distributed noise. The estimation strategy proved

to be as efficient as the classic EKF scheme, in which successive linearization takes place, even in a situation of loss of all state variables measurements. Finally, an online parameter estimation algorithm based on the maximization of the probability of occurrence of the linear model given the measurement of previous sampling instant is proposed in order to deal with model structural uncertainties. The technique is an extension of the multi-model scenario-based estimation for a continuous set of models. The proposed methodology was tested in the ESP system, considering all state measurements to be unavailable and the viscosity as the parameter to be estimated. The proposed algorithm showed a similar control and state estimation performance to the one from Chapter 4, which does not contemplate the online parameter estimation strategy. In addition, it proved to be robust to inaccurate initial guess of the parameter and to disturbances in the parameter.

All the three approaches proved to be suitable in the proposed algorithm, despite some tuning improvements expected to improve control aggressiveness. The SKFs have the advantage of not requiring an available nonlinear model as the linear model net could be obtained from data information and identification techniques. The viscosity estimation has presented a great overall performance. However, in regions of high intake pressure setpoint, the estimated viscosity value does not reflect the real value. That can be explained by higher model uncertainties in this region that mislead the estimated viscosity value in order to reach a trustworthy state estimation. This result comes from the fact that the parameter estimation strategy uses the viscosity as a degree of freedom to select the most probable model for the best Kalman Filter performance. Finally, it is important to point out that the proper tuning is a challenge in this kind of algorithm as there are several tuning matrices and values to be arbitrated.

Chapter 6

Final Remarks

6.1 Developments Overview

In the introduction of this document we pointed the main motivations to develop a sophisticated automatic control for ESPs systems. Among them, one can highlight:

- Large number of operating parameters to be monitored;
- Need for ensuring operation within constraints;
- Keeping optimal and stable operation;
- Most ESPs failures are caused by manual operation;
- An ESP failure can result in a multimillion-dollar losses due to maintenance and loss of production;

PAVLOV *et al.* (2014) point out the main control targets for the ESP operation, they are keeping pump inlet pressure in a desired setpoint while minimizing power consumption, this way it is possible to control well flow rate in the optimal energy cost. In addition, they discriminate all operational constraints that must be satisfied in order to guarantee safe operation. Apart from these aspects, several other challenges are naturally imposed to the ESP system, in this work we proposed to focus our efforts in:

- nonlinearities due to process input variables and parameters;
- loss of instrumentation due to extreme subsea environment;
- measurement uncertainty;
- model structural uncertainty.

When using linear MPC for controlling nonlinear processes, one must ensure that the linear models sufficiently captures the system response over a broad operating range.

In chapter 3 we extend the work of PAVLOV *et al.* (2014), BINDER *et al.* (2014) and KRISHNAMOORTHY *et al.* (2016) by considering a linear MPC with model adaptation accounting for process nonlinearity. Two linear models were developed, one for operations with large valve openings (low gain) and the other for small valve openings (high gain). It is shown that both models do not work well for the opposite situation of valve opening that they were designed for, therefore, an adaptive strategy was proposed. Moreover, the final MPC strategy had its performance tested within servo and regulatory control approaches resulting in a broader range of operation.

In chapter 4, the problem of measurement uncertainty and instrumentation loss are addressed. For that, a robust adaptive MPC coupled with Kalman filter is proposed and three adaptive approaches are compared. It is shown that for a situation of loss of measurement of the state variables, a single internal model, such as proposed by KRISHNAMOORTHY *et al.* (2016), or a simple scheduling strategy, such as the one proposed in chapter 3, are not enough to the accurate state estimation, resulting in a large offset in the inlet pressure estimation. Two scheduling strategies based on interpolation approaches of a net of linear models are proposed and compared to the classical successive linearization strategy. The proposed scheduling strategies presented a similar performance compared to the successive linearization strategy, avoiding the need of obtaining a local linear model at each sampling time by interpolating among a number of linear models previously obtained by identification instead. Moreover, the state estimation performance was very efficient for the situation of loss of all state measurements in all three scheduling approaches.

Finally, in chapter 5, the problem of model structural uncertainty is tackled by proposing an algorithm to estimate the viscosity of the oil by using it as a degree of freedom to find the most probable linear model to occur in a Kalman Filter scheme. The proposed parameter estimation strategy served as a soft-sensor of the viscosity value for operation with mild intake pressure, as for high intake pressure the model uncertainties were high enough to distrust the viscosity value in detriment of high quality model for an accurate state estimation. In addition, an algorithm is proposed coupling the parameter estimation, the switching model strategy based on the model net previously obtained, the Kalman Filter for state estimating and, finally, the MPC algorithm to find the control action. Hence, the three main challenges proposed were overcome, which are system nonlinearities, measurement and model structural uncertainties.

6.2 Work Contributions

In the time of conclusion of this work, it was found in the literature any work of adaptive MPC applied to ESP systems. In addition, although interpolation in a linear model net applied to model scheduling in a MPC is not a new idea, no work was found using this strategy in a MPC coupled with a KF to select the internal model of both strategies. To conclude, the proposed parameter estimation strategy is an extension of the multi-model Kalman Filter presented by SIMON (2006), for the case of a continuous set of linear models. The resulted robust adaptive MPC algorithm coupled with the state and parameter estimator is a new approach to avoid the min-max problem in the robust MPC context and it is the main contribution of the present work.

6.3 Future Work

This work presents a dual facet in terms of application and methodology. Both sides can be exploited in deeper developments in order to tackle still open matters to result in a trusted, stable and robust methodology for a wide set of scenarios.

In terms of application, the presented discussions can be used as basis for more developments, such as:

- Increase the model net to cope with measured disturbances, such as p_m, and unmeasured disturbances, such as fluid watercut and reservoir productivity index;
- Enhance the process model to cope with several wells working at the same time with multiple ESPs feeding the same manifold, a very common configuration of the production system;
- Apply this modelling approach in real systems with real data, so that more sophisticated data-driven strategies can be applied to increase the performance of the control strategy.
- Test the estimation performance for the loss of output measurements;
- Couple an input observer for the case of loss or mistrust in the input signals;
- Impose safety constraints for pump operation based on efficiency curves.

In terms of methodology, some open matters to the development of the proposed algorithm can be cited:

- Capability to deal with non-Gaussian noise in the measurements;
- Proof of guaranteed stability of the MPC with the scheduling strategy;
- Evaluate and enhance the estimation over biased measurements;
- Test the methodology in more complex system to stress it in terms of more complex dynamics behavior, such as dead time, inverse responses and gain inversion;
- Compare the proposed parameter estimation algorithm with more conventional ones based on Kalman Filter, such as the incorporation of the parameters in the state vector and considering them to have null dynamics;
- Perform comparison test with more established parameter estimation methods such as set-based estimation or scenario-tree in nonlinear schemes, which can be more reliable, but also more costly than the proposed approach.

Considering the high number of deepwater reservoirs in Brazil, the crescent trend of ESP use in oil production and a favorable environment for cooperative research between companies and universities, the application field of research in ESP systems is a fertile soil for technology and innovation advances in the country's research production for the near future.

Bibliography

ABDULLAH, M., ROSSITER, J. A., HABER, R., 2017, "Development of Constrained Predictive Functional Control using Laguerre Function Based Prediction", *IFAC-PapersOnLine*, v. 50, n. 1, pp. 10705–10710. doi: <10.1016/j.ifacol.2017.08.2222>. Availability: <https://doi.org/10.1016/j.ifacol.2017.08.2222>.

ANZEHAEE, M. M., BEHNAM, B., HAJIHOSSEINI, P., 2018, "Augmenting ARMarkov-PFC predictive controller with PID-Type III to improve boost converter operation", *Control Engineering Practice*, v. 79, n. January, pp. 65–77. doi: <10.1016/j.conengprac.2018.07.006>. Availability: <https://doi.org/10.1016/j.conengprac.2018.07.006>.

ASHIDA, Y., WAKITANI, S., YAMAMOTO, T., 2017, "Design of an Implicit Self-tuning PID Controller Based on the Generalized Output", *IFAC-PapersOnLine*, v. 50, n. 1, pp. 13946–13951. doi: <10.1016/j.ifacol.2017.08.2216>. Availability: <https://doi.org/10.1016/j.ifacol.2017.08.2216>.

BALDI, S., KORKAS, C. D., LV, M., et al., 2018, "Automating occupant-building interaction via smart zoning of thermostatic loads: A switched self-tuning approach", *Applied Energy*, v. 231, n. August, pp. 1246–1258. doi: <10.1016/j.apenergy.2018.09.188>. Availability: <https://doi.org/10.1016/j.apenergy.2018.09.188>.

BELLMAN, R., 1957, *Dynamic Programming*. New Jersey, Princeton.

BIDIKLI, B., BAYRAK, A., 2018, "A self-tuning robust full-state feedback control design for the magnetic levitation system", *Control Engineering Practice*, v. 78, n. May, pp. 175–185. doi: <10.1016/j.conengprac.2018.06.017>. Availability: <https://doi.org/10.1016/j.conengprac.2018.06.017>.

BINDER, B. J., KUFOALOR, D. K., PAVLOV, A., et al., 2014, "Embedded model predictive control for an electric submersible pump on a programmable

logic controller", *2014 IEEE Conference on Control Applications, CCA 2014*, , n. 2, pp. 579–585. doi: <10.1109/CCA.2014.6981402>.

BINDER, B. J., PAVLOV, A., JOHANSEN, T. A., 2015, "Estimation of flow rate and viscosity in a well with an electric submersible pump using moving horizon estimation", *IFAC-PapersOnLine*, v. 28, n. 6, pp. 140–146. doi: <10.1016/j.ifacol.2015.08.022>. Availability: <http://dx.doi.org/10.1016/j.ifacol.2015.08.022>.

BRDYS, M. A., CHOTKOWSKI, W., DUZINKIEWICZ, K., et al., 2002, "Two - Level dissolved oxygen control for activated sludge processes", *IFAC Proceedings Volumes (IFAC-PapersOnline)*, v. 35, n. 1, pp. 467–472. doi: <10.3182/20020721-6-ES-1901.01387>. Availability: <http://dx.doi.org/10.1016/S1474-6670(17)40870-6>.

BRUHN, C. H., GOMES, J. A. T., DEL LUCCHESE, C., et al., 2003, "Campos Basin: Reservoir Characterization and Management - Historical Overview and Future Challenges". In: 15220, O. (Ed.), *2003 Offshore Technology Conference*, Houston, USA.

CAMACHO, E. F., BORDONS, C., 2007, *Model Predictive Control*. 2nd ed. London. ISBN: 9781852336943.

CAMPETELLI, G., ZUMOFFEN, D. A., BASUALDO, M. S., et al., 2010, *Testing PFC controller on a well validated in silico model of a type I diabetic patient*, v. 9. IFAC. ISBN: 9783902661692. Availability: <http://dx.doi.org/10.3182/20100705-3-BE-2011.00042>.

CASTANO, J. A., HERNANDEZ, A., LI, Z., et al., 2014, *Implementation of robust EPSAC on dynamic walking of COMAN humanoid*, v. 19. IFAC. ISBN: 9783902823625. Availability: <http://dx.doi.org/10.3182/20140824-6-ZA-1003.00996>.

CASTANO, J. A., HERNANDEZ, A., LI, Z., et al., 2015, "Enhancing the robustness of the EPSAC predictive control using a Singular Value Decomposition approach", *Robotics and Autonomous Systems*, v. 74. doi: <10.1016/j.robot.2015.09.001>. Availability: <http://dx.doi.org/10.1016/j.robot.2015.09.001>.

CLARKE, D. W., MOHTADI, C., TUFFS, P. S., 1987a, "Generalized Predictive Control - Part I. The Basic Algorithm*", *Automatica*, v. 23, n. 2, pp. 137–148. doi: <10.1016/0005-1098(87)90087-2>.

CLARKE, D., MOHTADI, C., TUFFS, P., 1987b, "Generalized predictive control Part II. Extensions and interpretations", *Automatica*, v. 23, n. 2, pp. 149–160.

CUTLER, C. R., RAMAKER, B. L., 1980, "Dynamic matrix control - A computer control algorithm", *Joint Automatic Control Conference*, v. 17, n. 72. doi: <10.1109/JACC.1980.4232009>.

CZERWIŃSKI, K., ŁAWRYŃCZUK, M., 2018, "Dynamic Matrix Control Algorithm Implementation on ARM Cortex-R5 MCU: Performance Analysis", *IFAC-PapersOnLine*, v. 51, n. 6, pp. 330–335. doi: <10.1016/j.ifacol.2018.07.175>.

DAHLIN, J., WILLS, A., NINNESS, B., 2018, "Sparse Bayesian ARX models with flexible noise distributions", *IFAC-PapersOnLine*, v. 51, n. 15, pp. 25–30. doi: <10.1016/j.ifacol.2018.09.085>. Availability: <https://doi.org/10.1016/j.ifacol.2018.09.085>.

DARBY, M. L., NIKOLAOU, M., JONES, J., et al., 2011, "RTO: An overview and assessment of current practice", *Journal of Process Control*, v. 21, n. 6, pp. 874–884. doi: <10.1016/j.jprocont.2011.03.009>. Availability: <http://dx.doi.org/10.1016/j.jprocont.2011.03.009>.

DAS, S., KUMAR, R., BHAUMIK, A., 2018, "Speed sensorless model predictive current control of doubly-fed induction machine drive using model reference adaptive system", Availability: <https://doi.org/10.1016/j.isatra.2018.10.025>.

DELOU, P. A., AZEVEDO, J., KRISHNAMOORTHY, D., et al., 2019a, "Model Predictive Control with Adaptive Strategy Applied to an Electric Submersible Pump in a Subsea Environment". In: *12th IFAC Symposium on Dynamics and Control of Process Systems, including Biosystems*, Florianópolis - SC, Brazil, a.

DELOU, P. A., SOUZA JR., M. B., SECCHI, A. R., 2019b, "A Robust Adaptive MPC coupled with Kalman Filter for an Electric Submersible Pump System: A multi-model approach". In: *I Brazilian Congress on Process Systems Engineering (PSE-BR 2019)*, Rio de Janeiro - RJ, Brazil, b.

DELOU; DEMUNER; SECCHI, A. R., 2018, "Estratégias de Controle Avançado Aplicadas à Planta Tennessee-Eastman". In: *COBEQ. São Paulo: Blucher*, pp. 1249–1252.

DI CAPACI, R. B., VACCARI, M., PANNOCCHIA, G., et al., 2018, "Identification and estimation of valve stiction by the use of a smoothed model", *IFAC-PapersOnLine*, v. 51, n. 18, pp. 684–689. doi: <10.1016/j.ifacol.2018.09.344>. Availability: <https://doi.org/10.1016/j.ifacol.2018.09.344>.

DIEHL, F. C., ALMEIDA, C. S., ANZAI, T. K., et al., 2018, "Oil production increase in unstable gas lift systems through nonlinear model predictive control", *Journal of Process Control*, v. 69, pp. 58–69. doi: <10.1016/j.jprocont.2018.07.009>. Availability: <https://doi.org/10.1016/j.jprocont.2018.07.009>.

EL-SAMAHY, A. A., SHAMSELDIN, M. A., 2018, "Brushless DC motor tracking control using self-tuning fuzzy PID control and model reference adaptive control", *Ain Shams Engineering Journal*, v. 9, n. 3, pp. 341–352. doi: <10.1016/j.asej.2016.02.004>. Availability: <http://dx.doi.org/10.1016/j.asej.2016.02.004>.

ELLIS, M., DURAND, H., CHRISTOFIDES, P. D., 2014, "A tutorial review of economic model predictive control methods", *Journal of Process Control*, v. 24, n. 8, pp. 1156–1178. doi: <10.1016/j.jprocont.2014.03.010>.

FERNANDES, L. S., FILHO, F. C., PAULO, J. B., et al., 2013, "Gain scheduling adaptive control applied to a particular mixer-settler equipment", *Control Engineering Practice*, v. 21, n. 8, pp. 1121–1127. doi: <10.1016/j.conengprac.2013.04.005>. Availability: <http://dx.doi.org/10.1016/j.conengprac.2013.04.005>.

FORBES, M. G., PATWARDHAN, R. S., HAMADAH, H., et al., 2015, "Model predictive controlin industry: Challenges and opportunities", *IFAC-PapersOnLine*, v. 28, n. 8, pp. 531–538. doi: <10.1016/j.ifacol.2015.09.022>. Availability: <http://dx.doi.org/10.1016/j.ifacol.2015.09.022>.

FURLAN, F. F., DE ANDRADE LINO, A. R., MATUGI, K., et al., 2016, "A simple approach to improve the robustness of equation-oriented simulators: Multilinear look-up table interpolators", *Computers and Chemical Engineering*, v. 86, pp. 1–4. doi: <10.1016/j.compchemeng.2015.12.014>.

GALLEGO, A. J., MERELLO, G. M., BERENGUEL, M., et al., 2019, "Gain-scheduling model predictive control of a Fresnel collector field", *Control Engineering Practice*, v. 82, n. January 2018, pp. 1–13. doi: <10.1016/j.

conengprac.2018.09.022>. Availability: <https://doi.org/10.1016/j.conengprac.2018.09.022>.

GARCIA, C. E., MORSHEDI, A. M., 1986, "QUADRATIC PROGRAMMING SO LUTION OF DYNAMIC MATRIX CONTROL (QDMC)", *Chem. Eng. Commun*, v. 46, n. 1-3, pp. 073–087. doi: <http://dx.doi.org/10.1080/00986448608911397>.

GONÇALVES, G. A. D. A., 2017, *On-line process model update in discrete-time predictive controllers: a Robust approach*. Ph.D. Thesis, Universidade Federal do Rio de Janeiro - COPPE, Programa de Engenharia Química, Brasil.

GONÇALVES, G. A., SECCHI, A. R., GUAY, M., 2016, "Discrete-time state and parameter estimation using a set-based approach", *Proceedings of the American Control Conference*, v. 2016-July, pp. 7073–7078. doi: <10.1109/ACC.2016.7526788>.

GRACIANO, J. E. A., JÄSCHKE, J., LE ROUX, G. A., et al., 2015, "Integrating self-optimizing control and real-time optimization using zone control MPC", *Journal of Process Control*, v. 34, pp. 35–48. doi: <10.1016/j.jprocont.2015.07.003>. Availability: <http://dx.doi.org/10.1016/j.jprocont.2015.07.003>.

GRIMM, G., MESSINA, M. J., TUNA, S. E., et al., 2007, "Nominally robust model predictive control with state constraints", *IEEE Transactions on Automatic Control*, v. 52, n. 10, pp. 1856–1870. doi: <10.1109/TAC.2007.906187>.

GROSDIDIER, P., FROISY, B., HAMMAIM, M., 1988, "the Idocom-M Controller", .

GROSDIDIER, P., MASON, A., AITOLAHTI, A., et al., 1993, "FCC unit reactor-regenerator control", *Computers and Chemical Engineering*, v. 17, n. 2, pp. 165–179. doi: <10.1016/0098-1354(93)80012-C>.

GROSDIDIER, P., KENNEDY, P., 1990, "Case study in multivariable control - Main fractionator slurry pumparound", *The Chemical Engineering Journal*, v. 44, n. 3, pp. 119–127. doi: <10.1016/0300-9467(90)80068-N>.

HAN, J., YU, S., YI, S., 2017, "Adaptive control for robust air flow management in an automotive fuel cell system", *Applied Energy*, v. 190, pp. 73–83. doi: <10.1016/j.apenergy.2016.12.115>. Availability: <http://dx.doi.org/10.1016/j.apenergy.2016.12.115>.

HARRIS, G., VERGARA, L., SOUZA, C. R. N., et al., 2012, "ESP systems enhance reliability in challenging environments", *Drilling & Completion*, pp. 2–5.

HEIRUNG, T. A. N., YDSTIE, B. E., FOSS, B., 2015, "Dual MPC for FIR systems: Information anticipation", *IFAC-PapersOnLine*, v. 28, n. 8, pp. 1033–1038. doi: <10.1016/j.ifacol.2015.09.104>. Availability: <http://dx.doi.org/10.1016/j.ifacol.2015.09.104>.

HODREA, R., NASCU, I., DE KEYSER, R., et al., 2012, *EPSAC predictive control applied to muscle relaxant administration*, v. 45. IFAC. ISBN: 9783902823106. Availability: <http://dx.doi.org/10.3182/20120829-3-HU-2029.00012>.

IANCU, M., CRISTEA, M. V., AGACHI, P. S., 2013, "Retrofit design of heat exchanger network of a fluid catalytic cracking plant and control based on MPC", *Computers and Chemical Engineering*, v. 49, pp. 205–216. doi: <10.1016/j.compchemeng.2012.11.001>. Availability: <http://dx.doi.org/10.1016/j.compchemeng.2012.11.001>.

IVO, O. F., 2018, *PERFORMANCE ANALYSIS OF DETERMINISTIC, MIN-MAX AND MULTI-STAGE NMPC APPLIED TO A SUBSEA GAS COMPRESSION SYSTEM*. Master Thesis, Universidade Federal do Rio de Janeiro - COPPE, Programa de Engenharia Química, Brasil.

JIA, R., MAO, Z., WANG, F., et al., 2015, "Self-tuning final product quality control of batch processes using kernel latent variable model", *Chemical Engineering Research and Design*, v. 94, pp. 119–130. doi: <10.1016/j.cherd.2014.12.013>. Availability: <http://dx.doi.org/10.1016/j.cherd.2014.12.013>.

JIN, R., CHEN, X., GENG, Y., et al., 2018, "LPV gain-scheduled attitude control for satellite with time-varying inertia", *Aerospace Science and Technology*, v. 80, pp. 424–432. doi: <10.1016/j.ast.2018.07.020>. Availability: <https://doi.org/10.1016/j.ast.2018.07.020>.

JORDANOU, J. P., CAMPONOGARA, E., ANTONELO, E. A., et al., 2018, "Nonlinear Model Predictive Control of an Oil Well with Echo State Networks", *IFAC-PapersOnLine*, v. 51, n. 8, pp. 13–18. doi: <10.1016/j.ifacol.2018.06.348>.

KALMAN, R. E., 1960a, "A new approach to linear filtering and prediction problems", *Journal of basic Engineering*, v. 82, n. 1, pp. 35–45.

KALMAN, R. E., 1960b, "Contributions to the theory of optimal control", *Bol. Soc. Mat. Mexicana*, v. 5, n. 2, pp. 102–119.

KHALIL, H. K., 2002, *Nonlinear Systems*. N. 5. 3rd ed. New Jersey, Prentice Hall. ISBN: 0130673897, 9780130673893.

KHUSAINOV, B., KERRIGAN, E., SUARDI, A., et al., 2018, "Nonlinear predictive control on a heterogeneous computing platform", *Control Engineering Practice*, v. 78, n. October 2017, pp. 105–115. doi: <10.1016/j.conengprac.2018.06.016>. Availability: <https://doi.org/10.1016/j.conengprac.2018.06.016>.

KIM, S. K., 2015, "Self-tuning adaptive feedback linearizing output voltage control for AC/DC converter", *Control Engineering Practice*, v. 45, pp. 1–11. doi: <10.1016/j.conengprac.2015.08.007>. Availability: <http://dx.doi.org/10.1016/j.conengprac.2015.08.007>.

KIM, S. K., 2017, "Robust adaptive speed regulator with self-tuning law for surfaced-mounted permanent magnet synchronous motor", *Control Engineering Practice*, v. 61, n. January, pp. 55–71. doi: <10.1016/j.conengprac.2017.01.014>. Availability: <http://dx.doi.org/10.1016/j.conengprac.2017.01.014>.

KLOPOT, T., SKUPIN, P., METZGER, M., et al., 2018, "Tuning strategy for dynamic matrix control with reduced horizons", *ISA Transactions*, v. 76, pp. 145–154. doi: <10.1016/j.isatra.2018.03.003>. Availability: <https://doi.org/10.1016/j.isatra.2018.03.003>.

KRISHNAMOORTHY, D., BERGHEIM, E. M., PAVLOV, A., et al., 2016, "Modelling and Robustness Analysis of Model Predictive Control for Electrical Submersible Pump Lifted Heavy Oil Wells", *IFAC-PapersOnLine*, v. 49, n. 7, pp. 544–549. doi: <10.1016/j.ifacol.2016.07.399>. Availability: <http://dx.doi.org/10.1016/j.ifacol.2016.07.399>.

KWONG, W. H., 2000, "Improved simplified model predictive control algorithm and its application to a continuous fermenter", *Brazilian Journal of Chemical Engineering*, v. 17, n. 2, pp. 143–161. doi: <10.1590/S0104-66322000000200003>.

LEE, J. H., 2011, "Model predictive control: Review of the three decades of development", *International Journal of Control, Automation and Systems*, v. 9, n. 3, pp. 415–424. doi: <10.1007/s12555-011-0300-6>.

LI, D., YANG, N., NIU, R., et al., 2012, "FPGA based QDMC control for reverse-osmosis water desalination system", *Desalination*, v. 285, pp. 83–90. doi: <10.1016/j.desal.2011.09.037>. Availability: <http://dx.doi.org/10.1016/j.desal.2011.09.037>.

LI, X. L., JIA, C., LIU, D. X., et al., 2014, "Nonlinear adaptive control using multiple models and dynamic neural networks", *Neurocomputing*, v. 136, pp. 190–200. doi: <10.1016/j.neucom.2014.01.013>. Availability: <http://dx.doi.org/10.1016/j.neucom.2014.01.013>.

LI, Y., ZHANG, X., BAO, J., et al., 2017, "Control of electrolyte flow rate for the vanadium redox flow battery by gain scheduling", *Journal of Energy Storage*, v. 14, pp. 125–133. doi: <10.1016/j.est.2017.10.005>.

LIU, X., ZHANG, C., LI, K., et al., 2017, "Robust current control-based generalized predictive control with sliding mode disturbance compensation for PMSM drives", *ISA Transactions*, v. 71, pp. 542–552. doi: <10.1016/j.isatra.2017.08.015>.

MACIEJOWSKI, J. M., 2002, *Predictive control: with constraints*. 1st ed. Harlow, England, Prentice Hall.

MAO, T., ZHANG, Y., RUAN, Y., et al., 2018, "Feature learning and process monitoring of injection molding using convolution-deconvolution auto encoders", *Computers and Chemical Engineering*, v. 118, pp. 77–90. doi: <10.1016/j.compchemeng.2018.07.009>. Availability: <https://doi.org/10.1016/j.compchemeng.2018.07.009>.

MARCHETTI, A., CHACHUAT, B., BONVIN, D., 2009a, *Modifier-Adaptation Methodology for Real-Time Optimization*. Ph.D. Thesis, a.

MARCHETTI, A., FRANÇOIS, G., FAULWASSER, T., et al., 2009b, "Modifier Adaptation for Real-Time Optimization—Methods and Applications", *Ind. Eng. Chem. Res.*, v. 48, n. 13, pp. 6022–6033. doi: <10.3390/pr4040055>. Availability: <http://www.mdpi.com/2227-9717/4/4/55>.

MARQUIS, P., BROUSTAIL, J., 1988, "SMOC, a bridge between state space and model predictive controllers: Application to the automation of a hydrotreating unit", *IFAC Proceedings Volumes*, v. 21, n. 4, pp. 37–45. doi: <10.1016/B978-0-08-035735-5.50010-3>.

MARRUEDO, D., ALAMO, T., CAMACHO, E., 2002, "Input-to-state stable MPC for constrained discrete-time nonlinear systems with bounded additive uncertainties", *Proceedings of the 41st IEEE Conference on Decision and Control, 2002.*, v. 4, n. December, pp. 4619–4624. doi: <10.1109/CDC.2002.1185106>. Availability: <http://ieeexplore.ieee.org/document/1185106/>.

MAYNE, D. Q., RAWLINGS, J. B., RAO, C. V., et al., 2000, "Constrained model predictive control: Stability and Optimality", v. 36. doi: <10.1016/S0005-1098(99)00214-9>. Availability: <www.lafabricadelibros.com>.

MAYNE, D. Q., 2014, "Model predictive control: Recent developments and future promise", *Automatica*, v. 50, n. 12, pp. 2967–2986. doi: <10.1016/j.automatica.2014.10.128>. Availability: <http://dx.doi.org/10.1016/j.automatica.2014.10.128>.

MENDES, J., OSÓRIO, L., ARAÚJO, R., 2017, "Self-tuning PID controllers in pursuit of plug and play capacity", *Control Engineering Practice*, v. 69, n. December 2016, pp. 73–84. doi: <10.1016/j.conengprac.2017.09.006>.

MENDONÇA, J. E., MATTOS, C. H., RITTERSHAUSSEN, J. H., 2008, "The First Deepwater Installation of a Subsea ESP: RJS-477A, Campos Basin, Brazil". In: 10969, O. (Ed.), *1999 Offshore Technology Conference*, pp. 1–9, Houston.

MOON, U. C., LEE, Y., LEE, K. Y., 2018, "Practical dynamic matrix control for thermal power plant coordinated control", *Control Engineering Practice*, v. 71, n. October 2017, pp. 154–163. doi: <10.1016/j.conengprac.2017.10.014>. Availability: <https://doi.org/10.1016/j.conengprac.2017.10.014>.

MUSHIRI, T., MAHACHI, A., MBOHWA, C., 2017, "A Model Reference Adaptive Control (MRAC) System for the Pneumatic Valve of the Bottle Washer in Beverages Using Simulink", *Procedia Manufacturing*, v. 7, pp. 364–373. doi: <10.1016/j.promfg.2016.12.003>.

NAMARA, P. M., NEGENBORN, R. R., DE SCHUTTER, B., et al., 2016, "Distributed MPC for frequency regulation in multi-terminal HVDC grids", *Control Engineering Practice*, v. 46, pp. 176–187. doi: <10.1016/j.conengprac.2015.11.001>. Availability: <http://dx.doi.org/10.1016/j.conengprac.2015.11.001>.

NIVA, L., YLI-KORPELA, A., 2012, *Control of a benchmark boiler process model with DMC and QDMC*, v. 8. IFAC. ISBN: 9783902823243. Availability: <http://dx.doi.org/10.3182/20120902-4-FR-2032.00035>.

OGUNNAIKE, RAY, 1994, *Process Dynamics, Modeling, and Control*. New York, OXFORD UNIVERSITY PRESS. ISBN: 0195091191.

OLTEAN, S.-E., DULAU, M., DUKA, A.-V., 2016, "Model Reference Adaptive Control Design for Slow Processes. A Case Study on Level Process Control", *Procedia Technology*, v. 22, pp. 629–636. doi: <10.1016/j.protcy.2016.01.131>.

PARKS, P. C., PARKS, P. C., 1966, "Liapunov Redesign of Model Reference Adaptive Control Systems", *IEEE Transactions on Automatic Control*, v. 11, n. 3, pp. 362–367. doi: <10.1109/TAC.1966.1098361>.

PASCHKE, F., ZAICZEK, T., 2018, "Identification of dynamic models for the short-term temperature prediction in a single room", *IFAC-PapersOnLine*, v. 51, n. 2, pp. 79–84. doi: <10.1016/j.ifacol.2018.03.014>. Availability: <https://doi.org/10.1016/j.ifacol.2018.03.014>.

PAVLOV, A., KRISHNAMOORTHY, D., FJALESTAD, K., et al., 2014, "Modelling and model predictive control of oil wells with electric submersible pumps", *2014 IEEE Conference on Control Applications, CCA 2014*, , n. 3905, pp. 586–592. doi: <10.1109/CCA.2014.6981403>.

PEREZ, J. M. G. T., 2012, *Controle Preditivo Multivariável Com Modelo De Realinhamento E Robusto Quanto À Estabilidade*. Ph.D. Thesis, Universidade Federal do Rio de Janeiro - COPPE, Programa de Engenharia Química, Brasil.

PIN, G., RAIMONDO, D. M., MAGNI, L., et al., 2009, "Robust model predictive control of nonlinear systems with bounded and state-dependent uncertainties", *IEEE Transactions on Automatic Control*, v. 54, n. 7, pp. 1681–1687. doi: <10.1109/TAC.2009.2020641>.

PINTO, A., BRANCO, C., DE MATOS, J., et al., 2003, "Offshore Heavy Oil in Campos Basin: The Petrobras Experience". In: 15283, O. (Ed.), *2003 Offshore Technology Conference*, Houston, USA.

PRIOR, D., LOPEZ, S., 1999, "Grangemouth ethylene plant installs closed-loop optimization solution", *Oil & Gas Journal*, v. 97, n. 42, pp. 83–86.

PUSCHKE, J., MITSOS, A., 2018, "Robust feasible control based on multi-stage eNMPC considering worst-case scenarios", *Journal of Process Control*, v. 69, pp. 8–15. doi: <10.1016/j.jprocont.2018.07.004>. Availability: <https://doi.org/10.1016/j.jprocont.2018.07.004>.

QIN, S. J., BADWELL, T. A., 1997, "An overview of industrial model predictive control technology", *Control Engineering Practice*, v. 93, n. 316, pp. 232–256. doi: <10.1.1.52.8909>.

QIN, S. J., BADWELL, T. A., 2003, "A survey of industrial model predictive control technology", *Control Engineering Practice*, v. 11, pp. 733–764. doi: <10.1016/S0967-0661(02)00186-7>.

RAMDANI, A., GROUNI, S., SOUFI, Y., 2016, "Application of predictive controller tuning and a comparison study in terms of PID controllers", *International Journal of Hydrogen Energy*, v. 41, n. 29, pp. 12454–12464. doi: <10.1016/j.ijhydene.2016.05.102>. Availability: <http://dx.doi.org/10.1016/j.ijhydene.2016.05.102>.

RAWLINGS AND MAYNE, D., 2009, *Model Predictive Control: Theory and Design*. Nob Hill Pub. ISBN: 9780975937709. Availability: <https://books.google.com.br/books?id=3{%}5C{_}rfQQAACAAJ>.

RICHALET, J., 1993, "Industrial applications of model based predictive control", *Automatica*, v. 29, n. 5, pp. 1251–1274. doi: <10.1016/0005-1098(93)90049-Y>.

RICHALET, J., RAULT, A., TESTUD, J. L., et al., 1978, "Model predictive heuristic control. Applications to industrial processes", *Automatica*, v. 14, n. 5, pp. 413–428. doi: <10.1016/0005-1098(78)90001-8>.

RICHALET, J., ABU EL ATA-DOSS, S., ARBER, C., et al., 1987, "Predictive Functional Control - Application to Fast and Accurate Robots", *IFAC Proceedings Volumes*, v. 20, n. 5, pp. 251–258. doi: <10.1016/S1474-6670(17)55325-2>.

SADEGHASSADI, M., MACNAB, C. J., GOPALUNI, B., et al., 2018, "Application of neural networks for optimal-setpoint design and MPC control in biological wastewater treatment", *Computers and Chemical Engineering*, v. 115, pp. 150–160. doi: <10.1016/j.compchemeng.2018.04.007>. Availability: <https://doi.org/10.1016/j.compchemeng.2018.04.007>.

SALAHSHOOR, K., KORDESTANI, M., 2014, "Design of an active fault tolerant control system for a simulated industrial steam turbine", *Applied Mathematical Modelling*, v. 38, n. 5-6, pp. 1753–1774. doi: <10.1016/j.apm.2013.09.015>. Availability: <http://dx.doi.org/10.1016/j.apm.2013.09.015>.

SHA'ABAN, Y. A., 2015, *Regulatory Level Model Predictive Control*. Ph.D. Thesis, University of Manchester.

SHI, J., ZHOU, H., CAO, Z., et al., 2014, "A design method for indirect iterative learning control based on two-dimensional generalized predictive control algorithm", *Journal of Process Control*, v. 24, n. 10, pp. 1527–1537. doi: <10.1016/j.jprocont.2014.07.004>. Availability: <http://dx.doi.org/10.1016/j.jprocont.2014.07.004>.

SIMON, D., 2006, *Optimal State Estimation: Kalman, H∞, and Nonlinear Approaches*. ISBN: 0471708585.

STOGIANNOS, M., ALEXANDRIDIS, A., SARIMVEIS, H., 2018, "Model predictive control for systems with fast dynamics using inverse neural models", *ISA Transactions*, v. 72, pp. 161–177. doi: <10.1016/j.isatra.2017.09.016>. Availability: <http://dx.doi.org/10.1016/j.isatra.2017.09.016>.

TAKACS, G., 2011, "How to improve poor system efficiencies of ESP installations controlled by surface chokes", *Journal of Petroleum Exploration and Production Technology*, v. 1, n. 2-4, pp. 89–97. doi: <10.1007/s13202-011-0011-9>.

TAO, G., 2014, "Multivariable adaptive control: A survey", *Automatica*, v. 50, n. 11, pp. 2737–2764. doi: <10.1016/j.automatica.2014.10.015>. Availability: <http://dx.doi.org/10.1016/j.automatica.2014.10.015>.

THOMAS, J. E., 2001, *Fundamentos de Engenharia de Petróleo*. Rio de Janeiro. ISBN: 85-7193-046-5.

TRAN, Q. N., ÖZKAN, L., BACKX, A. C., 2014, "Generalized predictive control tuning by controller matching", *Journal of Process Control*, v. 25, pp. 1–18. doi: <10.1016/j.jprocont.2014.10.002>. Availability: <http://dx.doi.org/10.1016/j.jprocont.2014.10.002>.

VARÓN, M. P., BANNWART, A. C., BIAZUSSI, J. L., et al., 2013, "Study of an Electrical Submersible Pump (ESP) as Flow Meter", *SPE Artificial Lift Conference-Americas*, , n. February 2016. doi: <10.2118/165065-MS>. Availability: <http://www.onepetro.org/doi/10.2118/165065-MS>.

WÄCHTER, A., BIEGLER, L. T., 2006, "On the implementation of an interior-point filter line-search algorithm for large-scale nonlinear programming", *Mathematical Programming*, v. 106, n. 1, pp. 25–57. doi: <10.1007/s10107-004-0559-y>.

WANG, L., 2009, *Model Predictive Control System Design and Implementation Using MATLAB*. N. 1st. 1st ed. London, Springer-Verlag London Limited. ISBN: 9781848823303.

WANG, Z., ZHANG, B., LI, X., et al., 2018, "Study on application of model reference adaptive control in fast steering mirror system", *Optik*, v. 172, pp. 995–1002. doi: <10.1016/j.ijleo.2018.07.095>. Availability: <https://doi.org/10.1016/j.ijleo.2018.07.095>.

WOJTULEWICZ, A., ŁAWRYŃCZUK, M., 2018, "Implementation of Multiple-Input Multiple-Output Dynamic Matrix Control Algorithm for Fast Processes Using Field Programmable Gate Array", *IFAC-PapersOnLine*, v. 51, n. 6, pp. 324–329. doi: <10.1016/j.ifacol.2018.07.174>.

YAN, W., ZHU, Y., 2018, "Informative Conditions for Identification of MISO ARMAX Model in Closed-loop Systems", *IFAC-PapersOnLine*, v. 51, n. 15, pp. 455–460. doi: <10.1016/j.ifacol.2018.09.187>. Availability: <https://doi.org/10.1016/j.ifacol.2018.09.187>.

ZABET, K., HABER, R., 2017, "Robust tuning of PFC (Predictive Functional Control) based on first- and aperiodic second-order plus time delay models", *Journal of Process Control*, v. 54, pp. 25–37. doi: <10.1016/j.jprocont.2017.01.008>. Availability: <http://dx.doi.org/10.1016/j.jprocont.2017.01.008>.

ZHANG, J., SUN, W., FENG, Z., 2018a, "Vehicle yaw stability control via H_-\infty gain scheduling", *Mechanical Systems and Signal Processing*, v. 106, n. 61773135, pp. 62–75. doi: <10.1016/j.ymssp.2017.12.033>. Availability: <https://doi.org/10.1016/j.ymssp.2017.12.033>.

ZHANG, K., ZHAO, J., ZHU, Y., 2018b, "MPC case study on a selective catalytic reduction in a power plant", *Journal of Process Control*, v. 62, n.

61673343, pp. 1–10. doi: <10.1016/j.jprocont.2017.11.010>. Availability: <http://dx.doi.org/10.1016/j.jprocont.2017.11.010>.

Appendix A

System Linearization Strategy

The linearization strategy followed the Taylor's expansion method truncated in the first order element. So the linear system can be written in the following matrix form:

$$\begin{aligned} \frac{dx(t)}{dt} &= Ax(t) + Bu(t) \\ y(t) &= Cx(t) + Du(t) \end{aligned} \tag{A.1}$$

In which, x, u and y are respectively state, input and output variables in a reference state deviation notation.

$$x = \begin{pmatrix} p_{bh} - p^*_{bh} \\ p_{wh} - p^*_{wh} \\ q - q^* \end{pmatrix} \tag{A.2}$$

$$u = \begin{pmatrix} f - f^* \\ z - z^* \end{pmatrix} \tag{A.3}$$

$$y = \begin{pmatrix} p_{p,in} - p^*_{p,in} \\ P - P^* \end{pmatrix} \tag{A.4}$$

Let $dx(t)/dt$ be represented by a function of x and u, such as:

$$\frac{dx(t)}{dt} = F(x, u) \tag{A.5}$$

The elements of matrices A, B, C and D can be calculated by the analytical derivatives of F and y over x and u:

$$a_{i,j} = \frac{\partial F_i}{\partial x_j}\Big|_{x^*,u^*},\ b_{i,j} = \frac{\partial F_i}{\partial u_j}\Big|_{x^*,u^*},\ c_{i,j} = \frac{\partial y_i}{\partial x_j}\Big|_{x^*,u^*} and\ d_{i,j} = \frac{\partial y_i}{\partial u_j}\Big|_{x^*,u^*} \tag{A.6}$$

The elements of the Jacobian matrix, A, are:

$$\begin{aligned}
a_{1,1} &= -\frac{\beta_1}{V_1} PI \\
a_{1,2} &= 0 \\
a_{1,3} &= -\frac{\beta_1}{V_1} \\
a_{2,1} &= 0 \\
a_{2,2} &= -\frac{\beta_2}{V_2}\left(\frac{C_c\, z^*}{2}\frac{1}{\sqrt{p^*_{wh} - p^*_m}}\right) \\
a_{2,3} &= \frac{\beta_2}{V_2} \\
a_{3,1} &= \frac{1}{M} \\
a_{3,2} &= -\frac{1}{M} \\
a_{3,3} &= -\frac{F_1{}' - F_2{}'}{M} + \frac{\rho g C_H}{M}\left(\frac{f^*}{f^0}\right)^2\left(C_{1,H0} + 2\, C_{2,H0}\, q^*\frac{f^*}{C_q f_0}\right)\frac{f^*}{C_q f_0}
\end{aligned} \tag{A.7}$$

The elements of matrix B are:

$$\begin{aligned}
b_{1,1} &= 0 \\
b_{1,2} &= 0 \\
b_{2,1} &= 0 \\
b_{2,2} &= -\frac{\beta_2}{V_2}\, C_c\, \sqrt{p^*_{wh} - p^*_m} \\
b_{3,1} &= \frac{1}{M} \\
b_{3,2} &= -\frac{1}{M}
\end{aligned} \tag{A.8}$$

The elements of matrix C are:

$$
\begin{aligned}
c_{1,1} &= 1 \\
c_{1,2} &= 0 \\
c_{1,3} &= F_1{}' \\
c_{2,1} &= 0 \\
c_{2,2} &= 0 \\
c_{2,3} &= C_P \left(\frac{f^*}{f_0}\right)^3 \left[C_{1,P0} + 2\, C_{2,P0}\, \frac{q^* f^*}{C_q f_0} + 3\, C_{3,P0} \left(\frac{q^* f^*}{C_q f_0}\right)^2\right] \frac{f^*}{C_q f_0}
\end{aligned}
\tag{A.9}
$$

Finally, the elements of matrix D are:

$$
\begin{aligned}
d_{1,1} &= 0 \\
d_{1,2} &= 0 \\
d_{2,1} &= C_P \left[\left(\frac{f^*}{f_0}\right)^3 \left(C_{1,P0} + 2\, C_{2,P0}\, \frac{q^*\, f^*}{C_q f_0} + 3\, C_{3,P0} \left(\frac{q^*\, f^*}{C_q f_0}\right)^2\right)\right] \\
d_{2,2} &= 0
\end{aligned}
\tag{A.10}
$$

in which,

$$
\begin{aligned}
F_i{}' = 0.158 \frac{2\rho L_i q^*}{D_i A_i^2} \left(\frac{\mu}{\rho D_i q^*}\right)^{1/4} + \\
0.158 \frac{1}{4} \frac{\rho L_i q^{*2}}{D_i A_i^2} \left(\frac{\mu}{\rho D_i q^*}\right)^{-3/4} \left(\frac{-\mu}{\rho D_i q^{*2}}\right), i = 1, 2
\end{aligned}
\tag{A.11}
$$

It is noteworthy that a relative deviation approach enhances the controllability of the system. This is a normalization strategy to deal with different order of magnitude of the variables. The system notation adopting the relative deviation is:

$$
\begin{aligned}
\frac{dz(t)}{dt} &= \hat{A} z(t) + \hat{B} v(t) \\
w(t) &= \hat{C} z(t) + \hat{D} v(t)
\end{aligned}
\tag{A.12}
$$

in which, z, v and w are respectively state, input and output variables in a reference

state relative deviation notation.

$$z = \begin{pmatrix} \dfrac{p_{bh} - p_{bh}^*}{p_{bh}^*} \\ \dfrac{p_{wh} - p_{wh}^*}{p_{wh}^*} \\ \dfrac{q - q^*}{q^*} \end{pmatrix} \tag{A.13}$$

$$v = \begin{pmatrix} \dfrac{f - f^*}{f^*} \\ \dfrac{z - z^*}{z^*} \end{pmatrix} \tag{A.14}$$

$$w = \begin{pmatrix} \dfrac{p_{p,in} - p_{p,in}^*}{p_{p,in}^*} \\ \dfrac{P - P^*}{P^*} \end{pmatrix} \tag{A.15}$$

Taking the system in a reference deviation notation, it is possible to find the equivalent matrices in the fractional reference deviation by applying the following transformations:

$$\hat{a}_{i,j} = a_{i,j} \frac{x_j^*}{x_i^*} \tag{A.16}$$

$$\hat{b}_{i,j} = b_{i,j} \frac{u_j^*}{x_i^*} \tag{A.17}$$

$$\hat{c}_{i,j} = c_{i,j} \frac{x_j^*}{y_i^*} \tag{A.18}$$

$$\hat{d}_{i,j} = d_{i,j} \frac{u_j^*}{y_i^*} \tag{A.19}$$

in which, $\hat{a}_{i,j}$, $\hat{b}_{i,j}$, $\hat{c}_{i,j}$ and $\hat{d}_{i,j}$ are the elements of matrices $\hat{A}_{i,j}$, $\hat{B}_{i,j}$, $\hat{C}_{i,j}$ and $\hat{D}_{i,j}$, respectively.

Appendix B

State-space MPC formulation

The state-space formulation presented in this section was inspired in the formulation presented by WANG (2009) for MIMO systems with the difference that here the feedthrough matrix is considered in the following discrete dynamic system:

$$\begin{aligned} x_m(k+1) &= A_m x_m(k) + B_m u(k) \\ y(k) &= C_m x_m(k) + D_m u(k) \end{aligned} \tag{B.1}$$

It is possible to show that:

$$\Delta x_m(k+1) = A_m \Delta x_m(k) + B_m \Delta u(k) \tag{B.2}$$

in which, $\Delta x_m(k) = x_m(k) - x_m(k-1)$ and $\Delta u(k) = u(k) - u(k-1)$. So, by doing the same with the output y, it is possible to show that:

$$\begin{aligned} \Delta y(k+1) &= C_m \Delta x_m(k+1) + D_m \Delta u(k+1) \\ \Delta y(k+1) &= C_m A_m \Delta x_m(k) + C_m B_m \Delta u(k) + D_m \Delta u(k+1) \end{aligned} \tag{B.3}$$

and, therefore:

$$y(k+1) = C_m A_m \Delta x_m(k) + C_m B_m \Delta u(k) + D_m \Delta u(k+1) + y(k) \tag{B.4}$$

Defining a new augmented state vector:

$$x(k) = \begin{bmatrix} \Delta x_m(k)^T \\ y(k)^T \end{bmatrix} \tag{B.5}$$

It is possible to write the following augmented model, equivalent to the one presented in Equation B.1:

$$\begin{aligned} x(k+1) &= \begin{bmatrix} A_m & o_m^T \\ C_m A_m & I \end{bmatrix} x(k) + \begin{bmatrix} B_m \\ C_m B_m \end{bmatrix} \Delta u(k) + \begin{bmatrix} 0_m^T \\ D_m \end{bmatrix} \Delta u(k+1) \\ y(k) &= \begin{bmatrix} 0_m & I \end{bmatrix} x(k) \end{aligned} \tag{B.6}$$

Defining the new matrices A, B, C and D so that the linear system presented in Equation B.6 is equivalent to the following:

$$\begin{aligned} x(k+1) =& Ax(k) + B\Delta u(k) + D\Delta u(k+1) \\ y(k) =& Cx(k) \end{aligned} \tag{B.7}$$

Now, it is possible to write the future state variable:

$$\begin{aligned} x(k_i+1|k_i) =& Ax(k_i) + B\Delta u(k_i) + D\Delta u(k_i+1) \\ x(k_i+2|k_i) =& A^2x(k_i) + AB\Delta u(k_i) + (AD+B)\Delta u(k_i+1) + D\Delta u(k_i+2) \\ x(k_i+3|k_i) =& A^3x(k_i) + A^2B\Delta u(k_i) + (A^2D+AB)\Delta u(k_i+1) + \\ & (AD+B)\Delta u(k_i+2) + D\Delta u(k_i+3) \\ & \vdots \\ x(k_i+L|k_i) =& A^Lx(k_i) + A^{L-1}B\Delta u(k_i) + (A^{L-1}D + A^{L-2}B)\Delta u(k_i+1) \\ & + (A^{L^2}D + B^{L-3}B)\Delta u(k_i+2) + \dots \\ & + (A^{L-N+1}D + A^{L-N}B)\Delta u(k_i+N-1) \\ & + D\Delta u(k_i+N) \end{aligned} \tag{B.8}$$

in which, $x(k_i+L|k_i)$ is the predicted state variables at k_i+L calculated with system information in the instant k_i, L and N are the prediction horizon and the control horizon, respectively. So, now it is possible to write the future outputs

based on the prediction of the state variables:

$$
\begin{aligned}
y(k_i+1|k_i) =& CAx(k_i) + CB\Delta u(k_i) + CD\Delta u(k_i+1) \\
y(k_i+2|k_i) =& CA^2x(k_i) + CAB\Delta u(k_i) + (CAD+CB)\Delta u(k_i+1) \\
&+ CD\Delta u(k_i+2) \\
y(k_i+3|k_i) =& CA^3x(k_i) + CA^2B\Delta u(k_i) + (CA^2D+CAB)\Delta u(k_i+1) + \\
&(CAD+CB)\Delta u(k_i+2) + CD\Delta u(k_i+3) \\
&\vdots \\
y(k_i+L|k_i) =& CA^Lx(k_i) + CA^{L-1}B\Delta u(k_i) \\
&+ (CA^{L-1}D + CA^{L-2}B)\Delta u(k_i+1) \\
&+ (CA^{L^2}D + CB^{L-3}B)\Delta u(k_i+2) + \dots \\
&+ (CA^{L-N+1}D + CA^{L-N}B)\Delta u(k_i+N-1) \\
&+ CD\Delta u(k_i+N)
\end{aligned}
\tag{B.9}
$$

It is possible to condensate the prediction of the outputs, deduced in Equation B.9, in a matrix notation as follows:

$$
Y = Fx(k_i) + \Phi\Delta U \tag{B.10}
$$

in which, vectors Y and ΔU are defined as:

$$
Y = \begin{bmatrix} y(k_i+1|k_i) \\ y(k_i+2|k_i) \\ y(k_i+3|k_i) \\ \vdots \\ y(k_i+L|k_i) \end{bmatrix} \tag{B.11}
$$

$$
\Delta U = \begin{bmatrix} \Delta u(k_i) \\ \Delta u(k_i+1) \\ \Delta u(k_i+2) \\ \vdots \\ \Delta u(k_i+N-1) \\ \Delta u(k_i+N) \end{bmatrix} \tag{B.12}
$$

and matrices F and Φ are:

$$F = \begin{bmatrix} CA \\ CA^2 \\ CA^3 \\ \vdots \\ CA^L \end{bmatrix} \tag{B.13}$$

$$\Phi = \begin{bmatrix} CB & CD & \dots & 0 & 0 \\ CAB & CAD + CB & \dots & 0 & 0 \\ CA^2B & CA^2D + CAB & \dots & 0 & 0 \\ CA^3B & CA^3D + CA^2B & \dots & 0 & 0 \\ \vdots & \vdots & \ddots & \vdots & \vdots \\ CA^{L-1}B & CA^{L-1}D + CA^{L-2}B & \dots & CA^{L-N+1}D + CA^{L-N}B & CD \end{bmatrix} \tag{B.14}$$

Now, it is possible to write the objective function for the linear MPC considering the reference trajectory of the controlled variables, $Y^{rt} = [y^{rt}(k_i + 1|k_i)^T, y^{rt}(k_i + 2|k_i)^T, y^{rt}(k_i + 3|k_i)^T, \dots, y^{rt}(k_i + L|k_i)^T]^T$, and the reference trajectory of the manipulated variables, $U^{rt} = [u^{rt}(k_i)^T, u^{rt}(k_i + 1)^T, u^{rt}(k_i + 2)^T, \dots, u^{rt}(k_i + N - 1)^T]^T$:

$$J = (Y - Y^{rt})^T W_Y (Y - Y^{rt}) + (U - U^{rt})^T W_U (U - U^{rt}) + \Delta U^T W_{\Delta U} \Delta U \tag{B.15}$$

such that,

$$U = \Delta U + \begin{bmatrix} u(k_i - 1) \\ u(k_i) \\ u(k_i + 1) \\ \vdots \\ u(k_i + N - 2) \\ u(k_i + N - 1) \end{bmatrix} \tag{B.16}$$

Finally, for the constrained case it is important to aggregate the three types of constraints in a single matrix form, as it is showed in Equation 2.8, so that any QP or NLP solvers could find the optimal manipulated variables sequence. For that, a similar manipulation of the constraints presented in Equation 2.24 to fit them

into matrix A and vector b. With proper mathematical handling, it is possible to show that:

$$A = \begin{bmatrix} -C_2 \\ C_2 \\ -I \\ I \\ -\Phi \\ \Phi \end{bmatrix}, \; b = \begin{bmatrix} -U^{lb} + C_1 u(k_i - 1) \\ U^{ub} - C_1 u(k_i - 1) \\ -\Delta U^{lb} \\ \Delta U^{ub} \\ -Y^{lb} + Fx(k_i) \\ Y^{ub} - Fx(k_i) \end{bmatrix} \tag{B.17}$$

in which C_1 is a $(mN) \times N$ matrix resulted from the vertical concatenation of N identity matrices of dimension $m \times m$ and C_2 is a $(mN) \times (mN)$ resulted from grouping the identity matrices in a inferior triangular manner, such that:

$$C_1 = \begin{bmatrix} I \\ I \\ I \\ \vdots \\ I \end{bmatrix}, \; C_2 = \begin{bmatrix} I & 0 & 0 & \dots & 0 \\ I & I & 0 & \dots & 0 \\ I & I & I & \dots & 0 \\ \vdots & \vdots & \vdots & \ddots & \vdots \\ I & I & I & \dots & I \end{bmatrix} \tag{B.18}$$